Dissertation

zur Erlangung des Doktorgrades der

Fakultät für Chemie und Pharmazie

der Ludwig-Maximilians-Universität München

Identification of novel septate junction components through genome-wide glial screens

Myrto Deligiannaki

aus Athen, Griechenland

2015

Diese Dissertation wurde im Sinne von §7 der Promotionsordnung vom 28. November 2011 von Frau Prof. Dr. Ulrike Gaul betreut.

Eidesstattliche Versicherung

Diese Dissertation wurde eigenständig und ohne unerlaubte Hilfe erarbeitet.

München, 07/04/2015

....

Myrto Deligiannaki

Dissertation eingereicht am: 07/04/2015

Erstgutachterin: Prof. Dr. Ulrike Gaul

Zweitgutachter: Prof. Dr. Klaus Förstemann

Tag der mündlichen Prüfung: 19/05/2015

Acknowledgements

Firstly, I would like to thank my advisor Ulrike Gaul for persistently encouraging my research and being a challenging mentor. I appreciate all her contributions of ideas, time and funding, as well as her support, which made my Ph.D. experience productive and stimulating.

I would also like to thank: the members of my thesis advisory committee, Magdalena Götz, Hiromu Tanimoto and Takashi Suzuki for the fruitful discussions and good advice; Klaus Förstemann for being my second thesis evaluator; all members of my defense committee: Ulrike Gaul, Klaus Förstemann, Nicolas Gompel, Magdalena Götz, Roland Beckmann and Daniel Wilson. I am also grateful to Hans-Jörg Schaeffer, Ingrid Wolf and everybody from the Max Planck International PhD programme who assisted me in various ways and provided excellent workshops.

A big thank you to members of the lab that contributed with their expertise to different aspects of my project: Abbie Casper for performing some of the experiments in the *pasiflora* project; Christophe Jung for his excellent work in developing the automated analysis of the dye assay and performing analysis of FRAP data; Claudia Ludwig and Susi Lange for sitting with me in the flyroom for hours counting flies during the screens - Claudia also for helping with generation of transgenic lines; Ulrich Unnerstall for his major contribution and patient help with the statistical analysis of the pan-glial screen.

I am particularly grateful to Sara Batelli for answering all my questions on molecular biology, for having productive discussions with me, and mostly for being a friend who stood all my bad moments. I am also indebted to Tina Schwabe for developing many of the tools I used, for allowing me to use her schematics and for making useful comments on my manuscript, as well as Xiaoling Li for our skype chats on the blood-brain barrier and her guidance at the beginning of my project. I would also like to thank all the members of the lab for creating a pleasant and interactive working atmosphere.

Special thanks to everybody who provided flies and reagents: E. Arama, V. Auld, W.Chia, L. Luo, the Vienna *Drosophila* Resource Center, the Bloomington *Drosophila* Stock Center, the TRiP at Harvard Medical School (NIH/NIGMS R01-GM084947), the *Drosophila* Genomics Resource Center and the Developmental Studies Hybridoma Bank.

My biggest thank you goes to my parents and sister for their understanding, trust and unquestioning support, and to Giorgos for moving to Germany, standing by me and simplifying my efforts in so many ways. Finally, I want to thank Matilda for recently bringing so much joy in my life.

Abbreviations

α2M	alpha2-Macroglobulin
ABC	ATP-Binding Cassette
AEL	After Egg Lay
AJ	Adherens Junction
BBB	Blood-Brain Barrier
Btl	Breathless
cAMP	cyclic Adenosine Mono-Phosphate
Caspr	Contactin-associated protein
cDNA	complementary DNA
CNS	Central Nervous System
Cold	Coiled
Cora	Coracle
Crb	Crumbs
Creb	Cyclic-AMP response element binding protein
Crim	Crimpled
CRISPR	Clustered Regularly Interspaced Short Palindromic Repeats
Crok	Crooked
Dlg	Discs large
EcR	Ecdysone Receptor
EGF	Epidermal Growth Factor
EMP	Epithelial Membrane Protein
FasIII	Fasciclin III
FERM	Four-point-one protein (4.1 protein), Ezrin, Radixin, Moesin
FLP	FLiPpase
FRAP	Fluorescence Recovery After Photobleaching
FRT	Flippase Recognition Target
GABA	Gamma-AminoButyric Acid
GAP	GTPase-Activating Protein
GEF	Guanine nucleotide Exchange Factor
GFP	Green Fluorescent Protein

Gli	Gliotactin
GO	Gene Ontology
GPCR	G-Protein Coupled Receptor
GPI	GlycosylPhosphatidylInositol
GTP	Guanosine TriPhosphate
IGF	Insulin Growth Factor
Ilp	Insulin-like peptide
Kune	Kune-kune
Lac	Lachesin
LDL	Low Density Lipoprotein
Lgl	Lethal giant larvae
Loco	Locomotion defects
Ly-6	Lymphocyte antigen-6
Mcr	Macroglobulin complement-related
Mdr65	Multiple drug resistance 65
Mega	Megatrachea
mir	microRNA
MLCK	Myosin Light Chain Kinase
MP20	lens fiber Membrane intrinsic Protein
MS	Mass-Spectrometry
Nrg	Neuroglian
Nrv2	Nervana2
Nrx-IV	Neurexin-IV
Pasi1	Pasiflora 1
Pasi2	Pasiflora 2
PBS	Phosphate Buffered Saline
PDZ	Post synaptic density protein (PSD95), Discs-large1 (Dlg1), Zonula occludens-1 protein (ZO-1)
PKA	Protein Kinase A
PMP22	Peripheral Myelin Protein 22
PNS	Peripheral Nervous System
Prd	Paired

Repo	Reversed polarity
RISC	RNA-Induced Silencing Complex
RGS	Regulator of G-protein Signaling
RNAi	RNA interference
RT	Room Temperature
RTK	Receptor Tyrosine Kinase
S2	Schneider 2
SD	Standard Deviation
Sinu	Sinuous
siRNA	small interfering RNA
SJ	Septate Junction
SPG	SubPerineurial Glia
Sb	Stubble
TEP	ThioEster Protein
TJ	Tight Junction
TMEM47	TransMEMrane protein 47
Tre1	Trapped in endoderm 1
Tub	Tubulin
UAS	Upstream Activating Sequence
UTR	UnTranslated Region
Vari	Varicose
VDRC	Vienna Drosophila Resource Center
wt	wild-type

Abstract

Epithelial barriers are central to the development of metazoans by compartmentalizing the body in distinct chemical milieus essential for the function of many organs. One such barrier is the blood-brain barrier, which isolates the nervous system from the body fluid to maintain its ionic homeostasis and ensure nerve pulse transmission. In *Drosophila*, the blood-brain barrier is formed late in embryogenesis by a thin epithelium of subperineurial glia that ensheath the nervous system. Similar to other epithelia, subperineurial glia seal the paracellular space by forming large multiprotein complexes at the lateral membrane, the septate junctions (SJs), which impede free diffusion and mediate barrier function.

To identify novel genes required for blood-brain barrier formation, we followed a genome-wide *in vivo* RNAi approach. We initially screened almost the whole genome for genes required in glia for adult viability and impressively identified 3679 potential candidates. Subsequently, we tested these candidates for requirement in subperineurial glia for adult survival and identified 383 genes. At a last step, we directly asked if blood-brain barrier formation is compromised in the knock-down of the genes by performing the embryonic dye penetration assay in a selection of candidates and identified five genes that play a role during barrier development. Three of these genes, *macroglobulin complement-related* (*mcr*) and the previously uncharacterized *pasiflora1* and *pasiflora2* are further characterized in the context of this thesis.

Here we show that all three proteins are novel components of the *Drosophila* SJ. Pasiflora1 and Pasiflora2 belong to a previously uncharacterized family of tetra-spanning membrane proteins, while Mcr was reported to be a secreted protein in S2 cells required for phagocytosis and clearance of specific pathogens. Through detailed phenotypic analysis we demonstrate that the mutants show leaky blood-brain and tracheal barriers, overelongated tracheal tubes and mislocalization of SJ proteins, phenotypes that are characteristic of SJ mutants. Consistent with the observed phenotypes, the genes are co-expressed in SJ-forming embryonic epithelia and glia and are required cell-autonomously to exert their function. In columnar epithelia, the proteins localize at the apicolateral membrane compartment, where

they colocalize with other SJ proteins, and similar to known SJ components, their restricted localization depends on other complex members. Using fluorescence recovery after photobleaching experiments, we demonstrate for Pasiflora proteins that they are core SJ components, as they are required for complex formation and themselves show restricted mobility within the membrane of wild-type epithelial cells, but fast diffusion in cells with disrupted SJs. Taken together, our results show that Pasiflora1 and Pasiflora2 are novel integral SJ components and implicate a new family of tetraspan proteins in the development of cell junctions. In addition, we find a new unexpected role for Mcr as a transmembrane SJ protein, which raises questions about a potential intriguing link between epithelial barrier function, phagocytosis and innate immunity and has potential implications for the function of occluding junctions.

Aim of the thesis

In my thesis project, I aimed at the identification and characterization of novel genes required for blood-brain barrier formation. For this purpose, I decided to carry out an unbiased genome-wide approach by exploiting the power of *in vivo* screening in *Drosophila*. My goals were: first, to perform a whole-genome RNAi screen for genes required in all glia for adult viability; second, to perform a blood-brain barrier-specific screen; and third, to select candidates and explore their role in barrier formation at the genetic, cellular and functional level.

Part 1

Genome-wide glial RNAi screens

1. 1 Introduction

1.1.1 Glia are central players of nervous system function

The nervous system is composed of two cell types, neurons and glia. Neurons, being the cells firing action potentials and transmitting the information have received most of the attention, while glia, originally thought to simply provide a static framework for neurons are much less studied. However, in recent years the idea of such a passive role for glia has been abandoned and an increasing repertoire of functions is being attributed to glia themselves, which are now appreciated as critical modulators in brain development and function. Importantly, the relative fraction of glial cells increases with the increasing complexity of nervous systems in evolution from around 5% in the worm to 90% in human, suggesting an important role for glia in higher brain functions (Pfrieger and Barres, 1995) (Fig. 1A). Glial dysfunctions also contribute to many neurological disorders, such as multiple sclerosis, fragile X syndrome, brain injury, and Alzheimer's disease and gliomas represent the majority of malignant brain tumors (Miller, 2005; Jacobs and Doering, 2010).

In *Drosophila*, glia constitute 10-25% of the nervous system cells (Fig. 1A) (Pfrieger and Barres, 1995; Kremer et al., in preparation). With the exception of midline glia, they are derived from a small set of uniquely identifiable glioblasts and neuro-glioblasts that delaminate from the neuroectoderm of the early embryo (Bossing et al., 1996; Schmidt et al., 1997). One of the earliest steps in the specification of *Drosophila* glia is the expression of the transcription factor Glial cells missing (Gcm), which in turn regulates the expression of numerous glial genes. One of its major targets is the transcription factor Reversed polarity (Repo), which is considered a definite marker of glial cell fate (Halter et al., 1995; Hosoya et al., 1995; Jones et al., 1995; Freeman et al., 2003). Once specified, most glia migrate significant distances within the developing nervous system until they reach their final sites.

Drosophila glia contribute to virtually all functions of the nervous system and are therefore essential for survival. They play diverse roles during development and many of these roles are recapitulated during adult life and are required for brain homeostasis and function. In particular, glia guide neurite growth and defasciculation by presenting growth cones with attractive and repulsive cues, and actively control the establishment of neuronal connectivity (Hidalgo et al., 1995; Hidalgo and Booth,

2000; Lemke, 2001). Furthermore, they establish and maintain ionic homeostasis and nerve pulse propagation by forming the blood-brain barrier (BBB), which ensheaths the entire nervous system, and by insulating axon bundles, individual axons and dendrites (Baumgartner et al., 1996; Schwabe et al., 2005; Awasaki et al., 2008; Stork et al., 2008). Glia also provide neurons with high energy metabolic substrates to sustain their activity and promote their survival (Buchanan and Benzer, 1993; Booth et al., 2000). Furthermore, glia protect the brain by phagocytosing unwanted and aberrant material. They engulf and degrade excessive dying neurons to adjust their cell number, as well as pruned axons and immature synaptic material to eliminate exuberant connections and refine neural circuits (Sonnenfeld and Jacobs, 1995; Awasaki and Ito, 2004; Watts et al., 2004; MacDonald et al., 2006; Kurant et al., 2008; Fuentes-Medel et al., 2009; Tasdemir-Yilmaz and Freeman, 2014). Moreover, glia modulate synaptic activity and regulate behavior by taking up neurotransmitters such as L-glutamate from the extracellular space (Rival et al., 2004; Grosjean et al., 2008). Glia have also been implicated in the circadian control of locomotor activity through the modulation of dopaminergic transmission (Suh and Jackson, 2007). In many of these cases, a variety of reciprocal signaling interactions between glia and neurons are necessary for proper development and function of the nervous system.

To perform such a wide spectrum of roles, glia are present in all brain regions and exhibit remarkable variety in morphologies. On the basis of their topology and neurons they associate with, *Drosophila* adult glia fall into different subtypes with significant morphological and functional similarities to their mammalian counterparts (Fig. 1C). Surface glia, which are further subdivided in perineurial and subperineurial glia (SPG), encapsulate the brain as a whole to form the BBB. These two subtypes also insulate the nerves of the peripheral nervous system (PNS) (also called peripheral glia), much like mammalian Schwann cells. Cortex or cell body glia are structurally similar to astrocytes and wrap neuronal somata and neuroblasts at the outer layer (cortex) of the central nervous system (CNS). Cortex glia make significant physical contact with the BBB and oxygen-providing trachea, suggesting that they might act as cellular conduits to supply gases and nutrients to target neurons. Neuropile glia similar to oligondendrocytes, extend sheath-like membrane structures around axons and axon tracts (ensheathing), as well as synapses (astrocyte-like glia) (Freeman and Doherty, 2006; Kremer et al., in preparation). Most of these

subtypes already exist in the embryo and perform similar functions (Fig. 1B). Finally, all glial subpopulations seem competent to perform engulfment of neuronal corpses. The situation is similar in mammals, where except for microglia, the major phagocytic glial subtype, Schwann cells perform motor axon pruning and astrocytes are prominent candidates to work along with microglia given that they express many phagocytic receptors (Fig. 1C) (Bishop et al., 2004; Farina et al., 2007; Napoli and Neumann, 2009).

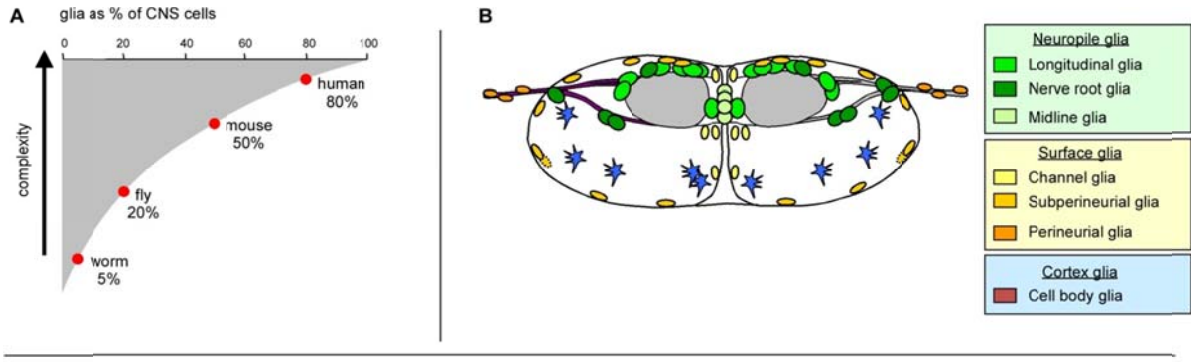

C

Functions	Distribution	Vertebrate glial subtype	*Drosophila* glial subtype
Trophic support of neurons	CNS cortex and surface	Astrocytes	Cortex and surface glia
Neuronal ensheathment, Trophic support of neurons	Ensheathing axons in CNS	Oligondendrocytes	Neuropile glia
Macrophage function	Throughout CNS and PNS	Microglia, astrocytes, Schwann cells	Cortex and neuropile glia
Ensheathment and support of peripheral nerves	Ensheathing nerves in PNS	Schwann cells	Peripheral glia

Figure 1. Glia are key players of nervous system function. (A) The fraction of glia within the CNS increases with the increasing complexity of the nervous system. (B) Schematic of *Drosophila* late embryonic ventral nerve cord (cross-section) depicting the different glial subtypes (prepared by Tina Schwabe and Ulrich Unnerstall based on data by Ito et al., 1995). (C) Comparison between mammalian and *Drosophila* glial subtypes based on their functions and distribution (modified from Freeman and Doherty, 2006).

1.1.2 Blood-brain barrier

The nervous system of higher animals is insulated from the body fluid by a BBB. The BBB impedes the passive influx of molecules into the brain and is required to maintain ionic homeostasis and ensure nerve pulse transmission. Its presence in insects, Crustacea, and Cephalopod mollusks, and its absence in lower

invertebrates suggests that barrier function is needed to perform complex integrative and analytical activities in the nervous system (Abbott et al., 1986). The BBB is also of outstanding clinical relevance, not only because its dysfunction is associated with severe pathology (e.g. multiple sclerosis, epilepsy, stroke, inflammation), but also because it presents a major obstacle for treating neurological diseases, by preventing the entry of possible therapeutic molecules into the brain (Zlokovic, 2008; Abbott, 2013).

1.1.3 Cellular architecture of the *Drosophila* blood-brain barrier

In *Drosophila* the BBB serves as a shield against the extraneous concentrations of ions and molecules of the hemolymph, such as high potassium levels and is essential for fly development; if it is compromised, action potentials cannot be propagated leading to paralysis and death at the end of embryonic development. The BBB is a squamous secondary epithelium formed late in embryogenesis (20h after egg lay, AEL) by a thin layer of SPG, which surround the CNS as a whole. Insulation is achieved by septate junctions (SJs) that seal the paracellular space (Schwabe et al., 2005; Schwabe et al., submitted). Like in other epithelia, SPG SJs consist of large multi-protein complexes composed of several, mainly transmembrane components, e.g. claudins and the cell adhesion molecules Neuroglian, Neurexin-IV and Contactin (Izumi and Furuse, 2014). To provide a tight barrier, SPG form deep interdigitations with their neighbors. This increases the length of intercellular membrane juxtaposition, and thus of the SJ belt, which ultimately determines the tightness of the seal. The barrier epithelium is attached via Dystroglycan and integrin receptors to a basement membrane, often called the basal lamina, which covers the outer surface of the nervous system and is secreted by CNS associated hemocytes (Olofsson and Page, 2005; Xie and Auld, 2011) (Fig. 2). SPG do not form a contiguous adherens junction belt, but spot adherens junctions, and do not express apical membrane determinants like Crumbs (Crb) and Bazooka (Fig. 2). However, SPG are clearly polarized and have distinct apical and basal membranes. Their polarity is evidenced by the restricted localization of membrane proteins, like Dystroglycan, which localizes at the basal, hemolymph-facing side of the epithelium, and the receptor Moody, which localizes at the apical, brain-facing membrane (Li et al., in preparation; Schwabe et al., submitted).

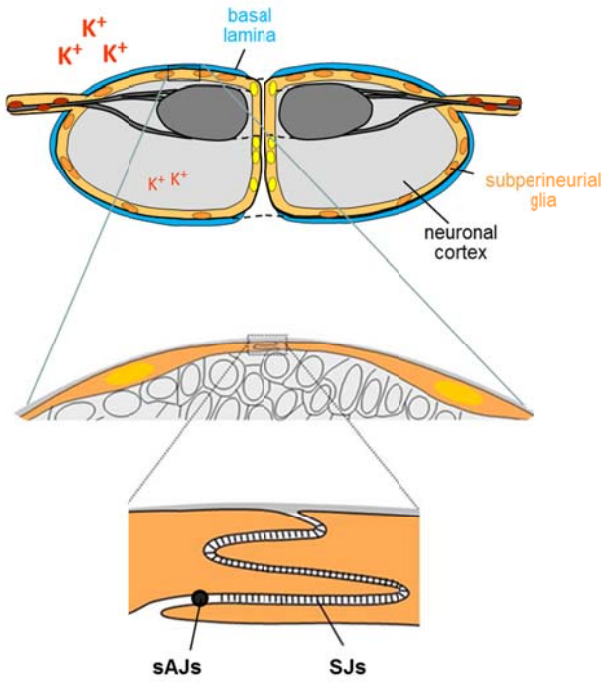

Figure 2. Structure of the *Drosophila* BBB. Schematic of 20 AEL embryonic nerve cord (cross-section). SPG (in orange) form a thin epithelium that surrounds the CNS. To provide impermeability, SPG form deep interdigitations with their neighbors and build SJs along the lateral membrane. Peripheral (in red) and channel glia (in yellow) are equivalent to SPG and insulate the peripheral nerves and CNS channels, respectively. sAJs: spot adherens junctions. Schematic prepared by Tina Schwabe and Ulrich Unnerstall.

Furthermore, the existence of localized transporters, such as the ABC transporter Mdr65 at the basal side, suggests that SPG perform directional transport to permit the uptake of nutrients and release of waste products from and to the hemolymph (Mayer et al., 2009).

During larval development, SPG need to adjust for the substantial growth of the CNS, while continuously providing insulation. Thus, instead of mitotic division, SPG undergo endoreplication and increase massively in size (Unhavaithaya and Orr-Weaver, 2012). In third-instar larval and adult CNS, between the basal lamina and the SPG epithelium there is an additional layer of non-SJ-forming perineurial glia. Perineurial glia are present in the embryo and first-instar larvae as individual cells associated with the SPG and subsequently undergo proliferation and form a sheath. The function of the perineurial layer is not known, but it likely provides

mechanical support to the SPG epithelium and contributes to barrier selectivity (Awasaki et al., 2008; Stork et al., 2008). A functionally and structurally equivalent SJ-forming glial epithelium ensheaths the nerves in the PNS (blood-nerve barrier) and the adult eye (blood-retinal barrier) (Auld et al., 1995; Baumgartner et al., 1996; Banerjee et al., 2006; Banerjee et al., 2008).

1.1.4 Moody signaling regulates blood-brain barrier development and maintenance

SPG are generated in the ventrolateral neuroectoderm and between 9 and 11 h AEL they extend filopodia-like processes and migrate to the CNS surface. When they reach their final sites, they become stationary and grow extensively. The growth of SPG is highly synchronous and isometric, such that all cells are of similar shape and size at any given time. By 13 h, SPG cover most of the CNS and begin contacting their neighbors. Epithelial closure is finished between 14.5 and 15.5 h. Subsequently, SJs start accumulating and insulation of the paracellular space is achieved from 18.5 h onwards, indicating that a functional BBB has been established (Fig 3B) (Schwabe et al., submitted).

BBB development is largely controlled by the Moody G-signaling pathway. The pathway consists of the orphan G-protein coupled receptor (GPCR) Moody, two heterotrimeric G-proteins (Gαi-βγ and Gαo-βγ), the RGS protein Loco, and cAMP-dependent protein kinase A (PKA) as one of the downstream effectors (Fig. 3A). All pathway components are expressed in SPG and in their loss of function, SPG SJs are disorganized leading to a leaky BBB. Live *in vivo* analysis over the entire time-course of BBB formation showed that in Moody pathway mutants, SPG growth is retarded and asynchronous resulting in a delay in cell contact formation and maldistribution of SJ material, which ultimately causes the impaired sealing of the barrier (Fig. 3B). PKA acts antagonistically downstream of Gβγ and effects proper SJ organization by regulating multiple aspects of cell behavior. It mainly controls membrane overlap between neighboring SPG, by negatively regulating MLCK and Rho1, and the coordinated actomyosin contractility in SPG. In addition, PKA affects the actin and microtubule cytoskeleton, as well as vesicle transport. Except for embryonic SPG, Moody is also expressed in other ensheathing glia of the CNS and PNS. In addition, it is expressed throughout larval development and in the adult and

is continuously required for insulation (Bainton et al., 2005; Schwabe et al., 2005; Li et al., in preparation; Schwabe et al., submitted).

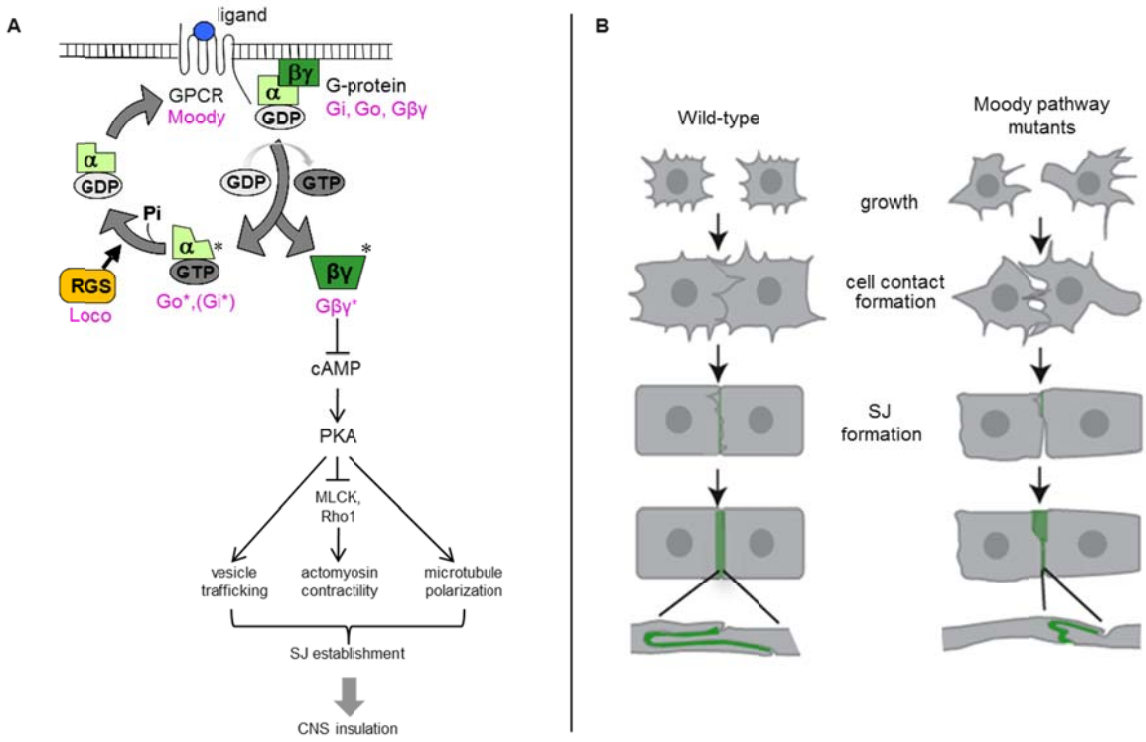

Figure 3. Moody signaling regulates BBB formation. (A) Upon ligand binding, Moody catalyzes the exchange of GDP for GTP at Gα, leading to dissociation of the complex. Once separated, Gβγ interacts with PKA, which can regulate various aspects of cell behavior. Signaling is terminated by GTP hydrolysis by Gα, which is stimulated by the RGS Loco. (B) Model of BBB development in wild-type and Moody pathway mutants. The pathway's primary role is the synchronization of SPG growth, which is a prerequisite for efficient contact formation and establishment of SJs (model from Schwabe et al., submitted).

1.1.5 The blood-brain barrier is more than a diffusion barrier

The BBB's strategic position at the interface between the nervous system and the rest of the body suggests that it might act as an orchestrating center transducing various signals to and from the CNS and connecting brain function with physiological states and responses of different organs. The BBB possesses highly active transport mechanisms to shuttle ions, amino acids, and energy-rich nutrients like sugars and

lipids inside the brain and remove waste products. Furthermore, SPG establish extensive gap junctions and once metabolites have entered the barrier epithelium, they can be distributed throughout the nervous system via these intercellular connections. Indeed, exciting recent findings revealed novel metabolic and signaling functions of the BBB and showed that it can sense and respond to systemic signals. In particular, the BBB is involved in the regulation of systemic insulin signaling, both independently and dependently of the nutritional status. For instance, SPG constantly release a secreted decoy of insulin receptor in the hemolymph, which mimics the receptor's extracellular domain, and interacts with several insulin-like peptides (Ilps) to inhibit signaling and restrict body size (Okamoto et al., 2013). In addition, SPG regulate systemic insulin signaling by conveying information about dietary lipids to the brain. When lipid content is high, lipid transfer particle is transported across the BBB by the LDL receptor-related proteins LRP1 and Megalin and induces Ilp release from specific neurons into the hemolymph (Brankatschk et al., 2014). Moreover, SPG regulate insulin signaling locally, within the nervous system. BBB glia respond to an unknown fat body-derived mitogen by secreting Ilps that locally activate IGF signaling in neuroblasts, releasing them from quiescence in a nutritionally-dependent manner. To express and secrete Ilps, SPG require the gap junction proteins Innexin1 and Innexin2 to translate metabolic signals into synchronized calcium oscillations (Chell and Brand, 2010; Speder and Brand, 2014). In contrast, Sousa-Nunes et al., suggested that neuroblast proliferation requires Ilp expression by cortex glia rather than SPG (Sousa-Nunes et al., 2011). In this case, the role of the BBB might be to coordinate a complex signaling network, relaying information from systemic signals to other glial subpopulations.

1.1.6 Insulating barriers of the mammalian nervous system

In mammals, the BBB is established by tight junctions (TJs) formed between endothelial cells that line brain capillaries. These are specialized TJs of extremely high electrical resistance that impede the paracellular flow of potentially damaging and fluctuating blood-borne solutes. Similar to *Drosophila* SJs, a major component of TJs are the claudins. To ensure chemical homeostasis, TJs work together with numerous transport systems in the vascular endothelium. Surrounding the endothelial cells, mesoderm-derived pericytes secrete a basal lamina and glial astrocytic endfeet completely surround the vessels (Fig. 4). Although the endothelial

TJs are the primary insulating agent, close interactions between all cell types are necessary for BBB function (Abbott et al., 2006; Daneman and Prat, 2015). Interestingly, in more primitive vertebrates such as elasmobranch fish, the BBB is formed by glia, the perivascular astrocytes, and the ancestral vertebrate is believed that had a glial BBB (Bundgaard and Abbott, 2008). Importantly, mammals also form SJs at the nodes of Ranvier of peripheral nerves between axons and myelinating Schwann cells, which are functionally, structurally and molecularly homologous with the *Drosophila* SJs (Poliak and Peles, 2003).

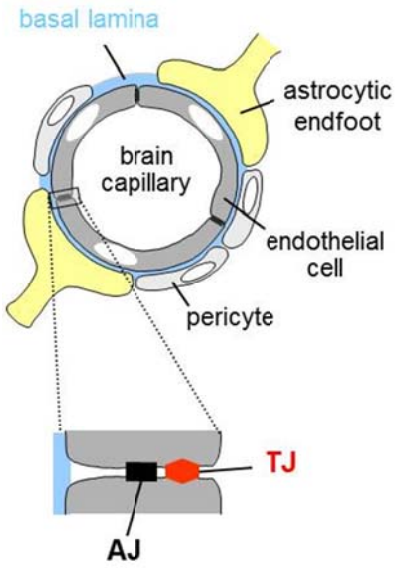

Figure 4. Structure of the mammalian BBB. Schematic of the mammalian BBB illustrating the different cell types contributing to barrier function. Although morphologically distinct from the *Drosophila* BBB, the principal insulating agent are claudin-based TJ strands.

1.1.7 *Drosophila* as a genetic model to identify and characterize novel genes

Since the beginning of the twentieth century, when T.H. Morgan decided to experiment with the fruitfly, studies in *Drosophila* have led the way in identifying novel gene functions and elucidating a plethora of biological processes. Importantly, many developmental and cellular functions are conserved between human and flies, with 75% of disease-associated genes having related sequences in *Drosophila* and over 30% functional homologues (Bier, 2005). *Drosophila* is one of the most versatile multicellular organisms for genetic analysis. This is not only due to the obvious benefits of low cost and short generation time and certain advantageous genetic

features, but also because the early start of experimentation was built on by succeeding generations of researchers who have developed an ever-increasing repertoire of high-quality techniques and resources. These include excellent genome annotation, genome-wide *in vivo* gene disruption (by transposable elements and transgenic RNAi), large-scale protein trap library in which endogenously expressed proteins are tagged with GFP, and many molecular tools for genetic manipulation (e.g. site-directed transgenesis, homologous recombination) and spatio-temporal control of gene expression (e.g. Gal4-UAS, FLP-FRT systems) (Morin et al., 2001; St Johnston, 2013).

One of the most important tools *Drosophila* provides is the ability to carry out large scale *in vivo* genetic screens (St Johnston, 2002). The simple genome structure, the limited gene redundancy, and the fact that regulatory regions are located near the genes they control have been proven great advantages for the identification of novel gene functions through classical forward genetic approaches (Nüsslein-Volhard and Wieschaus, 1980). In such screens, random mutations are induced (e.g. by radiation, chemicals or insertional mutagenesis), mutant individuals are recovered and the affected gene is mapped. Subsequently, the pioneering RNAi technique and the production of transgenic *UAS-RNAi* libraries have facilitated the implementation of large-scale reverse genetic screens, in which the identity of the perturbed genes is known, and have enabled the systematic analysis of gene function *in vivo* (Dietzl et al., 2007; Ni et al., 2011). When induced with a Gal4 driver, the *UAS-RNAi* transgene leads to the generation of double-stranded short interfering RNAs (siRNAs), which mediate the degradation of complementary mRNAs. Therefore, it results in the knock-down of the corresponding gene in a spatio-temporal expression pattern that depends on the Gal4 enhancer (Fig. 5). Importantly, RNAi works exceptionally well in *Drosophila* both *in vivo* and in cultured cells. After screening, a wealth of computational and experimental data are available in *Drosophila* to draw from for post-analysis. Once potential candidates are identified, advanced genetic and molecular tools together with a large repertoire of markers and superb imaging techniques allow for the straightforward characterization of gene functions and for a depth of experimental scrutiny unmatched in higher organisms.

Drosophila has also emerged as a very promising model organism to study glial biology. *Drosophila* glia exhibit remarkable morphological similarities to vertebrate glia and fulfill roles that are highly analogous and in many cases

molecularly conserved. The *Drosophila* nervous system is sophisticated, yet much simpler compared to the mammalian and neuronal and glial lineages are well defined. In addition, an abundance of tools exist in the fly to precisely manipulate single cells or whole populations of glia *in vivo*, and to image glia live in the intact brain. This is very critical because from the moment glia are born they are intimately

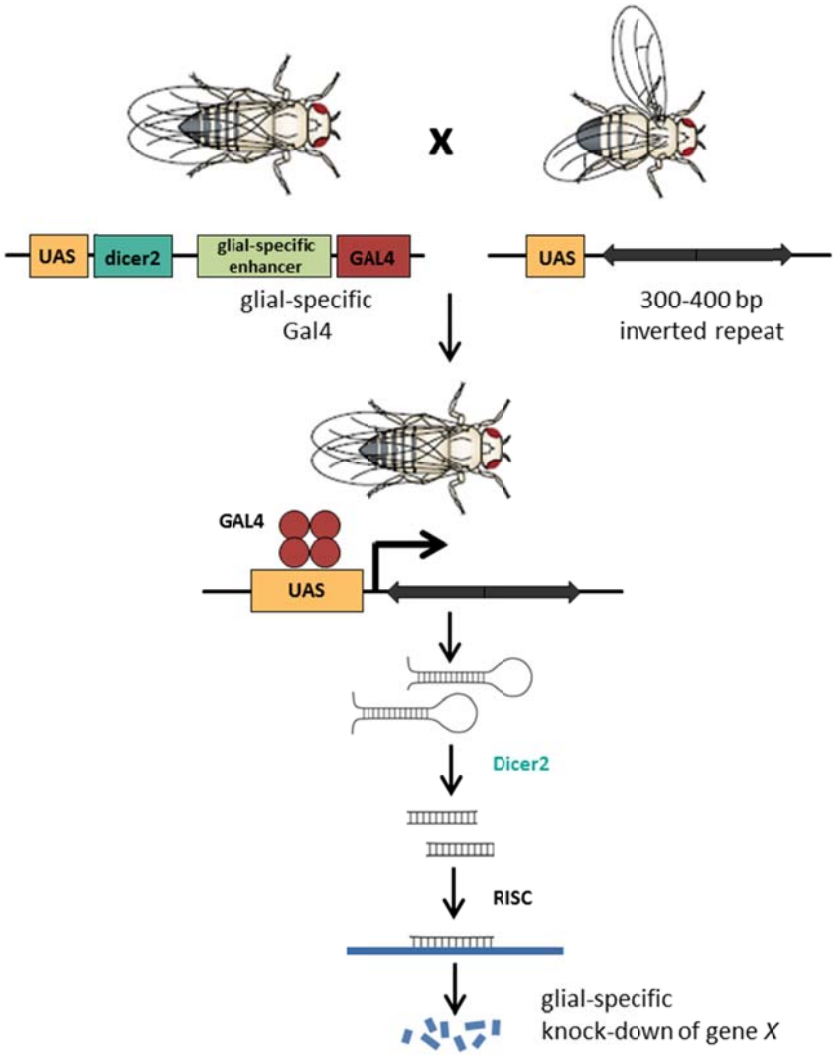

Figure 5. Glial-specific *in vivo* RNAi in flies. A female expressing glial-specific Gal4 is crossed with a male carrying an inverted repeat under the control of *UAS*. In the progeny carrying both transgenes, Gal4 is expressed in glia, binds to *UAS* and activates the transcription of the inverted repeat, leading to generation of hairpin RNAs. Hairpin RNAs are cleaved by the ribonuclease Dicer2 to generate siRNAs. siRNAs are loaded into the RISC complex and mediate the cleavage of complementary mRNAs, leading to glial-specific knock-down of the gene which the inverted repeat was designed for. In *Drosophila*, to efficiently phenocopy the impaired gene, overexpression of Dicer2 is needed.

associated with neurons, and these two cell types are highly interdependent for normal development and function. Importantly, *Drosophila* also allows the investigation of developmental features of glia, which in mammals can provechallenging due to the difficulty of accessing animals *in utero*, where critical glial developmental milestones occur.

1.1.8 Rationale

Although our insights on glial biology have profoundly advanced in the past years, it seems that we are still only scratching the surface of the many glial functions. Moreover, although we have gained much information on the *Drosophila* glial BBB and the role of Moody signaling in its formation, given its physiological importance, many questions remain open (Fig. 6). Several features of Moody signaling make it a rather complex pathway and suggest that is currently incomplete. Both the active G-proteins and PKA are able to transduce the signal to multiple effectors, integrating Moody signaling with a wide range of biological responses, such as cytoskeletal organization, cell–cell and cell–matrix adhesion, vesicular trafficking, cell polarity and possibly gene expression. In addition, the finding that loss of function of downstream effectors results in more severe defects than loss of Moody strongly suggests that G-proteins receive additional activating input. The GPCR Tre1, which is the closest paralog of Moody and is expressed in a subset of SPG is a strong candidate, however thus far, there is insufficient evidence to exclude or confirm this possibility (Schwabe et al., 2005). Moreover, the pathway's role in barrier maintenance in the adult has not been investigated in any detail. Furthermore, although strong insulation defects are observed in Moody signaling mutants, SPG do spread over the CNS to form an epithelium and some pathway mutants survive until later stages. Thus, when looked from a developmental perspective, it seems that additional independent pathways are involved in BBB establishment. In addition, the precise mechanism by which the barrier-forming SJs are established in the SPG epithelium and how their highly regular alignment is achieved remain poorly understood. Finally, the BBB except for a selective diffusion barrier appears to be a dynamic and communicative layer between the brain and the body. The BBB might act as a key integrator of various systemic stimuli to the brain and as a signaling center orchestrating major developmental and physiological events. Such fascinating novel roles of the BBB in animal physiology and behavior are expected to be unraveled in the coming years.

My goal was to identify novel genes required for BBB formation. Because the lab had exhausted the identification of BBB genes through a candidate gene approach; i.e. by screening known G-protein effectors for insulation defects, I decided to carry out a neutral genome-wide RNAi screen and subsequently select candidates to further explore their role in barrier formation at the genetic, cellular and functional level.

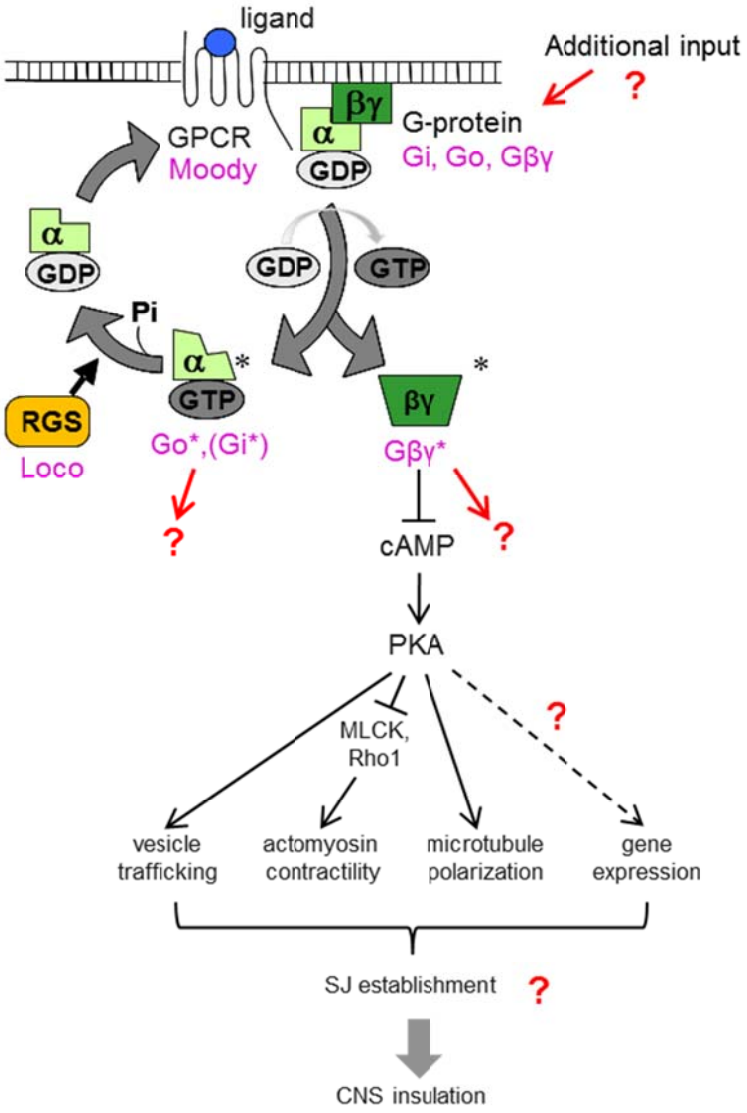

Figure 6. Open questions on BBB formation. Moody signaling is currently incomplete and components acting both upstream and downstream of G-proteins remain to be identified. In addition, how the barrier-forming SJs are established is still unknown.

1.2 Genome-wide RNAi screens identify glial and SPG genes

1.2.1 Overview of genome-wide RNAi screening

To identify novel glial genes required for BBB development, we followed a neutral genome-wide *in vivo* RNAi approach. We used glial-specific Gal4 drivers and the VDRC KK transgenic RNAi library (Dietzl et al., 2007), which at the moment comprised 10450 *UAS-RNAi* strains (75% genome coverage) each targeting a single gene. For the generation of *UAS-RNAi* lines, hairpins with no predicted off-targets were inserted into the genome via site-directed transgenesis thus minimizing position effects. To efficiently phenocopy the impaired gene, Dicer2, which processes double stranded RNA into siRNA , was co-expressed in all our screening steps. In order to screen genome-wide, we initially tested the lines for impaired adult viability using the strong pan-glial driver *repo-Gal* taking advantage of the fact that several glial functions, including BBB function are essential for fly survival. The lines that showed an effect in the *repo-Gal4* screen were subsequently re-tested for impaired adult viability with the SPG-specific but weaker *moody-Gal4* to identify candidates involved

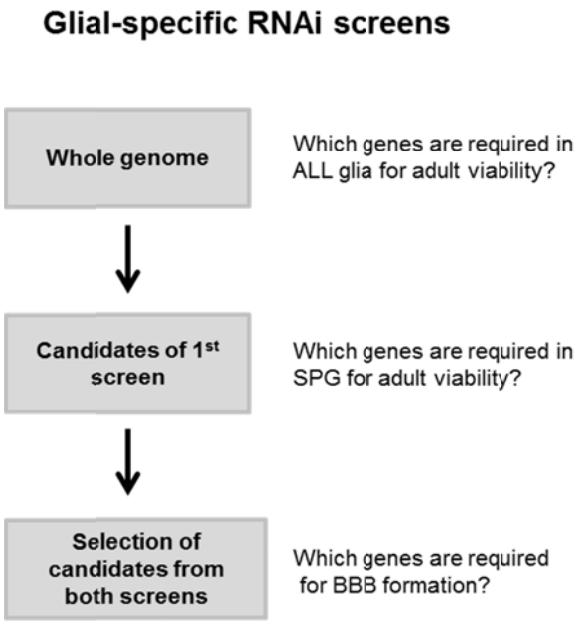

Figure 7. Overview of genome-wide screen to identify novel BBB genes. In order to screen at a genome-wide level, we initially screened for genes required in all glia for adult viability. As the number of candidates is being narrowed down, our question becomes more and more BBB-specific.

in BBB formation and/or maintenance. In both screens, the RNAi lines targeting housekeeping genes involved in basic cellular functions serve as internal positive controls as they are potentially cell-lethal. Finally, to directly ask if the genes are required for BBB formation, we performed the embryonic dye penetration assay in a selection of candidates using *repo-Gal4* (Fig. 7).

RNAi screens have the major advantage of being reverse genetic screens, meaning that the gene whose function is disrupted is known and one looks for the manifestation or not of the phenotype of interest. However, such screens also bear two limitations. First, RNAi results in variable and partial loss-of-function of the affected gene and might lead to false negatives. This is of particular concern for proteins that are expressed in particularly high levels, such as structural components of the cytoskeleton. Second, RNAi is prone to off-target effects due to targeting of additional mRNAs with homology to the introduced siRNA and thus false positives.

1.2.2 Primary pan-glial screen

In our primary screen, we checked 10450 *UAS-RNAi* lines for impaired adult viability using *repo-Gal4*, which drives strong expression in all glia except for midline glia from embryonic stage 13 throughout the development and lifespan of the fly. We crossed transheterozygote *repo*-Gal4/TM3 virgin females with *UAS-RNAi* males, removed the parents after sufficient egg lay to avoid overcrowded vials and scored the approximately 150 progeny of the first generation by counting the number of *UAS-RNAi;repo-Gal4* versus *UAS-RNAi;TM3* flies. The TM3 balancer carries the dominant marker Stubble (Sb) which causes shorter bristles compared to wild-type (wt) allowing the easy discrimination of the two genotypes. Assuming that the genotypes are equally viable, based on Mendelian rules they should appear in a 1:1 ratio; lower percentages in the flies with the knock-down would imply a role for the gene in glia. In order to identify glial genes required in all developmental stages, as well as in the adult, we counted the progeny 8-10 days after eclosion. Because after a few rounds of screening we realized that the screen was yielding many positive results, we continued by simply defining in which of the categories lethal, subviable, and viable each knock-down falls and only counted the exact number of progeny for each genotype for the class of subviable. In order to define the average percentages with which the two genotypes appear in the case that the glial knock-down is not affecting viability, we counted the exact number of progeny for each of the genotypes

in the crosses of 400 random RNAi lines and plotted the results as percentage of flies with glial knock-down (non-Sb). Theoretically, we expect a normal (binomial) distribution with mean 50%. We observe that our results indeed follow a normal distribution with mean 52% non-Sb progeny and standard deviation (SD) 5.2, in addition to the curve 'tail' that represents subviable and lethal knock-downs. By fitting the data, we observe that for percentages lower than 40% non-Sb flies, we retrieve more candidates compared to those expected from the normal distribution, suggesting that some represent truly subviable knock-downs (Fig. 8A). We observe a similar phenomenon for percentages lower than 40% when fitting the distribution curve to all the results counted in the screen, although in this case the fit is not as

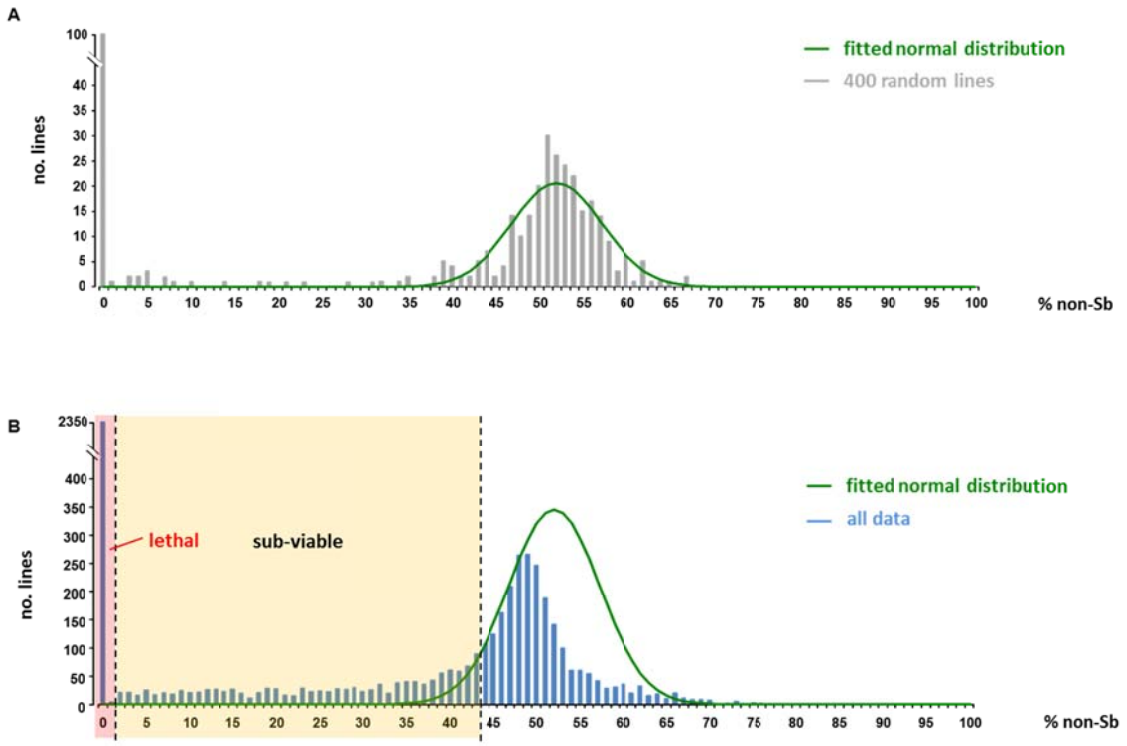

Figure 8. Distribution of *repo-Gal4* screen data. Plots of *repo-Gal4* screen results with the *x* axis showing the percentage of progeny with glial-specific knock-down (non-Sb) and the *y* axis the number of RNAi lines. (A) Grey bars depict the 400 random RNAi lines for which the exact numbers of Sb and non-Sb progeny were counted. In green, the fitted normal distribution. The lines that showed no effect follow a normal distribution with mean 52% and SD 5.2. (B) Blue bars depict all the RNAi lines for which the exact number of progeny was determined. The knock-downs that were considered lethal and subviable are highlighted.

good because we were biased towards counting the results that showed an effect. Based on the fitting procedure, we considered as complete lethal and subviable knock-downs that resulted in 0-0.49% and 0.5-40% progeny with glial-specific knock-down, respectively (Fig. 8B).

The screen was very successful and identified 3679 candidates (35.2% of library, 28% of genome) as potential glial genes. From these, knock-down of 2438 genes (23.3% of library) caused complete adult lethality, and of 1241 genes (11.9% of library) adult subviability (Fig. 9A). Based on classification by gene ontology terms (GO, Flybase), among the 3679 candidates, 1696 (46.1%) are known genes with a name and biological function assigned, 1030 (28%) are uncharacterized but have some prediction for their structure and/or function, and 953 (25.9%) are uncharacterized genes with no predictions. From the genes with a known or predicted function, 981 (36%) are likely ubiquitously expressed housekeeping genes (Fig. 9B). In this category we included all genes whose products are required for the maintenance of basic cellular functions, such as DNA replication, general transcription, RNA splicing, translation, chromatin assembly and proteasome-mediated protein degradation. After excluding housekeeping genes, the *repo-Gal4*

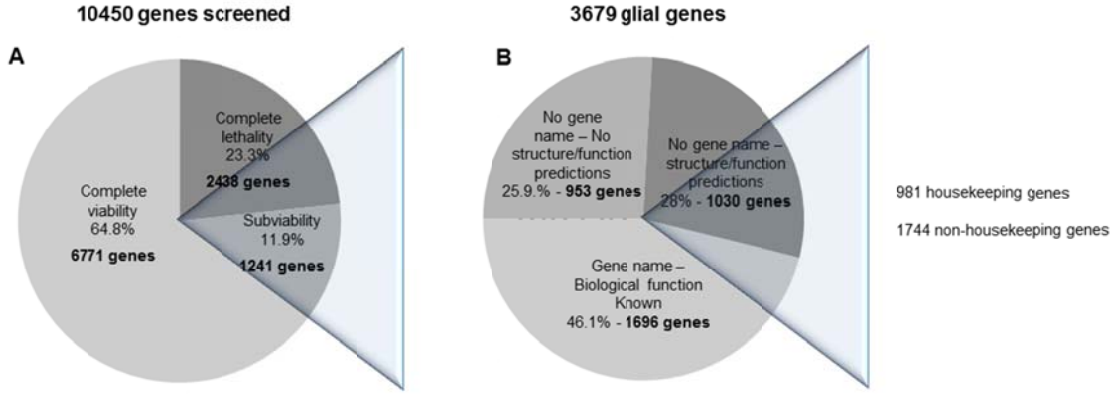

Figure 9. Results of *repo-Gal4* screen. (A) Chart depicting the number of genes whose pan-glial knock-down resulted in adult lethality, subviability or had no effect. (B) Chart depicting the candidates which resulted in lethality or subviability classified based on the current knowledge on their structure and/or biological function (GO terms, Flybase). Among the identified genes with a known or predicted function, two-thirds are potentially interesting, non-housekeeping genes.

screen revealed a great number of candidates (2697) that potentially play a specific role in glial development and/or function, and offers valuable material for studying multiple aspects of glial biology.

Importantly, among our results we identify both known glial genes, which serve as internal positive controls, as well as many interesting novel candidates. These include components of numerous signaling pathways (e.g. GPCR, RTK, Ecdysone, Hippo, JAK/ STAT, Decapentaplegic), as well as a great number of transcription factors. We additionally find several proteins with roles in cell shape regulation and epithelial morphogenesis (e.g. actin- and microtubule-binding proteins, motors, RhoGEFs and RhoGAPs, components of the adherens, septate and gap junctions) that might be of particular interest for studying BBB development. We also identify many potential candidates with respect to Moody signalling; i.e. Tre1 and 30 more GPCRs (without including gustatory receptors) that might be acting together with Moody upstream of the G-proteins, as well as G- and RGS proteins, three adenylate cyclases potentially involved in the generation of cAMP, kinases that may act downstream of G-proteins, and several proteins that might function in response to PKA, like components of vesicular trafficking, cytoskeletal regulators and the transcription factors CrebA and CrebB-17A. We also find proteins involved in circadian rhythm (e.g. Timeless, Clock, PDFR, Reg-5, Takeout), phagocytosis (e.g. Simu, Eater, PGRPs, ABC transporters, Ced-6) and ionic and neurotransmitter homeostasis (e.g. GABA, acetylcholine and glutamate receptors, glutamate dehydrogenase, K^+ channels, and aquaporins) and many more fascinating molecules. Surprisingly, among our candidates we find genes that are not expected to cause lethality, since their genomic mutants survive to adulthood (e.g. 11 gustatory receptors, phagocytosis receptors). One possible explanation for this result is that competition for resources exists between the two genetically distinct progeny of the first generation, leading to increased death of the flies that express the siRNA and disrupt a given process. Another explanation might be that the siRNA targets more than one mRNAs, e.g. multiple members of the family of gustatory receptors.

The retrieval of known glial genes suggests an efficient screening procedure. To further check the performance of the screen, we implemented different kinds of analysis in our results. First, we checked how well we retrieve housekeeping genes; knock-down of these genes is expected to kill glial cells and lead to death of the animal. We observe that housekeeping genes are enriched and we overall retrieve

category	# genes tested	fraction recovered
nucleosome	44	0.93
chromatin assembly or disassembly	49	0.86
general RNA polymerase II transcription factor activity	42	0.74
transcription initiation from RNA polymerase II promoter	47	0.79
transcription from RNA polymerase II promoter	156	0.56
transcription from RNA polymerase I promoter	4	1.00
mediator complex	23	0.78
spliceosome	165	0.67
mRNA polyadenylation	15	0.87
mRNA cleavage	11	0.91
nuclear export	6	1.00
structural constituent of ribosome	140	0.90
ribosome biogenesis	13	0.92
translation	279	0.71
protein folding	75	0.49
response to DNA damage	74	0.61
DNA replication	47	0.57
mitotic spindle elongation	68	0.91
cytoskeleton organization	93	0.55
glycolysis	24	0.63
mitochondrial electron transport	45	0.71
all genes	**9682**	**0.36**

Figure 10. The *repo-Gal4 screen* successfully retrieves housekeeping genes. Genes are classified based on their known or predicted involvement in an essential housekeeping function (GO terms, Flybase) and the fraction recovered for each term is shown. Housekeeping genes are enriched when compared with the fraction recovered for all genes with a known or predicted function (0.36).

them with very high percentages that in some cases reach 90%, like for genes associated with nucleosome and ribosome biogenesis and mitosis. The smaller fraction recovered for genes that fall in other GO classes, such as cytoskeleton assembly and DNA repair might reflect biological redundancy between the gene products and/or result from incompleteness of the RNAi knock-down (Fig. 10). Second, we determined how well we retrieve components of signaling pathways known to be required in glia. The multi-component EGF pathway is required in longitudinal and peripheral glia for their survival and represents a good example. Neuronally-derived EGF activates the EGF receptor on the glial membrane leading

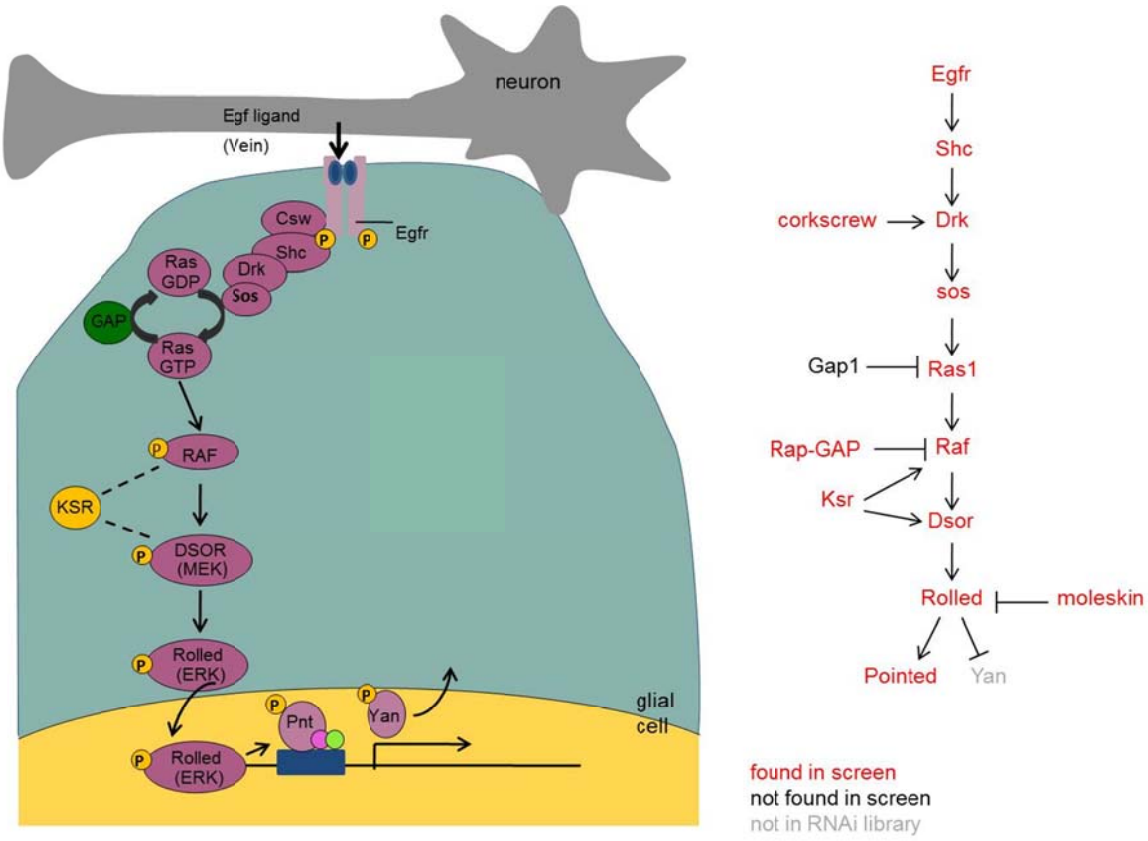

Figure 11. The *repo-Gal4 screen* successfully retrieves the complete EGF signaling pathway. The multi-component EGF pathway is activated in glia in response to neuronally-derived EGF leading to activation of target genes essential for glial survival.

to a cascade of intracellular protein phosphorylations ultimately resulting to the nuclear translocation of the transcription factor Pointed. In the nucleus, Pointed regulates a number of target genes essential for glial survival (Hidalgo et al., 2001; Shilo, 2014). Impressively, we identify 13 of the 15 core pathway components (Fig. 11). Similarly, we retrieve components of the Ecdysone pathway, which is required in glia during metamorphosis to prune axons, such as the Ecdysone receptor (EcR), the transcription factor Broad, and many primary and secondary ecdysone-responsive genes (Fig. 12) (Awasaki and Ito, 2004; Watts et al., 2004; Awasaki et al., 2006). Third, we compared our results with a microarray-based transcriptome profile of embryonic glia previously performed in the lab (U. Gaul, unpublished). The genes that were found as differentially expressed in glia were clustered in groups of

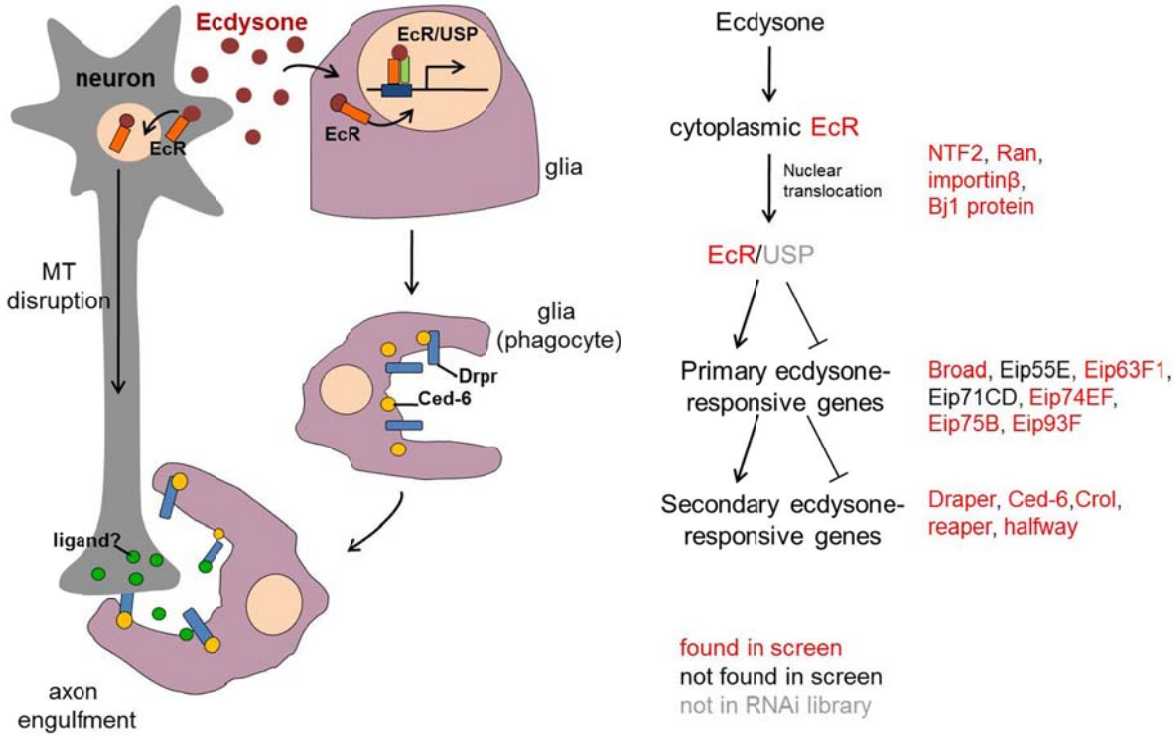

Figure 12. The *repo-Gal4* screen successfully retrieves Ecdysone signaling components and responsive genes. During metamorphosis, hemolymph-derived ecdysone is sensed by EcR expressed in both neurons and glia. In the neuron, activation of EcR leads to the transcription of target genes that mediate fragmentation of axon microtubules, while in glia of genes required for engulfment and degradation of the dying neuron. The screen successfully revealed EcR signaling components and target genes required in the glial cell. MT: microtubule.

expression levels measured as actual number of transcripts. We observe a linear correlation between gene expression levels and efficiency of retrieval in the functional RNAi screen, confirming the long-standing belief that gene expression correlates with functional requirement in a given cell. Furthermore, this finding also indicates that *repo-Gal4* is a very strong driver and that highly expressed genes are efficiently knocked-down in our screen (Fig. 13).

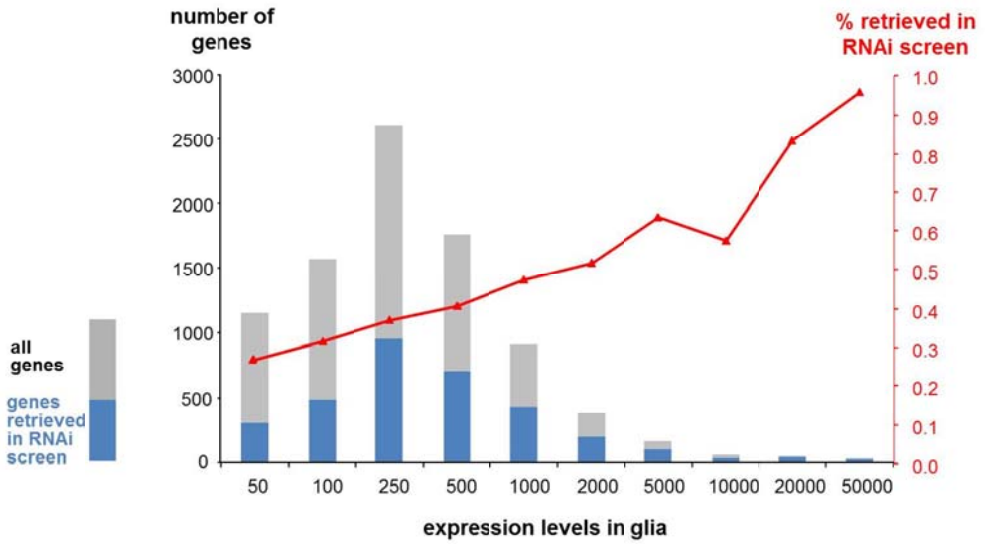

Figure 13. The higher the expression levels of a gene in glia, the higher the likelihood that it is retrieved in the *repo-Gal4* screen. Comparison of *repo-Gal4* screen results with microarray-based embryonic glia transcriptome profile. The genes identified as differentially expressed in glia in the microarray screen are grouped based on expression levels measured as number of transcripts and are depicted in the *x* axis. Grey bars show the number of genes for each expression cluster and are depicted in the left *y* axis. Blue bars show the number of genes that were retrieved in the *repo-Gal4* screen for each cluster. The percentage of genes retrieved in the *repo-Gal4* screen for each cluster is plotted with red triangles and is shown in the left *y* axis. Red graph is used to visualize that there is a linear correlation between expression levels and percentage of retrieval in the functional RNAi screen.

1.2.3 Secondary blood-brain barrier-specific screen

We then continued to identify genes that are specifically required in SPG for adult survival, using the *moody-Gal4* driver. *moody-Gal4* starts being weakly expressed at late embryonic stage 16 in a subset of SPG and other ensheathing glia, such as peripheral and channel glia, and strongly labels all SPG at third instar larval CNS. We crossed *moody-Gal4/TM3* females with all the lines that caused lethality or subviability in the *repo-Gal4* screen and followed the same procedure to check for impaired adult survival. We tested 3900 lines because we manually selected and included some interesting genes that resulted in slightly higher viability than the threshold of 40% that we established. In contrast to the *repo-Gal4* screen, in the *moody-Gal4* screen the exact number of progeny for each genotype was determined. We plotted the results as percentage of flies with knock-down (non-Sb)

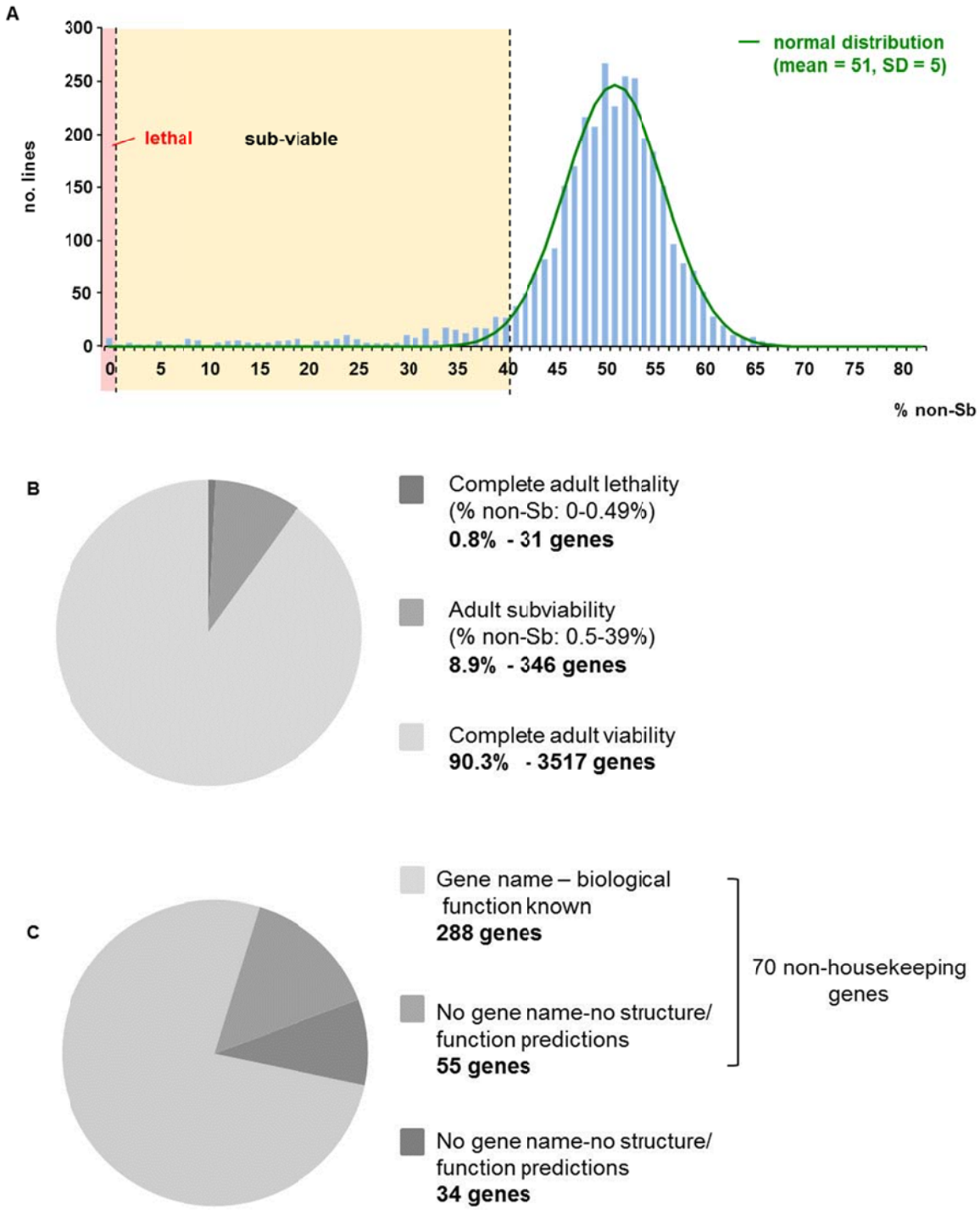

Figure 14. Results of *moody-Gal4* screen. (A) Distribution of the 3900 genes tested. The *x* axis depicts the percentage of progeny with SPG-specific knock-down (non-Sb). The *y* axis shows the number of genes. The lines that had no effect show a normal distribution with mean 51% and SD 5. Based on the distribution we defined the groups of subviable and complete lethal. (B) Chart depicting the number of genes identified whose SPG-specific knock-down resulted in adult lethality, subviability

or had no effect. (C) Chart depicting the candidates which resulted in lethality or subviability classified based on the current knowledge on their structure and/or biological function (GO terms, Flybase).

and observed a normal distribution with a mean of 51% progeny with glial-specific knock-down for most crosses that correspond to the knock-downs that had no effect. Based on this distribution and following the same procedure as in the *repo-Gal4* screen, we defined the groups of subviable and lethal (Fig.14A).

The *moody-Gal4* screen resulted in the identification of significantly less candidates. Knock-down of only 31 genes (0.8% of lines tested) caused complete adult lethality (0-0.49% flies with SPG-specific knock-down), while 346 genes (8.9% of lines tested) caused adult subviability (0.5-39% flies with SPG-specific knock-down), leaving us with 377 genes potentially required in SPG (Fig. 14A,B). Among these, 288 have a gene name and a function assigned, 55 are uncharacterized but have predictions for their structure and/or function and 34 genes are completely unknown and have no predictions. Furthermore, between the genes with a known or predicted function, 273 are potentially housekeeping and 70 non-housekeeping (Fig. 14C). Among the non-housekeeping candidates, few are known SPG genes, e.g. the G-signaling components Moody and Gβ13F, the SJ-associated proteins Nrx-IV, ATPα, Lac, Cora, Vari and Crok, and the integrin β subunit Myospheroid (Schwabe et al., 2005; Xie and Auld, 2011; Izumi and Furuse, 2014).

The identification of a small number of genes in the *moody-Gal4* screen partly results from the fact that the knock-down is performed in a small subset of glia and partly from the weakness of *moody-Gal4* at least during embryonic stages. Two lines of evidence suggest that *moody-Gal4* is a rather weak driver and resulted in a substantial number of false negatives. First, housekeeping genes were not retrieved with high efficiency, although SPG are indispensable for fly survival (Fig. 15). Second, some non-housekeeping genes known to be required in SPG were not identified (e.g. *pka-C1*, *wunen2*) (Ile et al., 2012; Li et al., in preparation) and knock-down of some genes that are expected to cause complete lethality, like SJ components, only led to mild subviability. However, the approximately 100 interesting candidates identified from the *moody-Gal4* screen (non-housekeeping and unknown function) represent a more than sufficient number in order to continue towards our goal of identifying a couple of novel genes required for BBB development.

Biological function	*moodyGal4* screen		*repoGal4* screen	
	number of genes tested	fraction recovered	number of genes tested	fraction recovered
mitotic spindle elongation	61	0.77	68	0.91
nucleosome	40	0.65	44	0.93
chromatin assembly or disassembly	42	0.57	49	0.86
structural constituent of ribosome	126	0.49	140	0.90
translation	180	0.42	279	0.71
ribosome biogenesis	11	0.360	13	0.92
nuclear export	6	0.330	6	1.00
mRNA polyadenylation	13	0.31	15	0.87
translation initiation	33	0.3	48	0.75
spliceosome	112	0.27	165	0.67
response to DNA damage	46	0.24	74	0.61
mRNA cleavage	10	0.2	11	0.91
general RNA polymerase II transcription factor activity	31	0.16	42	0.74
3'-5'-exoribonuclease activity	7	0.14	9	0.67
tRNA processing	8	0.125	13	0.69
cytoskeleton organization	56	0.125	93	0.55
DNA replication	28	0.11	47	0.57
structural constituent of cytoskeleton	17	0.06	38	0.45
glycolysis	15	0	24	0.63
mitochondrial electron transport	32	0	45	0.71

Figure 15. Retrieval of housekeeping genes in the *moody-Gal4* compared to the *repo-Gal4* screen. Genes are classified based on their known or predicted involvement in an essential housekeeping function (GO terms, Flybase). *moody-Gal4* is weak compared to *repo-Gal4* and does not retrieve housekeeping genes with high efficiency although knock-down of such genes is cell-lethal and *moody-Gal4* expressing SPG are indispensable for fly survival.

1.2.4 Small-scale screen to identify genes required for blood-brain barrier formation

To directly identify novel players involved in BBB formation, we knocked-down a selection of candidates with *repo-Gal4* and performed the dye penetration assay. We injected a 10 kDa rhodamine-conjugated dextran in the body cavity of 20 AEL embryos (Fig. 16A), when the barrier is closed, and followed its penetration into or exclusion from the CNS 15 min after injection. In the wt, dye does not diffuse into the nervous system, but it rapidly penetrates into the nerve cord of mutants with a defective BBB (Fig. 16C). *repo-Gal4* is strongly expressed from stage 13 onwards (10 AEL), thus providing a large time window for efficient knock-down to take place. All knock-downs were checked for dye penetration in parallel to negative (w^{1118}) and

positive control embryos (*loco* zygotic mutants). In order to quantify the dye accumulation in a systematic and fast fashion, we developed an automated analysis software using *Definiens*. The software automatically measures mean pixel intensity after excluding overexposed areas, such as the body cavity and channels that run through the CNS (Fig. 16B). Importantly, when knocking-down genes expected to impair BBB integrity, such as the SJ components Lac and Nrx-IV, we observe strong dye penetration, demonstrating that BBB phenotypes can be detected using RNAi (Fig. 16C). In total, 74 genes were tested with this assay: 45 candidates from the *repo-Gal4* screen, which included 20 GPCRs, two RGS proteins and other receptors and interesting molecules and 29 from the *moody-Gal4* screen. We identified five

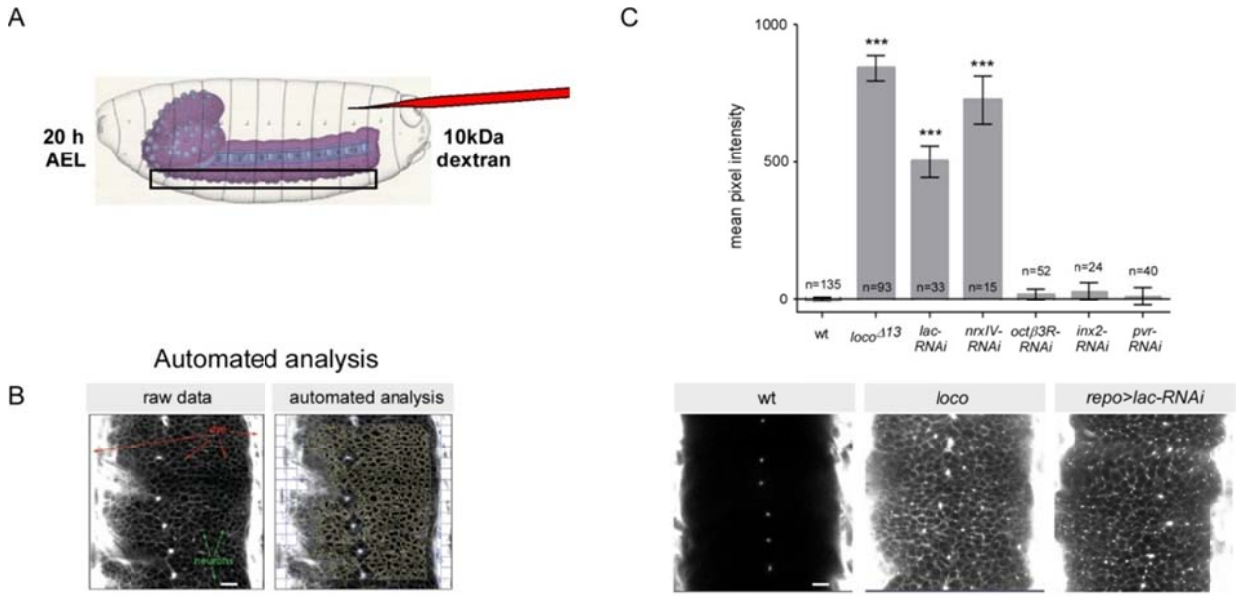

Figure 16. Embryonic dye penetration screen. (A) Schematic showing the dye penetration assay. A box highlights the ventral-most region of the CNS that is imaged (modified from Hartenstein V., Atlas of *Drosophila* development). (B) Example of automated analysis for pixel intensity measurements. The software automatically excludes overexposed areas, such as the body cavity and channels running through the CNS. (C) Example of dye assay for some of the RNAi lines tested using *repo-Gal4*. Graph on top shows quantification of the assay. Columns represent intensity of dye penetration into nerve cord as measured by mean pixel intensity after subtracting the average of wt (w^{1118}) control embryos (performed in parallel). The number of injected embryos is indicated at each column. Asterisks indicate significance compared to w^{1118}. *** $p<0.001$, ±SEM. Dye diffuses into the nerve cord of *loco* positive controls and in the RNAi-mediated knock-down of SJ proteins Lac and Nrx-IV. Below the graph, single confocal sections of representative 20 h AEL dye-injected embryos of different genotypes. Anterior is up. Scale bars are 10 µm.

genes whose pan-glial knock-down caused BBB permeability suggesting that they are novel genes required for BBB development. All were pursued further to characterize their specific roles, but three (*pasiflora1*, *pasiflora2*, *mcr*) will be discussed in the context of this thesis.

1.3 Discussion

1.3.1 Genome-wide glial screening

We performed a genome-wide RNAi screen for genes required in glia for adult survival using the pan-glial *repo-Gal4* driver and the VDRC KK transgenic *UAS-RNAi* library. The *repo-Gal4* driver is very strong and efficiently led to the identification of a big number of potential glial genes: 3679 genes or 28% of the genome. Previously it has been estimated that in *Drosophila*, disruption of approximately 30% of the genomic loci results in lethality and 75% of lethal loci are pleiotropic, meaning that their gene products are expressed and utilized at multiple places and times (Miklos and Rubin, 1996). These observations further support that the 28% of the genome we identify as required in glia is a remarkably high number. The success of the screen is also reflected in the very high efficiency of retrieval of both housekeeping and known glial genes. For some GO terms and signaling pathways, gene retrieval almost reaches 100% suggesting that the screen is close to saturation. After excluding housekeeping genes, which are needed in every cell type, the *repo-Gal4* screen identified 2697 interesting molecules possibly required for glial development and/or function. To help uncover true candidates, the results of the screen can be integrated with those of glial transcriptome analyses by us (U. Gaul, unpublished) and others (Egger et al., 2002; Freeman et al., 2003; Altenhein et al., 2006) and the available information from *in situ* experiments (BDGP website), which have different strengths and caveats; candidates identified on the basis of multiple lines of evidence can be assigned to higher confidence groups.

By determining the survival rate at 10 days old adults, the identified candidates might exert their function at any developmental stage and/or during adult life and cover a wide repertoire of glial functions. The results of our pan-glial screen potentially offer the whole set of essential glial genes and represent valuable material that can contribute to many glial projects in the lab, such as BBB development and maintenance, glial phagocytosis, and glial control of homeostasis

in the adult. The identified candidates also offer hints about truly novel glial functions and can be the starting point for addressing exciting new questions on glial biology. The lab has recently characterized 650 glial Gal4 drivers, including five drivers, each with strong and specific expression in one glial subpopulation (perineurial, SPG, cortex, ensheathing, astrocyte-like) (Kremer et al., in preparation). The results of the pan-glial RNAi screen in combination with the Gal4 collection can be used to decipher differential functions of glial subpopulations at a large scale, carry out various more specific glial screens, and study the role of particularly appealing candidates. In addition, by checking the RNAi lines with the strong *repo-Gal4* driver, several strains efficiently silencing housekeeping genes, such as the basal transcriptional machinery were identified, which might also be of interest to relevant projects in the lab.

The remarkable technique of RNAi has opened exciting new avenues for screening. Compared to forward screens, RNAi screens have the advantages that they can cover the whole genome and that they are overall faster because the step of mapping the mutation, which can sometimes be labor-intensive and time-consuming, is eliminated. However, they also bare some limitations, the most important being the incompleteness of knock-down, which calls for strong drivers. The recently developed CRISPR-Cas9 system provides a fast means to create complete knock-outs and is emerging as a promising alternative to RNAi that might allow for the realization of impressive screens under complete loss of function conditions (Bassett et al., 2013; Kondo and Ueda, 2013). However, currently, given the gaps in our knowledge of how the system operates in eukaryotic cells, it does not seem that we fully understand all the potential problems to apply the technique at a genome-wide level. CRISPR may complement RNAi approaches and can be used for the fast validation and further characterization of individual candidates, but at least in the near future RNAi will likely remain the method of choice for carrying out large scale reverse genetic screens.

1.3.2 Screening for blood-brain barrier genes – achievements and future directions

The secondary *moody-Gal4* screen revealed 383 genes that when knocked-down specifically in SPG result in reduced adult viability. Among the candidates, most are housekeeping and some are known SPG genes, such as Moody signaling and SJ

components. After excluding these candidates, the screen revealed approximately 100 interesting or completely uncharacterized genes, allowing us to continue with directly identifying novel genes required for BBB formation. In contrast to *repo-Gal4*, *moody-Gal4* is a rather weak driver in particular during embryonic development. *moody-Gal4* starts being weakly expressed late in embryogenesis (late stage 16-stage 17) in only a subset of SPG, suggesting that *moody-Gal4*-mediated knock-down will not capture genes required during BBB formation. However, many of the genes involved in establishing the barrier in the embryo are also expected to be required for its maintenance at later stages during which *moody-Gal4* is strongly expressed. The low rates of retrieval of housekeeping genes indeed suggest that the screen resulted in a significant number of false positives. Because *moody-Gal4* is highly expressed in third instar larval SPG, this result might also indicate that after development, cells cannot be efficiently killed by RNAi. Nevertheless, manual exploration of the available data and specifically of the approximately 400 lines that just escaped the threshold we established (40-44% viable flies with SPG-knock-down) suggests that housekeeping and known or potential SPG genes (e.g. *kune*, *megalin*, *rho1*, *crebB-17A*, *tre-1*) might be enriched in these groups. Therefore, a closer look at these candidates, as well as their comparison with the RNA-seq-based tissue-specific expression profile and microarray-based SPG transcriptome, might help identify true and exciting SPG genes (Graveley et al., 2011; DeSalvo et al., 2014).

To overcome the problem of the weakness of *moody-Gal4* and improve the functional RNAi screening for SPG genes, it will be important to optimize the screening conditions to yield more positive results. For instance, pilot screens of a selection of candidates, together with many positive controls could be carried out to search if other SPG-specific drivers are stronger (e.g. driver with two copies of *moody-Gal4*, *GR54C07-Gal4*). In addition, different sensitized genetic backgrounds could be tried, i.e. the screen could be performed in flies which carry a mutation that affects BBB formation and/or maintenance. When barrier function is already disrupted, the residual gene activity in incomplete knock-downs that showed no effect in the *moody-Gal4* screen might no longer suffice. Suitable sensitized backgrounds would be the removal of one copy of *Gβ13F*, *pka-C1*, or of a SJ component since homozygous mutants of these genes have very strong insulation defects. Except for increasing the effectiveness of the screen, selection of the

appropriate sensitized background may be used to bias the screen towards detection of specific candidates. For example, loss of function of genes involved in Moody signaling may bias the screen towards identification of additional pathway components. Such genetic modifier screens have been proven very successful in identifying missing pathway components; e.g. for the identification of several proteins of the Sevenless pathway involved in R7 photoreceptor development (Simon, 1994). In a small-scale preliminary screen, we tested 200 random RNAi lines using *moody-Gal4* in a *pka-C1* heterozygous mutant background. Importantly, although loss-of-function mutations in almost all genes are recessive, *pka-C1* heterozygous mutants show mild dye leakage into the CNS (Li et al., in preparation). Using the sensitized background, we identify 12 additional candidates (6% more), including the known SPG genes *rho1* and *kune*, suggesting that a couple of hundred more genes could be found with this strategy.

As a last step in our screening procedure, we have performed the embryonic dye penetration assay using *repo-Gal4* and identified five genes whose glial-specific knock-down impairs BBB integrity. The genes tested included 29 candidates from the *moody-Gal4* screen and 45 candidates from the *repo-Gal4* screen. Genes whose knock-down caused adult subviability with *moody-Gal4* but not a permeable embryonic BBB might include molecules that serve functions in BBB maintenance during later stages or that play roles in SPG other than barrier function. For instance, the gap junction protein Innexin2 was one such candidate, which in the meantime was shown to be required in larval SPG, together with Innexin1, for nutrient-dependent reactivation of neuroblast proliferation (Speder and Brand, 2014). Furthermore, because the phenotypic analysis of *moody* pathway mutants suggests that there is additional activating input into the G-proteins, we tested with the dye assay 20 GPCRs identified in the *repo-Gal4* screen, including Tre1, but unfortunately did not find any whose knock-down impairs BBB formation. Because even the *moody* deletion mutant has a rather weak dye penetration phenotype (Schwabe et al., 2005), it is possible that there is partial redundancy between the two (or more) receptors and that RNAi-mediated knock-down is insufficient to reveal additional GPCRs. Screen of genomic mutants or knock-down of GPCRs in a *moody* sensitized background (*moody-RNAi* or heterozygous *moody* mutant) might consist more suitable approaches in order to identify the receptors that act together with Moody to activate the G-proteins.

Part 2

Pasiflora1, Pasiflora2 and Mcr are novel components of the *Drosophila* septate junction

2.1 Introduction

2.1.1 Epithelia - an evolutionary novelty

The first epithelium was a novel structure capable of subdividing the body into morphologically and physiologically distinct compartments and consisted an evolutionary novelty that allowed for the development of metazoans with complex body plans (Leys and Riesgo, 2012). Epithelial sheets surround the body as a whole and line almost all surfaces and cavities within it. They act as selective diffusion barriers to isolate the organs from the body fluid and maintain their homeostasis and proper function. Given their wide distribution, epithelia also perform other functions, including protection against mechanical stress and dehydration, absorption, secretion, excretion, and gas exchange. To accomplish such diverse functions, epithelia adopt different cellular arrangements. Simple squamous epithelia are single layers of thin flattened cells, such as in the lung and blood vessels in vertebrates and BBB in *Drosophila*. Simple cuboidal and columnar epithelia are also single-layered, but consist of taller cells with expanded lateral membranes, like the epithelia of intestine, glands, and the *Drosophila* trachea (Fig. 17A).

All epithelia have three common features. First, epithelial cells have a polarized organization of the plasma membrane and underlying cytoskeleton. Their apical and basal membranes are segregated and have unique biochemical compositions. Within the epithelium, the component cells share an aligned polarity with the apical membrane facing the organ lumen or the outside of the organism (St Johnston and Ahringer, 2010). Second, their basal membrane is anchored to a specialized dense extracellular matrix, the basement membrane (Fig. 17B). The basement membrane not only provides mechanical support to the epithelium and separates it from the underlying tissue, but also plays crucial roles in regulating the growth, survival, differentiation and morphogenetic interactions of epithelial cells (Brown, 2000). Third, epithelial cells are attached to each other with different types of intercellular junctions. These include adhering junctions, which provide cohesion; occluding junctions, which seal the paracellular space; and gap junctions, which allow direct intercytoplasmic communication between the cells (Knust and Bossinger, 2002) (Fig. 17B). Many junctional proteins compose complex multi-protein families, such as the adherens junction-associated cadherins, the occluding junction-associated claudins, and the gap junction-associated innexins. Such large families

are often used in a tissue-specific manner during epithelial morphogenesis and might explain the diversified properties of different epithelia (Franke, 2009).

Based on their mode of formation, epithelia are distinguished in primary and secondary (Tepass, 1997; Schwabe et al., submitted). Primary epithelia, like the *Drosophila* trachea, epidermis, foregut, and hindgut arise by shape changes of the original blastoderm. In contrast, secondary epithelia, like kidney tubules and heart in vertebrates, as well as heart, midgut and BBB in *Drosophila* develop through mesenchymal intermediates in a process called mesenchymal-epithelial transition. Primary and secondary epithelia also differ in the ways they establish apical-basal polarity. In *Drosophila* primary epithelia, polarity is established by the mutually antagonizing actions of apical determinants, like Crb and Bazooka (Par-3) and proteins that define the basolateral domain, such as the Lgl group proteins Discs-large (Dlg), Scribbled (Scrib) and Lethal giant larvae (Lgl) (Fig. 17B) (Laprise and Tepass, 2011). Neither Crb nor Bazooka are found in secondary epithelia, making more enigmatic the mechanisms by which polarity is established; however, recent findings suggest that in the *Drosophila* BBB, interactions with the basement membrane, as well as occluding junctions are involved (Schwabe et al., submitted).

2.1.2 Occluding junctions mediate epithelial barrier function

A common role shared by all epithelia is that they define compartment boundaries and act as barriers to generate and maintain distinct chemical microenvironments. To accomplish this role, epithelia selectively transport substances via localized membrane channels and transporters and impede free paracellular diffusion. To restrict diffusion, epithelial cells are densely packed and have a narrow intermembrane space, which is sealed by specialized occluding junctions. The sealing capacity of an epithelium is defined by its occluding junctions and can be determined by its ability to block tracers of different sizes (Asano et al., 2003; Schwabe et al., 2005).

2.1.3 Overview of *Drosophila* septate junctions - ultrastructure and subtypes

In most invertebrates, septate junctions (SJs) seal the epithelial paracellular space and provide barrier function (Noirot-Timothee et al., 1978; Tepass and Hartenstein, 1994; Schwabe et al., 2005) (Fig. 17B). The lowest phylum known to possess SJs is Porifera, however, it is still unclear whether sponge SJs act as occluding junctions

(Ledger, 1975). SJs have been described in several invertebrate groups, including nematodes, arthropods and mollusks, as well as vertebrates (discussed in section 2.1.6, Fig. 17B) and their ultrastructure has been defined by transmission electron microscopy. In cross-sections, SJs display a characteristic electron-dense ladder-like appearance between adjacent cells. In tangential sections, morphologically distinct SJs have been described in different organisms, e.g. straight, pleated, smooth, and paired SJs (Izumi and Furuse, 2014). *Drosophila* possesses pleated and smooth SJs. Pleated SJs appear as an array of regularly spaced, undulating rows of septa that span the intermembrane space; within the SJ, the opposing membranes maintain a constant distance of approximately 15 nm (Fig. 17C). These septa form circumferential spirals around the cell and prevent the passive flow of solutes by extending their travel distance through the paracellular route (Tepass and Hartenstein, 1994; Schwabe et al., 2005). Tracer studies have indicated that individual septa act as impartial filters; thus the more septa are arrayed, the tighter the seal (Abbott, 1991). So far, how the highly regular septa alignment is established remains elusive. Pleated SJs are found in the majority of *Drosophila* epithelia, e.g. epidermis, trachea, foregut, hindgut, salivary glands and the glial blood-brain and blood-nerve barriers and have been characterized in much deeper detail; for the rest of this thesis, the term SJs will refer to pleated SJs. In contrast, smooth SJs are not arranged as undulating rows when viewed tangentially, but as straight parallel bands and are found in the midgut, gastric caeca and Malphigian tubules (Flower and Filshie, 1975; Tepass and Hartenstein, 1994). So far, no functional difference between the barrier properties of the two SJ subtypes has been described, while their structural differences are thought to reflect variation in the molecular architecture. In columnar epithelia, SJs localize at the apicolateral membrane just basally of adherens junctions (Fig. 17B). Importantly, SJs are indispensable for *Drosophila* development and SJ mutants die at the end of embryogenesis due to various insulation defects.

2.1.4 Molecular composition and morphogenesis of *Drosophila* septate junctions

The SJ consists of a large multiprotein complex. Although at the ultrastructural level SJs have been described in a big number of invertebrate species, most of our knowledge on their molecular composition comes from studies in the genetically

tractable *Drosophila*. In the fruitfly, more than 20 proteins have been identified, mainly through genetic screens, that when missing lead to disruption of SJs and loss of barrier integrity (Izumi and Furuse, 2014) (Fig. 17B). Most are transmembrane and lipid-anchored proteins that localize at the SJ, such as the claudins Megatrachea (Mega; Pickel - Flybase) (Behr et al., 2003), Sinuous (Sinu) (Wu et al., 2004), and Kune-kune (Kune) (Nelson et al., 2010), the cell adhesion molecules Neurexin-IV (Nrx-IV) (Baumgartner et al., 1996), Contactin (Cont) (Faivre-Sarrailh et al., 2004), Neuroglian (Nrg) (Genova and Fehon, 2003), and Lachesin (Lac) (Llimargas et al., 2004), the sodium pump with its two subunits ATPα and Nervana2 (Nrv2) (Genova and Fehon, 2003; Paul et al., 2003), Melanotransferrin (Mtf; Transferrin 2 - Flybase) (Tiklová et al., 2010) and Macroglobulin complement-related (Mcr) (Bätz et al., 2014; Hall et al., 2014). The homophilic cell adhesion molecule Fasciclin III (FasIII) also localizes at SJs and has been widely used as a SJ marker (Woods et al., 1997), however, flies carrying a null mutation in *fasIII* are viable, suggesting that the protein is dispensable for SJ formation (Whitlock, 1993). The complex also includes the intracellular proteins Coracle (Cora) and Varicose (Vari) that directly interact with the cytoplasmic tail of Nrx-IV via their FERM and PDZ domains, respectively and link the junctions to the cytoskeleton (Fehon et al., 1994; Lamb et al., 1998; Ward et al., 1998; Ward et al., 2001; Wu et al., 2007; Bachmann et al., 2008; Moyer and Jacobs, 2008). A hallmark of SJ proteins is that they are interdependent for localization and removal of one component is sufficient to destabilize the whole complex and mislocalize other SJ proteins. In addition, half of the known SJ proteins can be readily co-immunoprecipitated from tissue extracts and detected by mass spectrometry (MS), further suggesting that they function together in a multi-protein complex (Genova and Fehon, 2003; Faivre-Sarrailh et al., 2004; Tiklová et al., 2010; Jaspers et al., 2012). Fluorescence Recovery After Photobleaching (FRAP) experiments have been instrumental in classifying most SJ proteins as core components based on their limited mobility after photobleaching and the observation that in their loss-of-function other SJ proteins diffuse fast into the bleached region due to impaired complex formation (Laval et al., 2008; Oshima and Fehon, 2011) (Fig. 2). Intriguingly, the specific roles of individual SJ proteins within the complex remain largely unknown.

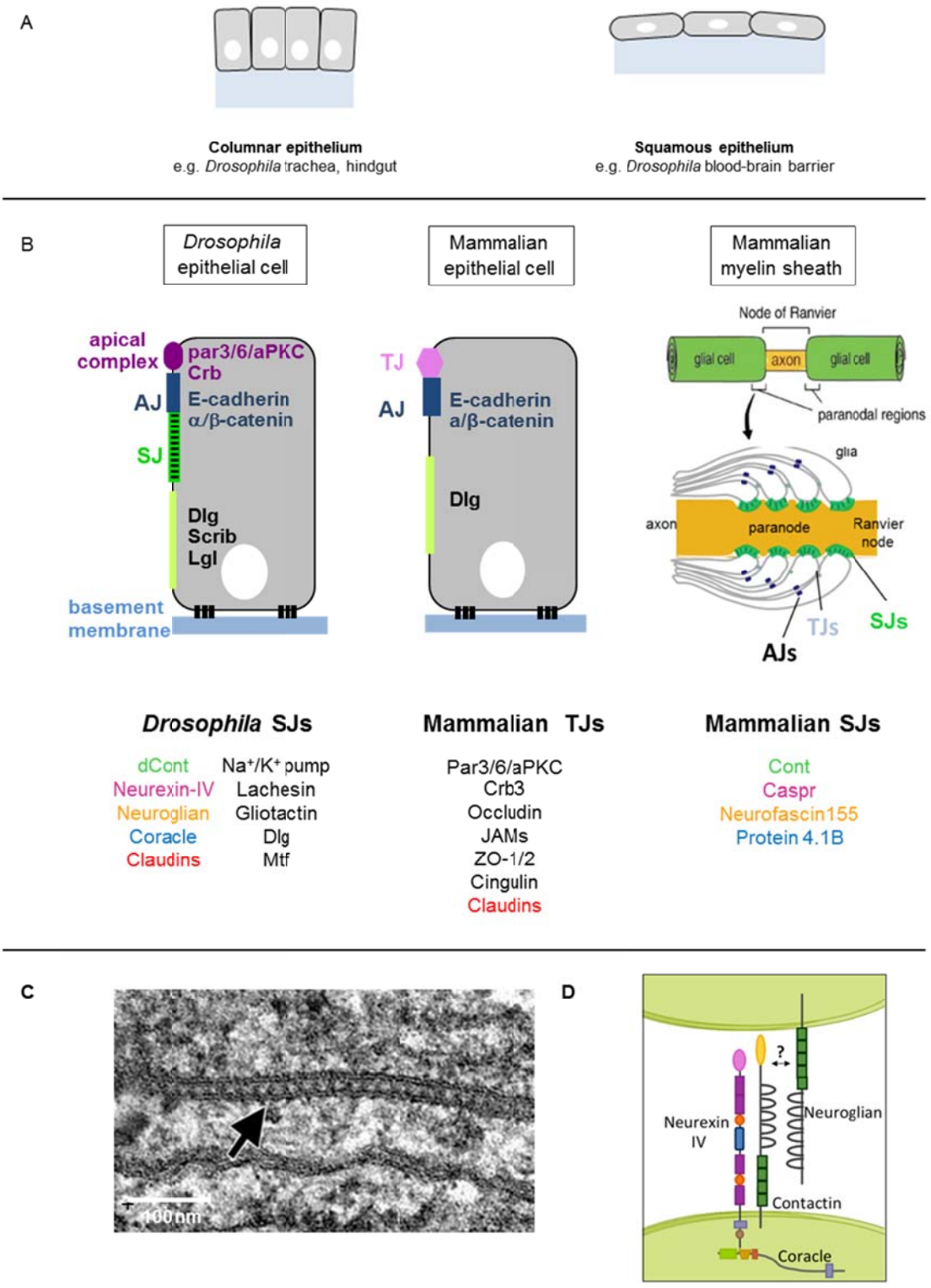

Figure 17. Occluding junctions in *Drosophila* and mammalian epithelia. (A) Examples of columnar and squamous epithelia, which consist of cells with expanded lateral membranes and thin flattened cells, respectively. (B) Subcellular localization and molecular composition of *Drosophila* and mammalian junctions. Key components are conserved. (C) Transmission electron microscopy of the

BBB epithelium of first instar larvae. The arrow points at SJs, which appear as ladder-like regular septa that span the paracellular space. (D) Schematic depicting known and potential interactions between *Drosophila* SJ components based mostly on studies of the mammalian paranode. Schematic for Ranvier node was prepared by Tina Schwabe, SJ micrograph is from Schwabe et al., 2005.

Accompanying epithelial morphogenesis, SJs are remodeled to mature to insulating junctions (Fig. 18). At embryonic stage 12, SJ proteins accumulate evenly along the lateral membrane of columnar epithelial cells. Core SJ proteins acquire their immobility after photobleaching at stage 13, indicating that it is at this stage that fully stable SJ complexes have formed (Oshima and Fehon, 2011). Subsequently, SJ proteins gradually localize at more apical compartments and by stage 15 are restricted to the apicolateral membrane. SJ maturation coincides with the appearance of the sealing capacity of the epithelium. The Ly-6 proteins Crooked (Crok), Crimpled (Crim), and Coiled (Cold) are required for SJ formation, however, they do not reside at SJs and instead localize to cytoplasmic puncta. In *ly-6* mutants, the FRAP kinetics of SJ proteins mirrors that of core complex mutants and therefore Ly-6 proteins are thought to be involved in the assembly of SJ (sub)complexes in an intracellular compartment (Nilton et al., 2010; Oshima and Fehon, 2011) (Fig. 18). The subsequent relocalization of SJs requires endocytosis from the basolateral membrane and recycling to the apicolateral compartment (Tiklová et al., 2010; Oshima and Fehon, 2011). Gliotactin (Gli) and Dlg localize at SJs (Woods and Bryant, 1991; Woods et al., 1997; Schulte et al., 2003), but in contrast to core components and Ly-6 proteins, in their loss-of-function the complex is properly formed and SJ proteins, although mislocalized, retain their restricted mobility. Moreover, at least Dlg does not display the characteristic immobility after photobleaching of core SJ proteins, but diffuses fast (Oshima and Fehon, 2011). This suggests that Gli and Dlg are required for localization of the complex rather than its assembly and is in line with previous observations that have reported Gli as non-essential for septa formation and have failed to demonstrate physical interactions between Gli or Dlg and known SJ proteins (Fig. 18). In addition, Gli and Dlg show a unique co-localization at tricellular contacts formed at the convergence of SJs from three adjacent cells, suggesting that they play a distinct role there (Ward et al., 1998; Schulte et al., 2003; Schulte et al., 2006).

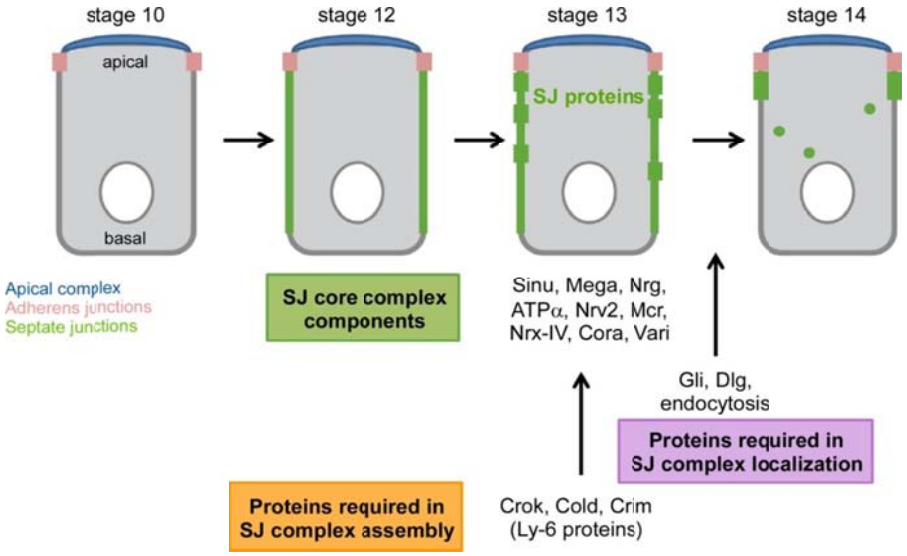

Figure 18. Timeline and players of SJ morphogenesis in columnar epithelia. The SJ complex consists of several core components. Ly-6 proteins are required for assembly of (sub)complexes at stage 13, while endocytosis and the SJ proteins Gli and Dlg are essential for complex relocalization at the apicolateral membrane at stage 14 (modified from Oshima and Fehon, 2011).

2.1.5 Other functions of *Drosophila* septate junctions

Except for their well established role as paracellular diffusion barriers, SJs also perform other functions. In the BBB epithelium, SJs contribute to the establishment and/or maintenance of cell polarity by acting as a fence within the lateral membrane that prevents intermixing of molecules between the apical and basal membrane compartments (Schwabe et al., submitted). In addition, some SJ proteins are also part of a complex that plays a developmentally earlier, independent role in promoting cell polarity. During late stages in the maturation of primary epithelia, which however precedes the development of SJs, a complex formed by Nrx-IV, Cora, the Na^+/K^+ ATPase and the SJ localizing-protein Yurt is required for maintaining polarity by restricting the size of the Crb domain and functionally substituting for the Lgl group proteins (Laprise et al., 2009). Finally, SJs are involved in the regulation of tracheal tube length with the majority of SJ mutants displaying overelongated dorsal trunks (Wu and Beitel, 2004). SJs control tube length, at least partly, by regulating apical secretion of the chitin deacetylases Serpentine and Vermiform that terminate tube elongation by a yet unidentified mechanism (Luschnig et al., 2006; Wang et al., 2006).

2.1.6 Vertebrate tight and septate junctions

In vertebrate epithelia, the block to paracellular diffusion is mediated by tight junctions (TJs) (Farquhar and Palade, 1963; Balda and Matter, 2008). In contrast to SJs, TJs localize apically of the *zonula adherens* (Fig. 17B) and using electron microscopy appear as a series of apparent fusions of the membranes of adjacent cells (kissing points). These fusions are composed of strands of intramembranous particles from opposing cells that associate to constitute a paired TJ and obliterate the paracellular space. Similar to invertebrate SJ septa, each strand acts independently from the others and the sealing capacity of TJs increases with the increasing number of strands. Within paired TJs, aqueous pores are postulated to occur, which are selectively permeable to small molecules. TJs consist of a series of proteins embedded in the plasma membrane, such as Occludin, Tricellulin, and junctional adhesion molecules (JAMs), which in turn are attached to cytoskeletal and scaffold proteins, including Zonula occludens (ZO)-1/2/3 and Cingulin. TJs also contain Crb3, Par-3, Par-6 and aPKC (atypical protein kinase C), which in *Drosophila* associate with the apical and sub-apical regions. Although the set of proteins composing the TJ is different from that of the SJ, the two complexes share a key molecular component, the claudins (Fig. 17B).

Mammals also possess SJs at the nodes of Ranvier in the PNS, where they form the paranodal junction between axons and myelinating glia (Fig. 17B) (Poliak and Peles, 2003). Importantly, mammalian SJs are composed (in part) of the homologous molecules found in *Drosophila* SJs (Fig. 17B). Studies of the paranodal junction have also unraveled some of the interactions bridging together SJ proteins in the multi-subunit complex. Caspr (Nrx-IV homologue) forms a complex with Contactin in *cis* in the axonal membrane and its intracellular region, like in *Drosophila*, binds the scaffold protein 4.1B (Cora homologue). Moreover, Neurofascin 155 (Nrg homologue) has been suggested to be the glial ligand of the Caspr/Contactin complex (Fig. 17D) (Einheber et al., 1997; Bhat et al., 2001; Boyle et al., 2001; Pillai et al., 2009). Like *Drosophila* BBB SJs, paranodal SJs serve the same dual function as a paracellular barrier impeding ion flow across the paranode and as a fence restricting the intermixing of neuronal membrane proteins such as Na^+ and K^+ ion channels. The myelin loops of Schwann cells also contain claudin-containing TJs, which contribute to paracellular barrier function and saltatory conduction of action potentials (Miyamoto et al., 2005).

2.1.7 Claudins – determinants of barrier selectivity

The major constituent of TJ strands are the claudins (Furuse et al., 1998a; Furuse et al., 1998b; Furuse and Tsukita, 2006; Günzel and Yu, 2013). Claudins comprise a family of 20-34 kDa proteins with four membrane-spanning regions and both termini facing intracellularly. The larger first extracellular loop of claudins contains the conserved family-signature motif W-x(15-20)-[GN]-L-W-x(2)-C-x(8-10)-C-x(15-16-)-[RQ]. In mammals, there are over 25 members which show cell- and tissue-specific expression. The identification and analysis of claudins led to a fundamental breakthrough in our understanding of barrier function. Claudins can oligomerize in strands homo- and hetero-philically on the same cell and homo- and hetero-typically on neighboring cells. It is now clear that TJ size- and charge-selectivity depends on claudins and in particular on their first extracellular loop. This loop lines the TJ pore and defines its diameter conferring size selectivity to TJ strands. In addition, critical amino acid residues of the claudin loop residing within the pore can be charged, thereby generating charge selectivity. These observations have led to a model in which different combinations and proportions of claudin molecules regulate tightness of paired TJs and might explain the diversified barrier properties of different epithelia. The second extracellular loop appears to be important for transcellular binding that narrows the paracellular space. The C'-tail is essential for protein stability and intracellular transport to the TJ, while the C'- terminus in most claudins contains a

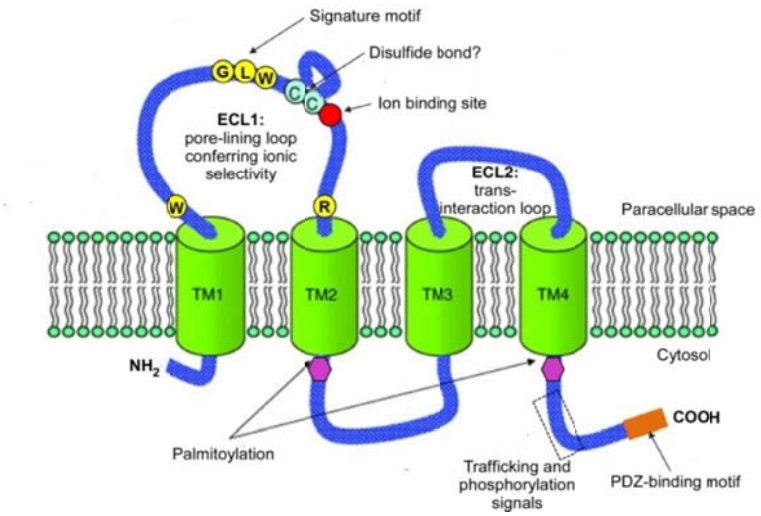

Figure 19. Predicted topology and secondary structure of claudins showing putative functional domains. TM: predicted transmembrane domain, ECL: extracellular loop (modified from Lal-Nag and Morin, 2009)**.**

PDZ-binding domain (most frequently VY) that allows binding to cytoplasmic proteins. In *Drosophila*, three claudins have been identified as components of the SJ, but their precise roles within the complex remain unknown (Behr et al., 2003; Wu et al., 2004; Nelson et al., 2010) (Fig. 19).

Claudins are part of the PMP22/EMP/MP20/Claudin mammalian superfamily of tetra-spanning membrane proteins (pfam00822), which includes claudins, peripheral myelin protein (PMP22), epithelial membrane proteins (EMPs), lens fiber membrane intrinsic protein (MP20), and more distantly related proteins, such as members of the TMEM47 family, voltage gated calcium channel γ subunits and clarins (Adato et al., 2002; Simske, 2013) (Fig. 20). Most superfamily members seem to perform diverse functions at specialized cell-cell contacts, including adhesion, barrier formation, regulation of channel activity and protein aggregation. The *Drosophila* and *Caenorhabditis elegans* genomes also encode members of the superfamily, which although highly divergent at the sequence level, they often perform similar functions with those assigned to their vertebrate counterparts.

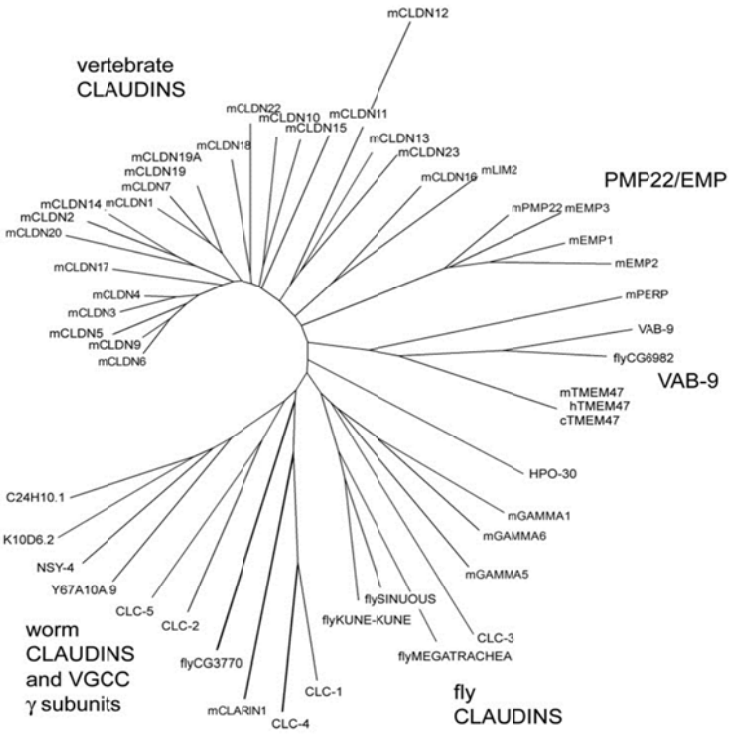

Figure 20. Phylogenetic tree of pfam00822 tetraspan proteins from vertebrates and invertebrates. The proteins are highly divergent at the sequence level, however, they often serve similar functions. Figure is from Simske, 2013**.**

2.2 Pasiflora proteins are novel core components of the septate junction

2.2.1 The novel *pasiflora* genes are required for blood-brain barrier formation

Among the candidates identified, the RNAi lines 102223 and 105806 caused complete adult lethality in the *repo-Gal4* screen and adult subviability in the *moody-Gal4* screen (23% and 17% survivors for 102223 and 105806, respectively; 51% for negative controls). Pan-glial knock-down of both genes results in leaky BBB (Fig. 21C-E) and late embryonic lethality (1% hatch, wt: 99%) (Fig. 21G). The lines correspond to the previously uncharacterized genes *CG7713* and *CG8121*, which belong to the same family (With et al., 2003). Inspired by the paralysis resulting from the BBB defect, we named the genes *pasiflora1* (*pasi1*, *CG7713*) and *pasiflora2* (*pasi2*, *CG8121*) from the Greek mythological goddess who was inducing paralysis in her victims. Our results suggest that the family members *pasiflora1* and *pasiflora2* are novel genes required for BBB formation.

To better analyze the phenotypes in complete loss of function, we sought to generate genomic mutants. The viable line *P{EP}G4182* carries a P-element insertion 219 bp upstream of the *pasiflora1* 5'UTR. We mobilized the P-element, created imprecise excisions and isolated a line, *pasiflora1*$^{\Delta}$ that deletes the entire *pasiflora1* locus and 59 bp of the neighboring *CG7379* 3'UTR (Fig. 21A). *pasiflora1*$^{\Delta}$ have a permeable BBB and although they survive as late embryos, they are unable to hatch and die at the end of embryonic development (0% hatch) (Fig. 21D, G). A similarly leaky BBB is observed in embryos transheterozygous for *pasiflora1*$^{\Delta}$ and the deficiency chromosomes *Df(3R)BSC566* and *Df(3R)ED5785* which uncover the locus (Fig. 21D,E). The dye leakage is severe, but significantly weaker than that of the amorphic *nrx-IV*^{4304} SJ mutant (Fig. 21B, E). However, *nrx-IV* is only zygotically expressed, while *pasiflora1* is also maternally provided (Fig. 23A, BDGP website; Baumgartner et al., 1996; Graveley et al., 2011). Because in *pasiflora1*$^{\Delta}$, part of the *CG7379 3'*UTR is deleted, we also tested the *CG7379* RNAi line 103928 that caused adult subviability in the *repo-Gal4* screen (29% surivors; negative controls 52%) and showed no effect in the *moody-Gal4* screen (49% survivors; negative controls 51%). Pan-glial knock-down of *CG7379* does not impair embryonic BBB integrity (data not shown). To ultimately prove that the glial loss of *pasiflora1* is causing the leaky BBB, we sought to rescue the dye penetration of *pasiflora1*$^{\Delta}$. Pan-glial overexpression of *pasiflora1* restores BBB function (Fig. 21D, E), further showing that there are no

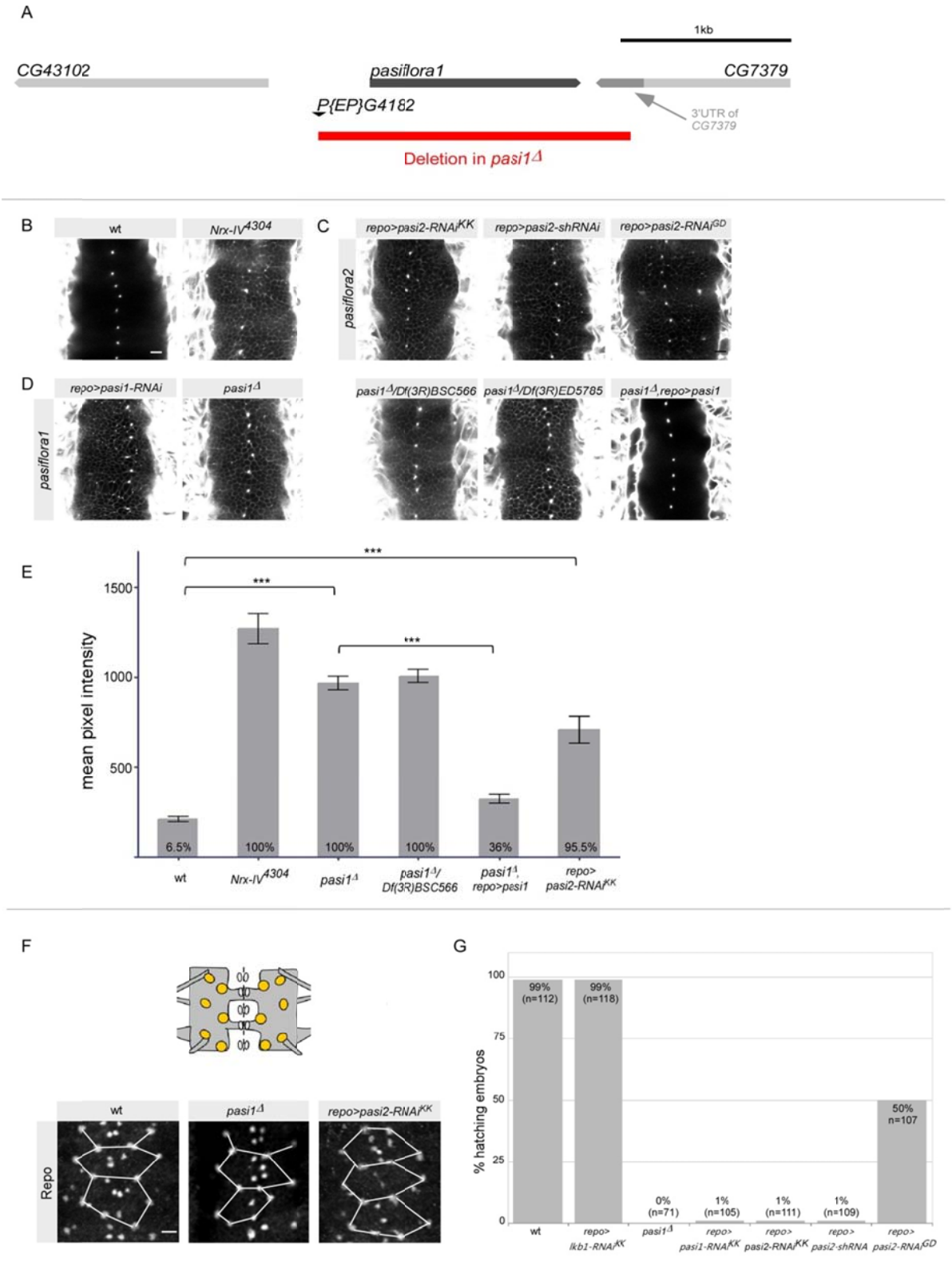

Figure 21. ***pasiflora genes*** **are required for BBB formation.** (A) Schematic of the *pasiflora1* genomic region. The deletion in the *pasi1*$^{\Delta}$ mutant spans the whole *pasiflora1* locus and part of the

3UTR' of the neighboring gene *CG7379*. (B-D) Single confocal sections of 20 h AEL dye-injected embryos. Dye diffuses into the nerve cord of *nrx-IV* positive controls (B) and in the loss of *pasiflora1* (D) and *pasiflora2* (C), as opposed to wt embryos (B). Pan-glial overexpression of *pasiflora1* CDS rescues the dye penetration of *pasiflora1*$^{\Delta}$ (D). Anterior is up. Scale bars are 10 µm. (E) Quantification of dye penetration assay. Raw data are plotted. Columns represent intensity of dye penetration into nerve cord as measured by mean pixel intensity. The percentage of embryos showing penetration is indicated at the bottom of each column. Brackets and asterisks indicate significance of pairwise comparisons. *** $p<0.001$, ±SEM, n=22-107. (F) Ventral surface views of stage 16 embryonic nerve cord stained with Repo. The full complement of SPG is detected in loss of function of *pasiflora* genes. The positions of nuclei are similar between the genotypes, as visualized by overlay of connecting lines. Schematic on top shows imaged area with SPG labeled orange. Three abdominal neuromeres are shown. Maximum projections of 4 µm z-stacks. Anterior is up. Scale bars are 10 µm. n=8-15. (G) Quantification of embryonic survival for different genotypes. Columns represent the percentage of embryos that hatched. The number of aligned embryos is indicated at the top of each column.

additional mutations on the chromosome contributing to BBB breakdown and indicating that *pasiflora1* is required cell-autonomously.

In the vicinity of the *pasiflora2* locus, no lines with P-element insertions were available. Since the gene belongs to the same family, we decided to pursue *pasiflora2* using RNAi. Moreover, the KK line is very potent as it causes strong BBB permeability and embryonic lethality with *repo-Gal4* (1% hatch) (Fig. 21C, E, G). The fact that impaired BBB is observed in the glial-specific knock-down suggests that *pasiflora2* is also cell-autonomously required. To exclude off-target effects of the line, we tested additional RNAi strains, which target different sequences of the mRNA. Two additional lines were used; the VDRC line GD43952 and a line we generated, which expresses a short 21 nt siRNA (*shRNAi*, TRiP design, Ni et al., 2011). Both lines show embryonic lethality and dye penetration with *repo-Gal4*, but the GD line leads to milder defects (Fig. 21C, G). For all our following experiments to study *pasiflora2*, we used the KK RNAi line.

To exclude that the leaky BBB is a result of earlier defects in glia specification and/or migration, we analyzed the number and positions of SPG. To this end, we stained stage 16 embryos with the Repo antibody, which labels all glial nuclei except for midline glia, and focused on the ventral-most SPG. In the wt, the number of glia is very stereotyped, and four SPG are found per abdominal neuromere in the ventral-most 4 µm of the nerve cord (Ito et al., 1995; Beckervordersandforth et al., 2008).

We detect the full set of SPG in both *pasiflora1*$^{\Delta}$ and *repo-Gal4;UAS-pasiflora2-RNAi* embryos. The positions of nuclei are somewhat variable in both control and mutant embryos, but overall we do not observe major differences between the genotypes (Fig. 21F). In summary, our results show that *pasiflora1* and *pasiflora2* are novel genes with a specific role in BBB formation.

2.2.2 *pasiflora* genes are required for tracheal tube size and barrier function

We noticed that the tracheal tubes of *pasiflora1*$^{\Delta}$ do not fill with air (data not shown), indicating that the tracheal paracellulalar barrier is also compromised. To confirm this observation, we performed the dye penetration assay in late stage 17 embryos and visualized the dorsal trunks. In the wt, dye is excluded from the tracheal lumen, but it rapidly diffuses into the tubes of *pasiflora1*$^{\Delta}$ homozygous and *pasiflora1*$^{\Delta}$ over the two deficiency chromosomes, but not in embryos with ubiquitous knock-down of *CG7379* (*tubulin-Gal4*). As expected, the tracheal defects are not restored in our rescue experiment with the glial *repo-Gal4* driver, further supporting that *pasiflora1* is cell-autonomously required (Fig. 22B and data not shown). Leaky tracheal tubes are also observed in embryos with ubiquitous knock-down of *pasiflora2*, while knocking-

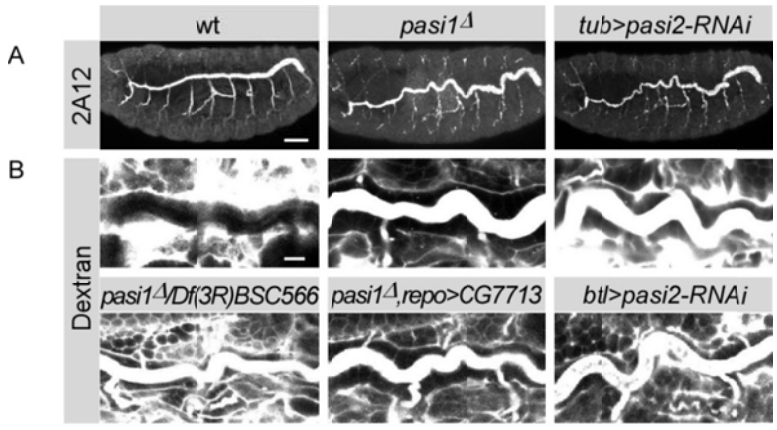

Figure 22. *pasiflora* genes are required for tracheal barrier formation and control of tube length. (A) Lateral views of stage 16 embryos stained with the 2A12 antibody. The dorsal trunks appear over-elongated and convoluted in the loss of *pasiflora* genes compared to wt. Maximum projections of 16-18 µm z-stacks. Scale bars are 40 µm. n=8-10. (B) Single confocal sections of 20 h AEL dye-injected embryos of different genotypes. Dye does not diffuse in the tracheal lumen of wt, but penetrates in *pasiflora1* and *pasiflora2* loss-of-function. Glial overexpression of *pasiflora1* does not rescue the tracheal phenotype of *pasiflora1*$^{\Delta}$. Lateral views of dorsal trunk. Anterior is left and dorsal is up. Scale bars are 10 µm. n=5-16.

down *pasiflora2* with the more trachea-specific *breathless-Gal4* leads to qualitatively similar phenotypes but with lower penetrance (Fig. 22B). Both *pasiflora* mutants also show excessively elongated and convoluted dorsal trunks, a result that was confirmed by staining stage 16 embryos with the 2A12 antibody that recognizes the luminal protein Gasp (Fig. 22A). Over-elongated dorsal trunks are observed in the majority of SJ mutants and are believed to be, at least partly, due to the role of SJs in apical secretion of chitin deacetylases that terminate tube elongation (Luschnig et al., 2006; Wang et al., 2006). In summary, the *pasiflora* genes are required for tracheal barrier function and control of tube size.

2.2.3 *pasiflora* genes are expressed in SJ-forming embryonic epithelia and glia

To characterize the expression pattern of *pasiflora* genes, we performed RNA *in situ* hybridization in wt embryos. The genes show identical expression patterns throughout embryogenesis (Fig. 23A). Ubiquitous weak expression is first detected at stages 1-4, suggestive of maternal contribution. Zygotic transcripts are detected in epithelial tissues from stage 10 onwards. The tracheal placodes are labeled at stage 10 and the anterior hindgut at stage 11; expression persists in these tissues throughout development. During stages 14-16, trachea, foregut, hindgut, epidermis and salivary glands are marked. At stage 16, we detect weak staining in the nervous system and labeling of some cells that based on their position are likely to be exit and/or peripheral glia. A clearer *in situ* for *pasiflora1* showing similar expression is displayed on the BDGP website (http://insitu.fruitfly.org). Therefore, both genes are specifically expressed in embryonic epithelia and insulating glia, all tissues that form SJs.

Several attempts to generate specific antibodies recognizing the two proteins were unsuccessful. By conventional expression techniques, overexpression of the highly hydrophobic Pasiflora proteins is toxic to the bacteria. We therefore raised antibodies against a mixture of two 15-16 amino acid-long peptides (Fig. 23B, epitopes highlighted with red asterisks). Unfortunately, neither the sera nor the affinity purified antibodies showed specific labeling in wt embryos (data not shown).

2.2.4 Molecular features of Pasiflora proteins

Pasiflora1 and Pasiflora2 are small proteins of 19 and 29 kDa, respectively, with four transmembrane domains but no signal peptide, and no sequence similarity to any

known domains or motifs. Interestingly, their predicted topology, with two intracellular termini and a bigger first extracellular loop, strongly resembles that of claudins (Fig. 23B). To examine if the proteins localize at the plasma membrane or some intracellular membrane compartment, we analyzed their subcellular localization *in vivo* and in cell culture. Because we did not succeed in generating specific antibodies, we C'-terminally tagged both proteins with GFP and FLAG (Fig. 23B). We expressed the tagged proteins in Schneider cells (S2), as well as glia and SPG *in vivo*, which we imaged in stage 16 embryos (*repo-Gal4*) and 3rd instar larval CNS (*moody-Gal4*), respectively. We find that Pasiflora proteins localize at the plasma membrane both *in vivo* and in S2 cells (Fig. 23C).

Pasiflora1 and Pasiflora2 were previously identified as members of a family conserved in *Drosophila* and *Anopheles*, consisting of proteins with four transmembrane domains and two short conserved intracellular motifs in the second and third intracellular regions. The family includes nine members in the fly, amongst which the founding member *fire exit* is expressed in a subset of exit and peripheral glia (as demonstrated by *lacZ* enhancer trap pattern), without any known molecular or biological function (With et al., 2003). Pan-glial knock-down of *fire exit* causes adult subviability (19% survivors; 52% for negative control) but was not pursued further. We did not test additional family members for BBB defects either because their pan-glial knock-down did not impair viability (*CG10311*, *CG12825*, *CG13747*, *CG14767*, and *CG15098)* or because an RNAi strain was not available in the collection (*CG13288*).

Different lines of evidence indicate that *pasiflora* genes are co-expressed. First, RNA *in situ* hybridization showed that the genes are similarly expressed in embryonic epithelia (Fig. 23A). Second, both genes were identified as differentially expressed in embryonic glia based on microarray transcriptome profiling (U. Gaul, unpublished). Third, based on developmental RNA-seq, the genes group together in a co-expression cluster; interestingly, the SJ genes *kune* and *cold* are also part of the cluster. *Pasiflora2* is also included in a second co-expression cluster together with several SJ genes (*sinu*, *nrx-IV*, *mcr*, *gli*, *crok*, *cold*, *crim*) (Graveley et al., 2011). The notion that *pasiflora1 and pasiflora2* expression is tightly co-regulated is also supported by the observation by us and others that both genes, together with more than half of the known SJ-encoding mRNAs, are predicted targets of miR-184 (Hong et al., 2009; Iovino et al., 2009; www.microrna.org). Based on the observed

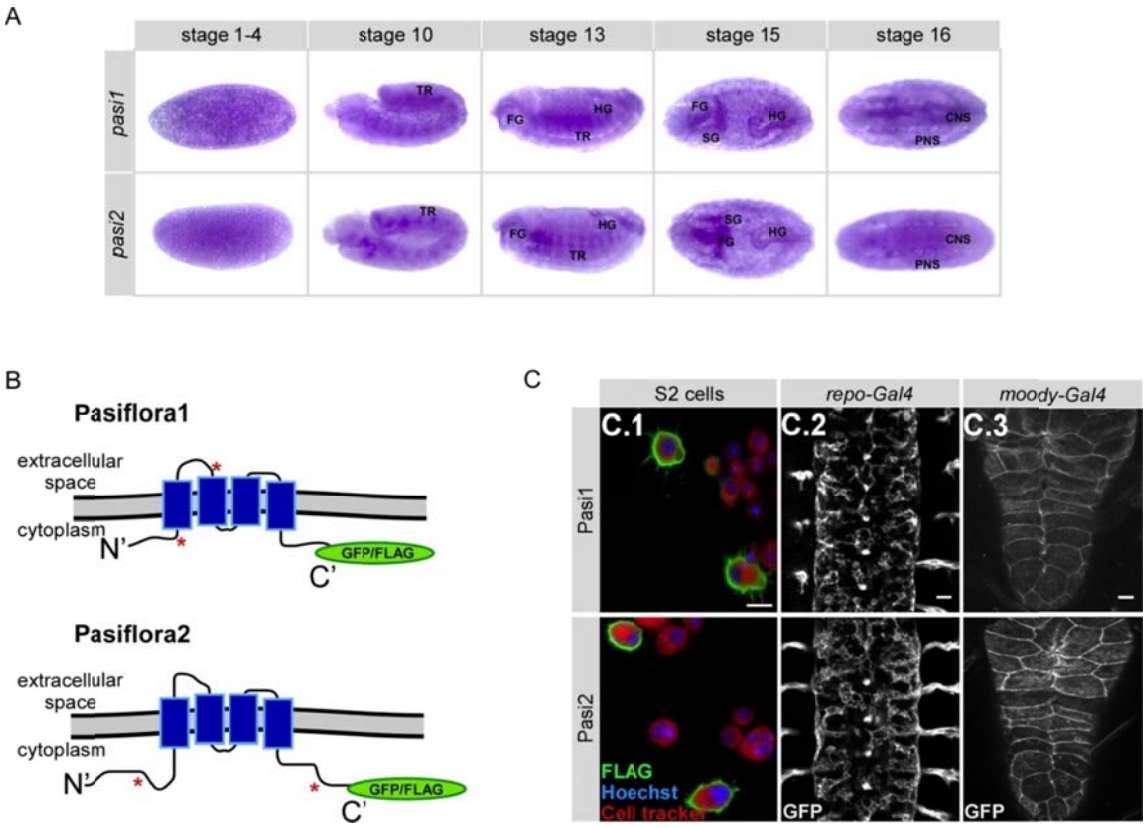

Figure 23 . Pasiflora1 and Pasiflora2 are tetra-spanning membrane proteins co-expressed in embryonic epithelia and glia. (A) RNA *in situ* hybridization with antisense probes for *pasi1* and *pasi2* in w^{1118} embryos. Both genes are expressed maternally (stage 1-4). Zygotic transcripts are detected from stage 10 onwards in epithelia and nervous system; trachea (TR), foregut (FG), hindgut (HG), salivary glands (SG), central (CNS) and peripheral nervous system (PNS). Anterior is left. (B) Predicted structure and topology of Pasiflora proteins. The site of fusion of GFP/FLAG tags is depicted with green ovals. The epitopes used for antibody production are highlighted with red asterisks. (C) Tagged versions of Pasiflora1 and Pasiflora2 localize at the plasma membrane. (C.1) Single confocal sections of S2 cells transiently transfected with Pasiflora-FLAG. Scale bars are 10 µm. (C.2) Ventral views of fixed stage 16 embryos expressing Pasiflora-GFP in glia. Maximum projections of 7 µm z-stacks. Scale bars are 10 µm. (C.3) Third instar larval CNS expressing live Pasiflora-GFP in SPG. Maximum projections of 10 µm z-stacks. Anterior is up. Scale bars are 20 µm.

phenotypes in *pasiflora* mutants, the expression patterns and the targeting by miR-184, we hypothesized that Pasiflora proteins are either SJ components themselves or play a role in complex assembly and/or trafficking. However, neither of the proteins was found a SJ co-immunoprecipitation experiment with a monoclonal antibody against the claudin Mega followed by MS although this study succeeded in

identifying at least 10 known SJ components (Jaspers et al., 2012). The properties of Pasiflora proteins and in particular their small size strongly disfavor their detection by liquid chromatography-coupled MS/MS and might explain why they escaped identification. Only a limited number of theoretical tryptic peptides is predicted for the proteins; three peptides for Pasiflora1 and <40 for Pasiflora2. Additionally, fully tryptic peptides have not been observed for either of the proteins and the only reported experimental, MS-based evidence is a single non-tryptic peptide for Pasiflora2 (www.peptideatlas.org). However, in the study by Jaspers et al. only fully tryptic peptides were included during the identification of MS spectra and only proteins with at least two peptides were reported. Notably, the two other claudins, Sinu and Kune, which have similar size and structure with the Pasiflora proteins, were also not detected in the MS.

2.2.5 *pasiflora* genes are required for localization of SJs

To confirm that *pasiflora* genes play a role in SJ formation, we analyzed the morphology and subcellular localization of SJs in the mutants. We first visualized the embryonic BBB using the live endogenously expressed markers Nrg-GFP and Lac-GFP (Morin et al., 2001). In wt late stage 17 embryos, both markers label SJs and trace the outlines of SPG, which make continuous contacts with their neighbors to seal the CNS. In *pasiflora1*$^{\Delta}$ and *repo-Gal4;UAS-pasiflora2-RNAi* embryos, SJs appear discontinuous and severely disorganized (Fig. 24A), demonstrating that both genes are required for SJ formation in the embryonic BBB.

SPG are very large but thin cells (only 0.2 μm tall) complicating the visualization of SJ localization along the lateral membrane during embryonic stages. We therefore turned to examine the hindgut and tracheal columnar epithelia. In the hindgut of wt stage 12 embryos, SJ proteins accumulate evenly along the lateral membrane, but at stage 15 are restricted to the apicolateral membrane compartment, as revealed by staining for Cora. In *pasiflora1*$^{\Delta}$ and *tubulin-Gal4;UAS-pasiflora2-RNAi* embryos, Cora localizes similarly to wt at stage 12, but fails to restrict apicolaterally at stage 15 and remains distributed along the lateral membrane. At stage 15 we observe similar mislocalization of additional SJ markers, such as Nrg-GFP, ATPα-GFP, and FasIII (Fig. 24C). Notably, in the variably penetrant phenotype of *pasiflora2* RNAi, the mislocalization phenotype is more pronounced for Cora and FasIII followed by Nrg, while ATPα is only mildly

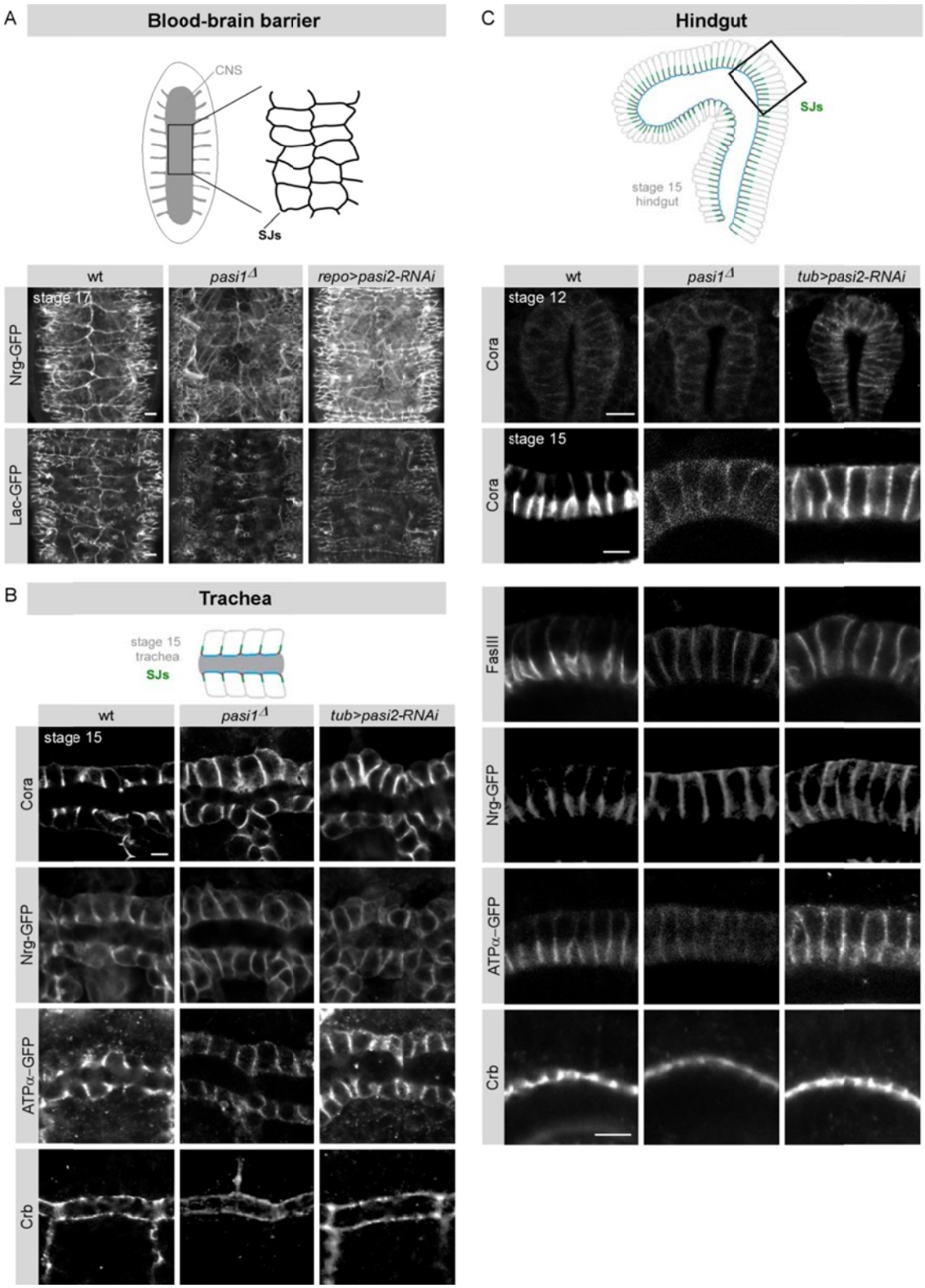

Figure 24. *pasiflora* genes are specifically required for localization of SJs. (A) Ventral surface views of nerve cord of 20 h AEL embryos expressing the live SJ markers Nrg-GFP and Lac-GFP.

SPG SJs are severely disrupted in the loss of *pasiflora* genes. Maximum projections of 8-11 µm z-stacks. Anterior is up. Scale bars are 10 µm. n=5-16. (B) Single confocal sections of stage 15 dorsal trunks stained for different junctional proteins. In *pasiflora* mutants, SJ proteins spread basolaterally. Cell polarity is preserved, as revealed by staining for Crb. Scale bars are 5 µm. n=6-12. (C) Single confocal sections of stage 12 and stage 15 hindguts stained for SJ proteins and Crb. In *pasiflora* mutants, SJ proteins localize at the lateral membrane similar to wt at stage 12, but fail to restrict apicolaterally at stage 15. Crb localization is preserved. Scale bars are 10 µm in stage 12 and 5 µm in stage 15 hindguts. n=5-21.

mislocalized. SJs are also mislocalized in tracheal cells. In the tracheal epithelium of wt stage 15 embryos, Cora, ATPα-GFP and Nrg-GFP accumulate in the apicolateral membrane, but spread basolaterally in the mutants (Fig. 24B). Furthermore, the intensity of SJ proteins appears lower in *pasiflora* mutants in all tissues examined. Dimmer SJ immunostaining has been reported for other SJ mutants as well, but in the cases where it was tested by western blots, the protein levels were overall not reduced (Genova and Fehon, 2003; Paul et al., 2003). This suggests that the weaker staining is not a result of reduced transcription or increased protein destabilization and degradation, but rather a consequence of the dispersed localization. Except for w^{1118}, we also tested genetically closer controls; i.e. a viable line with precise excision of *P{EP}G4182* and embryos with ubiquitous knock-down of a random RNAi (VDRC KK 108356) and confirmed that they have wt localization of SJs (data not shown). Collectively, our results show that *pasiflora* genes are required for the apicolateral localization of SJs in the embryonic hindgut and tracheal epithelia.

Some SJ proteins also play an earlier, independent role in maintaining cell polarity by restricting the size of the apical Crb domain (Laprise et al., 2009). To investigate if cell polarity is disturbed in the mutants, we analyzed the distribution of Crb in hindgut and trachea and observed that in both tissues, Crb localizes at the apical membrane similarly to wt (Fig. 24B,C). Thus, in columnar embryonic epithelia, *pasiflora1* and *pasiflora2* selectively affect SJ organization, but not the establishment or maintenance of cell polarity.

2.2.6 Pasiflora proteins localize at the SJ and their localization depends on other complex components

To determine if Pasiflora proteins accumulate in a specific membrane compartment, we analyzed the localization of GFP-tagged versions in the hindgut epithelium using

the *69B-Gal4* driver. Both proteins co-localize at the membrane with Cora, but not Crb, and display the characteristic dynamic expression of SJ proteins: at stage 12, they localize along the lateral membrane and at stage 15 become restricted apicolaterally (Fig. 25A). Occasionally, we detected a small amount of Pasiflora proteins, but not Cora, at the apical and basolateral membrane compartments. We believe that this is due to overly high protein levels under Gal4-UAS overexpression because we only observe it in a minority of cells and it correlates with the strength of expression in the given cell. Altogether, our results show that Pasiflora1 and Pasiflora2 are membrane proteins that localize at SJs.

Core SJ proteins are known to be interdependent for localization and removal

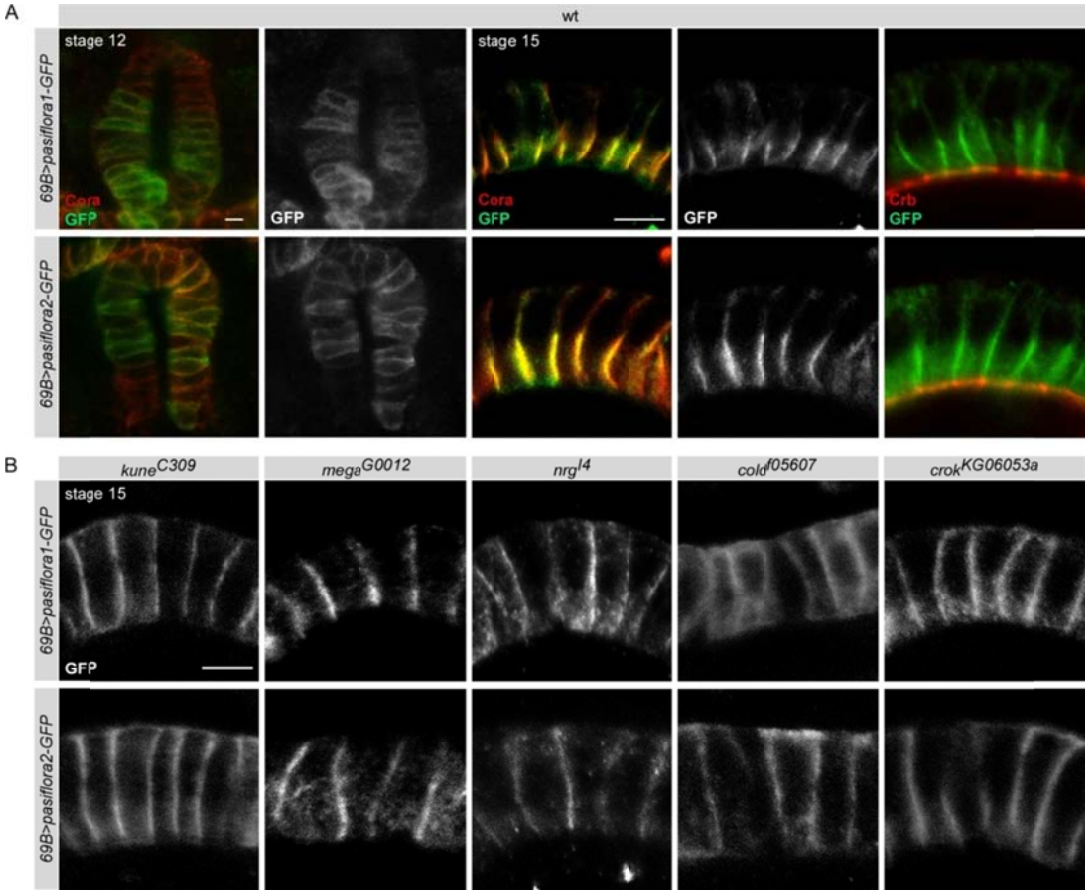

Figure 25. Pasiflora proteins localize at SJs and their localization depends on other complex components. Single confocal sections of hindguts of fixed embryos expressing Pasiflora1- and Pasiflora2-GFP. (A) In the wt, both proteins co-localize with Cora at SJs, but not with Crb. (B) In embryos mutant for different SJ genes, Pasiflora-GFP proteins lose their apicolateral accumulation and spread basolaterally. Scale bars are 5 μm. n=5-11.

of one component is sufficient to destabilize the entire complex and mislocalize other SJ proteins. To address whether Pasiflora1 and Pasiflora2 localization is similarly affected, we analyzed their distribution in the hindgut of stage 15 embryos homozygous for amorphic mutations in different SJ proteins. Co-staining for Cora served as readout of SJ integrity. In *kune*^{C309}, *mega*^{G0012}, and *nrg*^{l4} core component mutants, as well as in *cold*^{f05607} and *crok*^{KG06053a} embryos that affect complex formation, Pasiflora proteins and Cora lose their restricted localization and extend basolaterally (Fig 25B, data for Cora not shown). In summary, our results show that Pasiflora proteins localize at the SJ and their localization depends on other SJ proteins, suggesting that they are novel core complex components.

2.2.7 Pasiflora proteins are required for SJ complex assembly

To further show that Pasiflora proteins are core SJ components, we performed a series of FRAP experiments. In the epidermis of wt stage 15 embryos, when mature SJ complexes have formed, the fluorescence of GFP-tagged core SJ proteins exhibits slow recovery after photobleaching because the stable SJ complexes are very large and move slowly within the membrane. In mutants of core components or of proteins involved in complex assembly, the SJ complex is not properly formed and the free GFP-proteins can diffuse fast to the bleached region (Oshima and Fehon, 2011).

To determine if SJ complex formation is impaired in *pasiflora* mutants, we performed FRAP of Nrg-GFP in the epidermis of stage 15 embryos. For our analysis, we calculated the percentages of mobile fractions, and more importantly the characteristic time of diffusion, τ_D (see materials and methods for detailed analysis). In wt, Nrg-GFP shows very slow recovery and even 10 min after bleaching only 10% of the fluorescence has recovered. Recovery has not reached a plateau by this time, but the strong movements of the embryos did not allow us to systematically perform longer time-lapse recordings. By fitting the data, we extrapolate for Nrg-GFP in wt a τ_D of 29.5 min and 29% mobile fraction. In contrast, in both *pasiflora1*$^{\Delta}$ and *tubulin-Gal4;UAS-pasiflora2-RNAi* embryos, Nrg-GFP recovers fast (τ_D=2.2 and 4.5 min, respectively) and has a large mobile fraction (65% and 43%, respectively) (Fig.

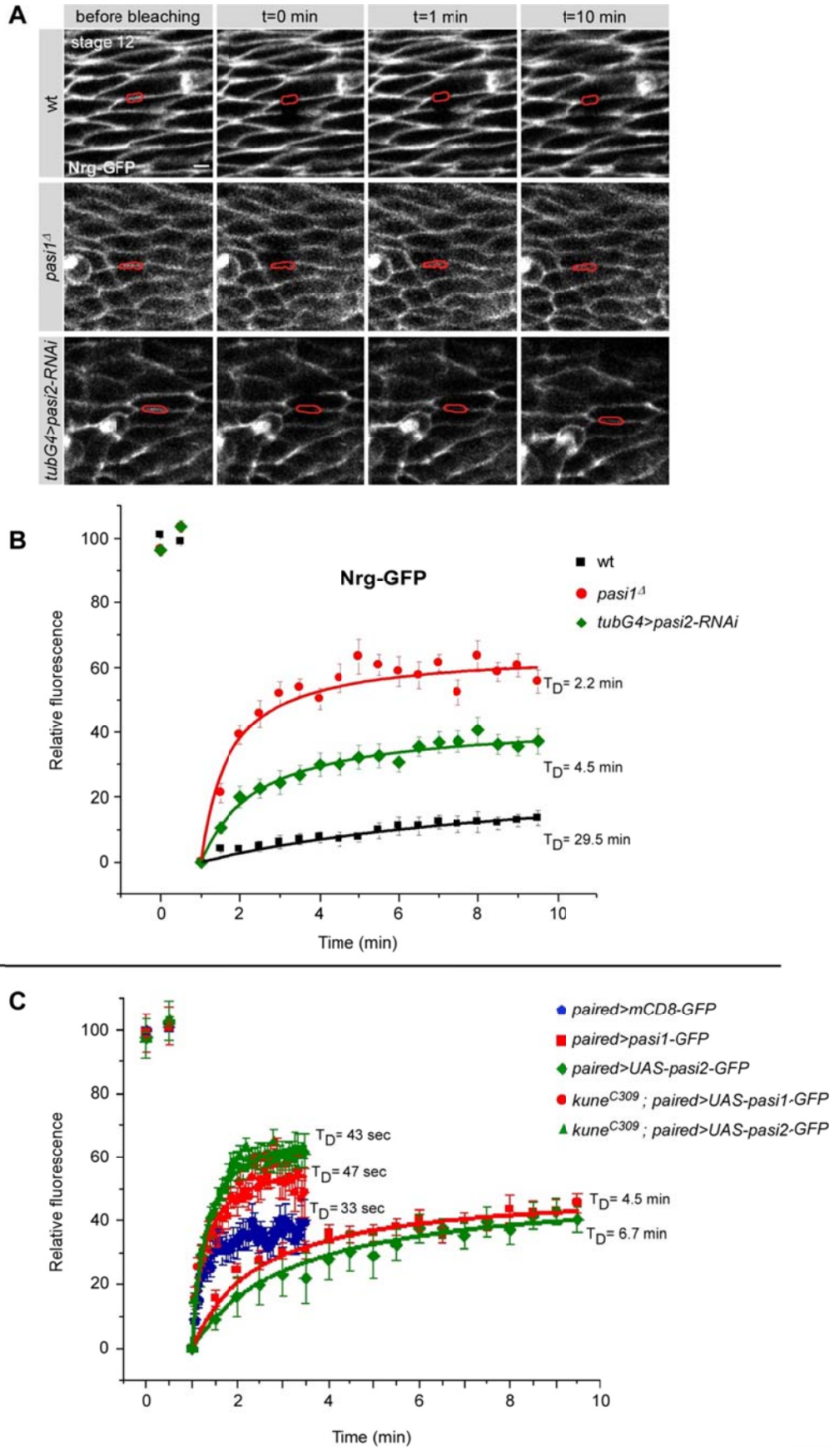
A
before bleaching
t=0 min
t=1 min
t=10 min
stage 12
wt
Nrg-GFP
pasi1Δ
tubG4>pasi2-RNAi
B
Nrg-GFP
wt
pasi1Δ
tubG4>pasi2-RNAi
Relative fluorescence
Time (min)
TD= 2.2 min
TD= 4.5 min
TD= 29.5 min
C
paired>mCD8-GFP
paired>pasi1-GFP
paired>UAS-pasi2-GFP
kuneC309 ; paired>UAS-pasi1-GFP
kuneC309 ; paired>UAS-pasi2-GFP
Relative fluorescence
Time (min)
TD= 43 sec
TD= 47 sec
TD= 33 sec
TD= 4.5 min
TD= 6.7 min

Figure 26. Pasiflora proteins are core components of the SJ. (A-B) *pasiflora* genes are required for SJ complex formation. (A) Single confocal sections of lateral epidermis of stage 15 embryos expressing live Nrg-GFP. Nrg-GFP shows restricted mobility after photobleaching in the wt, but diffuses fast to the bleached region in *pasiflor*a mutants. Bleached membranes are marked in red. Scale bars are 5 μm. (B) Quantification of relative fluorescence of Nrg-GFP over time in wt and *pasi* mutants, ±SEM. (C) Quantification of relative fluorescence of Pasiflora-GFP proteins over time showing that in wt, Pasiflora proteins are more immobile compared to a membrane bound mCD8-GFP. In *kune* mutants with disrupted SJs, Pasiflora proteins lose their restricted mobility. ±SEM. n=9-17.

26A,B). Therefore, the behavior of Nrg-GFP in *pasiflora* mutants is similar to that observed in mutants of core SJ components and proteins involved in complex assembly. Together with their localization at SJ, these results argue that Pasiflora proteins are core components required for formation of SJ complexes.

To further show that Pasiflora proteins are integral SJ components, we analyzed their mobility within the membrane in the epidermis of stage 15 embryos. To this end, we used *paired-Gal4* and expressed GFP-tagged Pasiflora proteins in epidermal stripes. As a control, we used membrane tagged mCD8-GFP and imaged embryos at stage 14, at a time when SJs are not yet fully mature and diffusion within the plasma membrane should not be impeded. mCD8-GFP recovers remarkably fast (τ_D=33 sec) and its mobile fraction is 40%. In contrast, the recovery of Pasiflora1- and Pasiflora2-GFP is significantly slower (τ_D=4.5 min and 6.7 min, respectively), with their mobile fractions being 50%. The faster recovery rate of Pasiflora-GFP proteins compared to Nrg-GFP could be due to overexpression conditions (Fig. 26C). Therefore, Pasiflora proteins are more immobile compared to other transmembrane proteins, suggesting that they are part of a membrane complex. Together with all our other data, this result strongly suggests that Pasiflora proteins are core components of the SJ complex. To ultimately prove this conclusion, we analyzed the mobility of Pasiflora-GFP proteins in epidermal cells of $kune^{C309}$ mutants that have disrupted SJs and observed that both proteins lose their restricted mobility and diffuse very fast (Pasiflora1-GFP: τ_D=47 sec, mobile fraction 59%; Pasiflora2-GFP: τ_D=43 sec, mobile fraction 67%) (Fig. 26C). Interestingly, their mobile fractions are larger compared to that of mCD8-GFP in wt stage 14 epidermal cells, further supporting the notion that SJs also serve a fence function that is likely

established before barrier function. Collectively, our results show that Pasiflora proteins are core components of the SJ complex (Fig. 27).

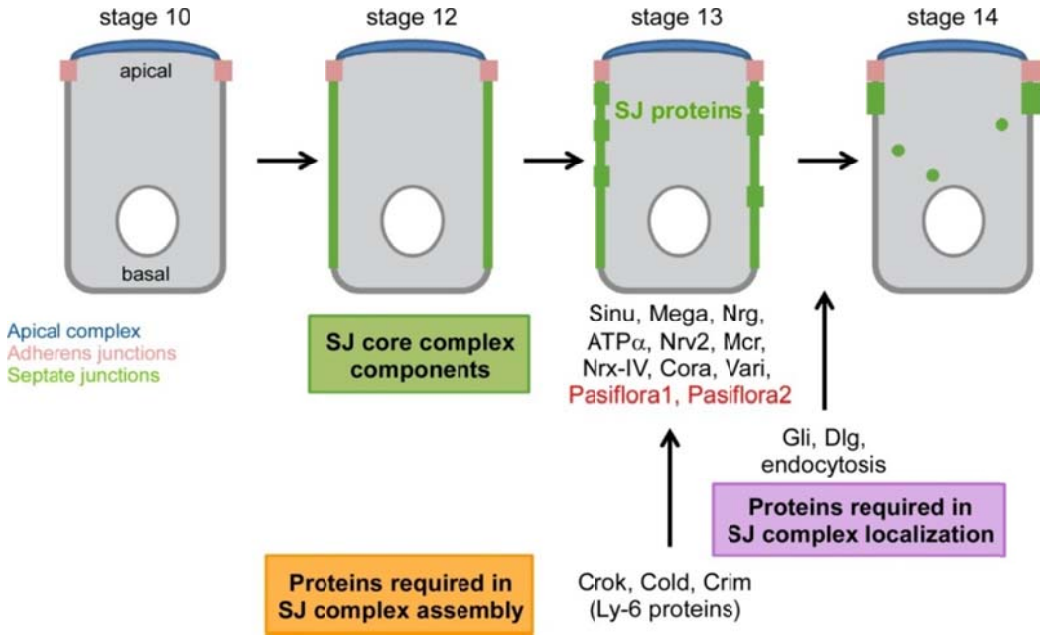

Figure 27. Timeline and players of SJ morphogenesis. The SJ complex consists of several core components, including the novel Pasiflora proteins. Ly-6 proteins are required for assembly of (sub)complexes at stage 13, while endocytosis and the SJ proteins Gli and Dlg are essential for complex relocalization at stage 14 (model modified from Oshima and Fehon, 2011).

2.3. Mcr is a novel septate junction component

2.3.1 Introduction –Mcr and other thioester proteins

Thioester proteins (TEPs) appeared early in animal evolution and are found in such diverse organisms as nematodes, insects, fish and mammals. In vertebrates, the TEP family includes complement factors (C3, C4A, C4B and C5), secreted broad-range protease inhibitors (α2-macroglobulin, PZP), and other less characterized members (e.g. CD109, CPAMD8, Ovostatin-1 and -2). TEPs contain a hypervariable region and most share the conserved motif GCGEQ, which allows for the formation of a highly reactive intrachain thioester bond. The thioester binds pathogen surfaces (in the case of complement factors) to mediate their opsonization and subsequent phagocytosis or lysis, and to proteases (in the case of protease inhibitors) to mediate their inhibition (Dodds and Law, 1998; Blandin and Levashina, 2004). The mechanism of protease inhibition is mostly studied for α2-macroglobulin (α2M) and involves steric hindrance. Upon proteolytic cleavage of a ‘’bait’’ region (that corresponds to the hypervariable region) from the attacking protease, α2M undergoes a conformational change that is linked to the cleavage of the thioester bond. α2M then covalently binds the protease to the exposed thioester, collapses about the protease and sterically shields its active site. The conformational change also exposes a conserved C’-terminal recognition domain that mediates clearance of the α2M-protease complex by receptor-mediated endocytosis (Borth, 1992).

Insects also encode several TEPs, which are thought to play roles in innate immunity, however, the functions of individual members are poorly understood. The *Drosophila* genome has six *tep* genes named *tep1-tep6*. Tep1-Tep4 are predicted secreted proteins expressed in hemocytes and are thought to be involved in the response to pathogens, while *tep5* appears to be a pseudogene. Tep6 or Macroglobulin complement-related (Mcr) is a diverged member of the family. While Mcr has N’- and C’-terminal α2M domains, LDLα domain and N’-terminal signal peptide also found in other TEPs, its thioester motif is mutated and it has a predicted C’-terminal transmembrane domain (Fig. 30A), suggesting that it might play distinct roles (Blandin and Levashina, 2004; Stroschein-Stevenson et al., 2006; Bou Aoun et al., 2011). Nevertheless, *Drosophila mcr* was identified in an RNAi screen for genes required for phagocytosis of the yeast *Candida albicans* and in a transcriptome profiling of genes upregulated after infection with the alphavirus Sindbis (Stroschein-

Stevenson et al., 2006; Mudiganti et al., 2010). Although both experiments were conducted in S2 cells leaving unanswered whether the protein plays a similar role in pathogen clearance *in vivo*, its expression in hemocytes at least during larval stages supports such a role (Bou Aoun et al., 2011; Hall et al., 2014) . In addition, the *Aedes aegypti* homologue of Mcr is part of a defense cascade that limits flaviviral infections in adult mosquitos (Xiao et al., 2014). The human protein most closely related to Mcr is CD109, a GPI-anchored protein whose functions have not been fully explored that however contains the sequence required to form the thioester bond (Lin et al., 2002; Solomon et al., 2004) (Fig. 28). Recently, two independent studies characterized Mcr as a component of the *Drosophila* SJ (Bätz et al., 2014; Hall et al., 2014). The experiments published were very similar to those that we had been performing, therefore we decided to abandon this project although it was close to its end. However, our work that led to the identification of Mcr as a novel SJ protein will be reported here.

2.3.2 *mcr* is required for blood-brain barrier formation

Through our glial screens, we identified the $mcr^{KK100197}$ RNAi line that caused complete adult lethality in the *repo-Gal4* screen and adult subviability in the *moody-Gal4* screen (32% survived; 52% for negative controls). Pan-glial knock-down of *mcr* results in embryonic lethality (2% hatch; wt: 99%) and dye penetration into the nerve cord (Fig. 28A, E). To exclude off-target effects, we generated a second *UAS-RNAi* line (*UAS-mcr-shRNAi*), which expresses a 21 nt siRNA targeting a non-overlapping sequence of the mRNA. Pan-glial knock-down using the *UAS-mcr-shRNAi* line also causes embryonic lethality (4% hatch) and leaky BBB (Fig 28A, D). Therefore, our results suggest that *mcr* is required in glia for BBB formation.

To study the phenotype of *mcr* under stronger loss of function conditions, we searched for lines with P-element insertions within or around the *mcr* locus. We found the adult homozygous lethal line $P\{EPgy2\}mcr^{EY07421}$ (thereafter called $mcr^{-/-}$) that has a P-element inside the *mcr* 5'UTR, 24 nucleotides downstream of the transcription start site. $mcr^{-/-}$ embryos show strong dye penetration into the nerve cord and die at the end of embryogenesis (0% hatch) (Fig. 28A, B, D). Because the P-element does not disrupt the coding sequence of *mcr*, $mcr^{-/-}$ likely represents a hypomorphic mutant; however, due to its strong phenotypes, we decided to use it to pursue studying *mcr*. Interestingly, *mcr* is the only *Drosophila tep* gene whose loss of

function is causing lethality, suggesting that it might have distinct functions from other family members (Bou Aoun et al., 2011). Embryos transheterozygous for *mcr*$^{-}$ and the deficiency chromosome *Df(2L)Trf-C6R31*, which deletes *mcr* and only four more genes, show dye leakage, further supporting that loss of *mcr* is causing the BBB phenotype (Fig. 28A, B). Moreover, we mobilized the P-element and isolated a line (*mcr*^{Pex1}) with a precise P-element excision. Similar to wt, *mcr*^{Pex1} homozygous embryos hatch (97% hatch), do not show dye penetration into the CNS and give rise to viable, fertile adults (Fig. 28 A,B,E), indicating that there are no second-site mutations in the chromosome contributing to the leaky BBB. Finally, pan-glial overexpression of *mcr* rescues the dye penetration of the *mcr*$^{-/-}$ mutant (Fig. A,B) demonstrating that *mcr* is required cell-autonomously in glia for BBB formation.

To exclude that the BBB permeability is a secondary consequence of earlier defects in glial specification and/or migration, we stained wt, *repo-Gal4;UAS-mcr-RNAi*^{KK}, and *mcr*$^{-/-}$ embryos with the Repo antibody and visualized the ventral-most SPG. The full complement of SPG nuclei is detected in all genotypes at their stereotyped positions (Fig 28C). Taken together, our results show that *mcr* is required in glia and plays a specific role during BBB formation.

2.3.3 *mcr* is required for tracheal tube size and barrier function

Our result that pan-glial overexpression of *mcr* rescues the embryonic BBB phenotype but not the lethality of the *mcr*$^{-/-}$ mutant prompted us to examine the embryos for additional developmental defects. To investigate if other barriers are compromised in *mcr*$^{-/-}$ embryos, we examined the trachea. We injected dye in the body cavity of late stage 17 embryos and visualized the dorsal trunks. In *mcr*^{Pex1} embryos, the dye is excluded from the tracheal lumen, but it rapidly diffuses into the tubes of *mcr*$^{-/-}$ embryos. In addition, the mutants have excessively elongated and convoluted dorsal trunks, as also visualized by staining stage 16 embryos with the 2A12 antibody. In addition, the 2A12 staining appears patchy and non-continuous in the mutant suggesting that its apical secretion into the tubes might be impaired. As expected, the tracheal defects of the mutant are not restored when overexpressing *mcr* in glia, further supporting that *mcr* is cell-autonomously required (Fig. 28E). In summary, our results show that *mcr* is required for tracheal paracellular barrier integrity and control of tube size.

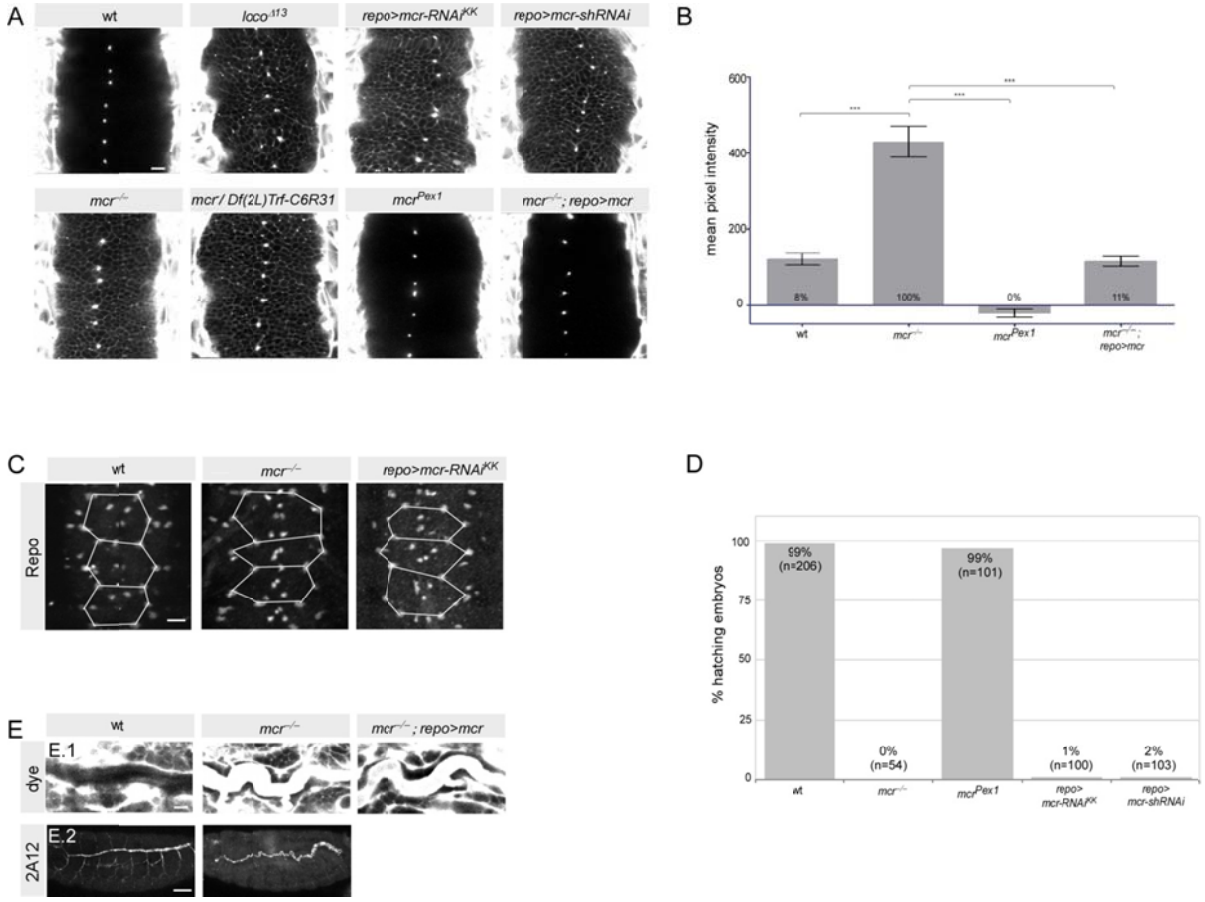

Figure 28. *mcr* is required for formation of blood-brain and tracheal barriers. (A-C) *mcr* is required for BBB formation. (A) Single confocal sections of 20 h AEL dye-injected embryos of different genotypes. Dye diffuses into the nerve cord of *loco* positive controls and in the loss of *mcr*, as opposed to wt (w^{1118}) embryos. Pan-glial overexpression of the *mcr* CDS rescues the dye penetration of the *mcr* mutant. Anterior is up. (B) Quantification of dye penetration assay. Raw data are plotted. Columns represent intensity of dye penetration into nerve cord as measured by mean pixel intensity. The percentage of embryos showing penetration is indicated at the bottom of each column. Brackets and asterisks indicate significance of pairwise comparisons. *** $p<0.001$, ±SEM, n=17-52. (C) Ventral surface views of stage 16 embryonic nerve cord stained with Repo. The full complement of SPG is detected in loss of function of *mcr*. The positions of nuclei are similar between the genotypes, as visualized by overlay of connecting lines. Three abdominal neuromeres are shown. Maximum projections of 4 µm z-stacks. n=8-19. (D) Quantification of embryonic survival of different genotypes showing that loss of *mcr* results in late embryonic lethality. Columns represent the percentage of embryos that hatched. The number of aligned embryos is indicated at the top of each column. (E) *mcr* is required for tracheal barrier formation and control of tube length. (E.1) Single confocal sections of 20 h AEL dye-injected embryos. Dye does not diffuse in the tracheal lumen of wt (mcr^{Pex1}), but penetrates in *mcr* mutants. Glial overexpression of *mcr* does not rescue the tracheal phenotype of the mutant. Lateral views of dorsal trunk. n= 7-14. (E.2) Lateral views of stage 16 embryos stained with

2A12. *mcr* mutants have over-elongated and convoluted dorsal trunks, as opposed to wt (mcr^{Pex1}). Maximum projections of 20 µm z-stacks. n=10-12. Anterior is left and dorsal is up. Scale bars are 10 µm except for images with 2A12 staining where they are 40 µm.

2.3.4 *mcr* is required for localization of SJs

Due to the phenotypes of permeable blood-brain and tracheal paracellular barriers, we hypothesized that SJs are compromised in the $mcr^{-/-}$ mutant. To visualize SJs in the embryonic BBB, we used the endogenously expressed live markers Nrg-, Lac-, and ATPα-GFP. In contrast to wt, where intact SJs are formed and all markers continuously label the periphery of SPG, in $mcr^{-/-}$ embryos, SJs appear severely disorganized and in many cases almost absent (Fig. 29A). Therefore, *mcr* is required for SJ formation between SPG.

To examine whether SJ localization along the lateral membrane is disturbed in $mcr^{-/-}$ embryos, we analyzed the hindgut and trachea columnar epithelia. In the hindgut of stage 15 wt embryos (mcr^{Pex1} or w^{1118}), the SJs markers Nrg-GFP, Cora, ATPα and FasIII accumulate at the apicolateral membrane, while in $mcr^{-/-}$ embryos, they lose their restricted localization and spread basolaterally (Fig. 29C). Interestingly, Nrg-GFP shows a differential behaviour and also spreads at the apical membrane (arrow in Fig.29C). In addition, ATPα is not as affected and its phenotype is highly variable and not fully penetrant; i.e some embryos show wt localization, some a mixture of cells with restricted and dispersed localization, and others with mislocalization in all cells. Similarly, in tracheal cells of stage 15 $mcr^{-/-}$ embryos, FasIII loses its apicolateral accumulation and spreads at the basolateral membrane compartment (Fig. 29B). In both trachea and hindgut, the localization of the apical membrane determinant Crb is preserved, indicating that loss of *mcr* does not affect the establishment or maintenance of cell polarity (Fig. 29B,C). Moreover, the levels of SJ proteins appear reduced in $mcr^{-/-}$ embryos in all tissues observed. Collectively, our results show that *mcr* is specifically required for the apicolateral localization of SJs in the columnar epithelia of hindgut and trachea.

2.3.5 Mcr is a plasma membrane protein

The suite of phenotypes observed in *mcr* mutants is commonly associated with disrupted SJs, therefore, we speculated that Mcr is a SJ component itself or is involved in the assembly and/or trafficking of SJ complexes. Furthermore, the *mcr*

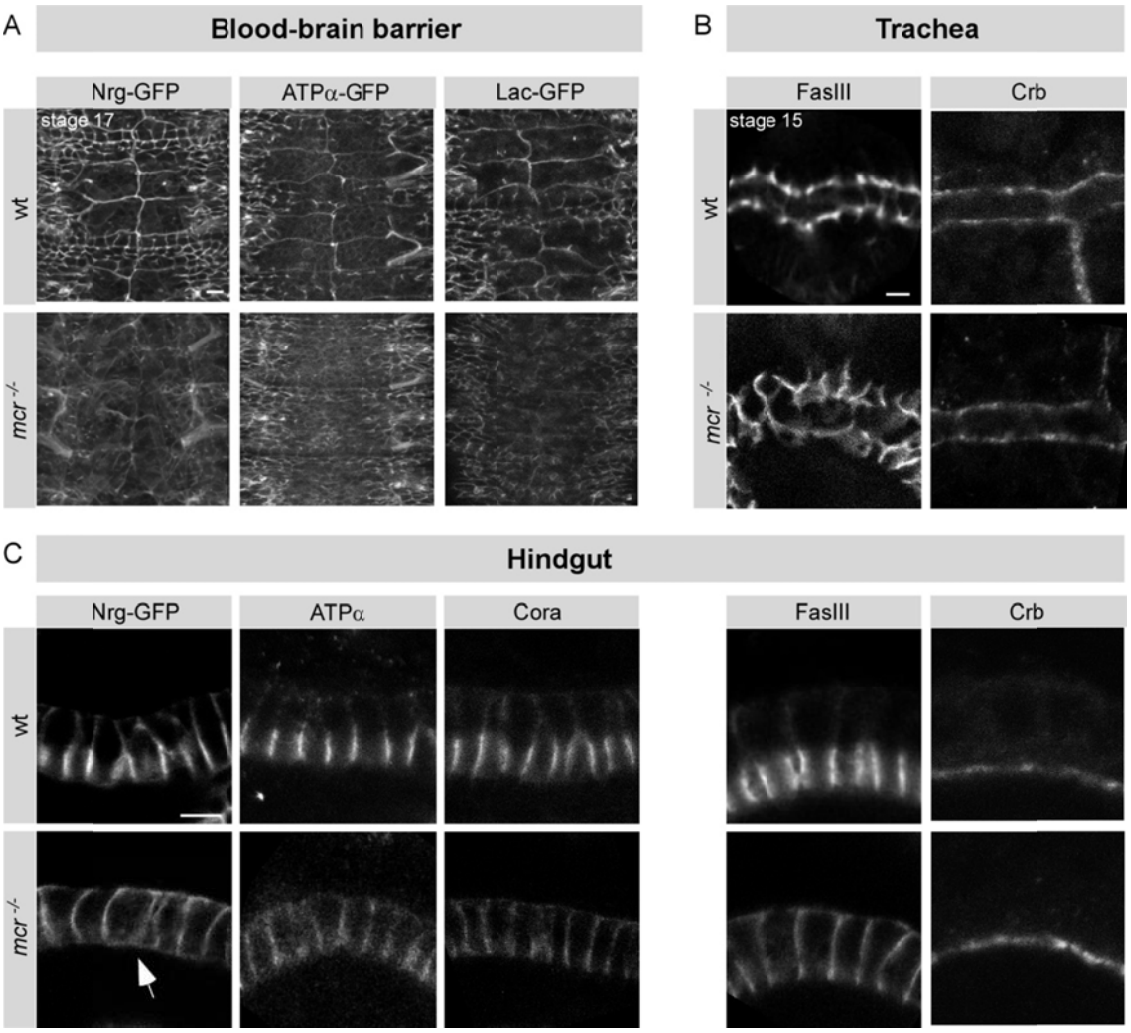

Figure 29. *mcr* is specifically required for localization of SJs. (A) Ventral surface views of nerve cord of 20 h AEL embryos expressing the live SJ markers Nrg-, ATPα- and Lac-GFP. SPG SJs are almost absent in the *mcr* mutant. Maximum projections of 10-11 µm z-stacks. Anterior is up. Scale bars are 10 µm. n=6-13. (B) Single confocal sections of stage 15 dorsal trunks stained for the SJ marker FasIII and the apical membrane determinant Crb. In *mcr* mutants, FasIII spreads basolaterally, but Crb localization is preserved. Scale bars are 5 µm. n=5-9. (C) Single confocal sections of stage 15 hindguts stained for SJ proteins and Crb. In *mcr* mutants, SJ proteins spread basolaterally, but ATPα shows milder and not fully penetrant phenotype. Note that Nrg-GFP also spreads at the apical membrane (arrow). Cell polarity is preserved. Scale bars are 5 µm. n=6-32.

mRNA is a predicted target of miR-184, which targets more than half of known SJ mRNAs (Hong et al., 2009; Iovino et al., 2009; www.microrna.org) and based on developmental RNA-seq, *mcr* is part of a co-expression cluster together with several

SJ genes (*sinu*, *nrx-IV*, *pasi2*, *gli*, *crok*, *cold*, *crim*) (Graveley et al., 2011), further strengthening our hypothesis. The only surprising finding for us was that full length Mcr was previously reported to be secreted in media by cultured S2 cells (Stroschein-Stevenson et al., 2006). First, a transmembrane rather than a secreted nature for Mcr would more easily explain our observation that the gene is cell autonomously required, and second, among the many proteins involved in the formation of SJs, no role for secreted proteins has been demonstrated so far.

Mcr is a large, 1760 amino acids long protein with a predicted molecular weight of 203 kDa. It contains an N'-terminal signal peptide and a C'-terminal transmembrane domain. Protein topology analysis predicts that Mcr is a single-pass membrane protein with a short intracellular C'-tail of only 15 amino acids and a large extracellular region, which contains the α2M and LDLα domains (Fig. 30A). We therefore sought to characterize if Mcr (also) localizes at the plasma membrane or some intracellular membrane compartment. We tagged Mcr at the C'-terminus with 3x-FLAG and expressed the fusion protein in S2 cells. In immunoblots using an anti-FLAG antibody, we detect a band of approximately 220 kDa, corresponding to the full length protein, only in cell lysates and not in culture media (Fig. 30B). In addition, in immunostainings Mcr localizes at the plasma membrane of S2 cells, while occasionally, we also detected weaker staining in the cytoplasm (Fig. 30B). Because Stroschein-Stevenson et al. detected the protein in media using an Mcr-specific antibody that targets an epitope at the N'-terminus, while we used C'-terminally tagged Mcr, it is possible that part of the Mcr protein pool is cleaved just upstream of the transmembrane domain and appears as a band of almost the full protein size in culture media. Although we cannot exclude that Mcr plays a role as a secreted protein as well, our results in S2 cells, together with the cell-autonomous requirement of the gene *in vivo* suggest that Mcr localizes at the plasma membrane and performs a function there.

We next sought to determine if Mcr also localizes at the plasma membrane *in vivo*. Surprisingly, although glial expression of FLAG-tagged Mcr rescues the BBB dye penetration of the $mcr^{-/-}$ mutant, we observe variable, very weak and in some cases undetectable FLAG staining in the embryo when using different Gal4 drivers (*repo-Gal4*, *btl-Gal4*, *69B-Gal4*; data not shown). Similarly, Mcr C'-tagged with GFP and two different sizes of linkers separating the molecules also shows inconclusive GFP expression both in S2 cells and in third instar larval CNS *in vivo* (*moody-Gal4*)

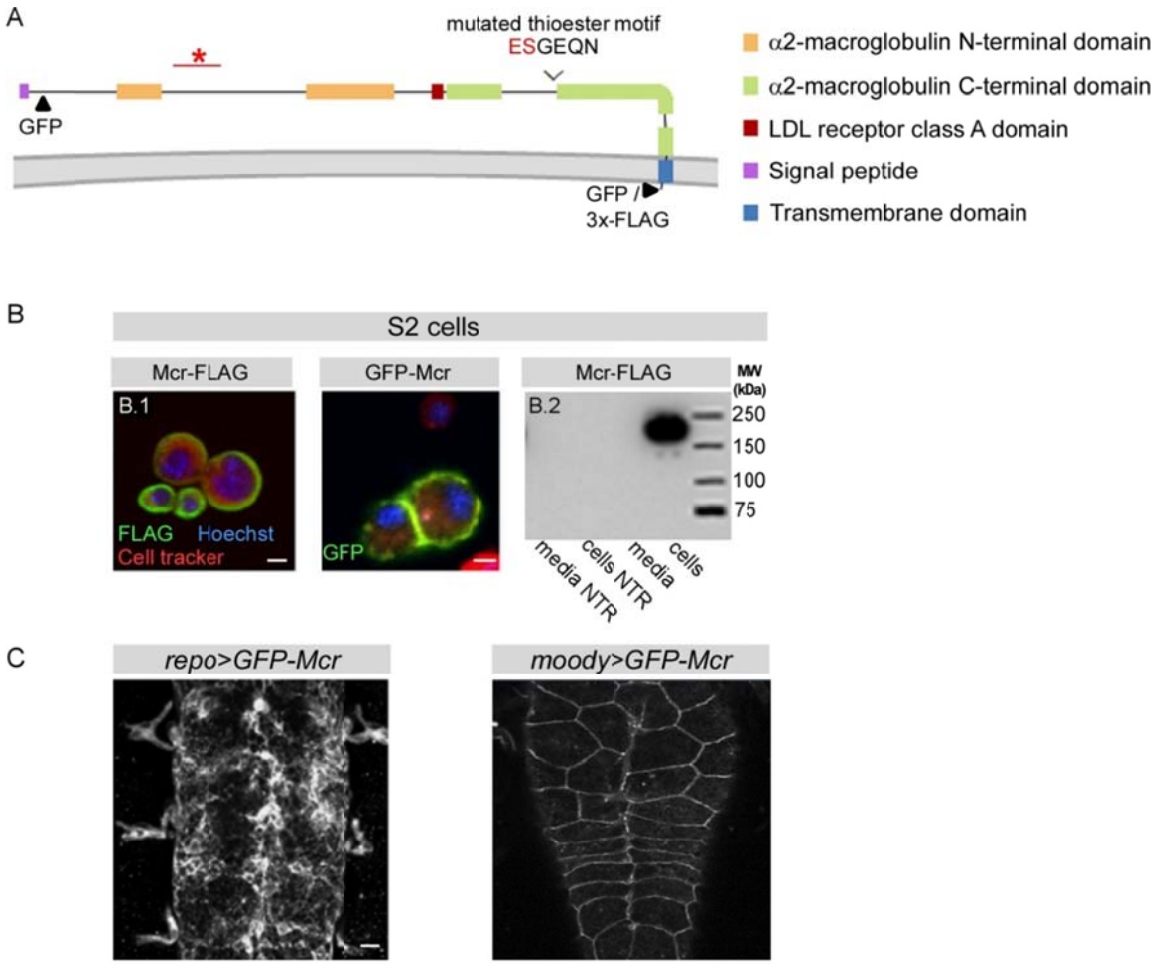

Figure 30. Mcr is a plasma membrane protein. (A) Predicted topology and domains of Mcr protein. The site of fusions of GFP/FLAG tags are highlighted with black arrowheads and the epitope used for antibody production with red asterisk. The mutated amino acids in the thioester motif are marked in red. (B) Tagged versions of Mcr localize at the plasma membrane in S2 cells. (B.1) Single confocal sections of S2 cells transiently transfected with C'-tagged Mcr-FLAG and N'-tagged GFP-Mcr. Scale bars are 10 μm. (B.2) Immunoblot of S2 lysates and media using a C'-terminally FLAG-tagged Mcr. NTR: Non-transfected cells. (C) N'-terminally tagged GFP-Mcr localizes at the plasma membrane *in vivo*. (C.1) Ventral views of fixed stage 16 embryos expressing GFP-Mcr in glia. Maximum projections of 15 μm z-stacks. Scale bar is 10 μm. (C.2 Third instar larval CNS expressing live GFP-Mcr in SPG. Maximum projections of 3 μm z-stacks. Scale bar is 20 μm. Anterior is up.

(data not shown). On the contrary, fusion of GFP at two different sites near the N'-terminus, downstream of the signal peptide leads to protein efficiently tagged with GFP. N-tagged Mcr-GFP localizes at the plasma membrane and marks the outlines

of glia in the embryo (*repo-Gal4*) and SPG in third instar larval CNS (*moody-Gal4*) (Fig. 30C). Therefore, our *in vivo* results show that Mcr localizes at the plasma membrane. In addition, our findings suggest that tagging of Mcr at the C'-tail might sterically inhibit GFP from fluorescing.

2.3.6 *mcr* is expressed in SJ-forming epithelia and glia

To characterize the expression pattern of *mcr* during embryogenesis, we performed RNA *in situ* hybridization in wt embryos using antisense *mcr* probes. Expression is first detected at stage 10 in tracheal placodes and at stage 11 in the hindgut. During stages 12-16 trachea, foregut, hindgut, epidermis and salivary glands are labeled, but not the endodermally-derived midgut. At stage 16 embryos all insulating glia of the CNS and PNS are marked, i.e. SPG, channel and peripheral glia (Fig. 31A). Therefore *mcr* is expressed in SJ-forming embryonic epithelia and glia.

To study the distribution of the Mcr protein we raised a polyclonal antibody against a non-conserved, 118 amino acids long peptide (Fig. 30A). Similar to the published data (Bätz et al., 2014; Hall et al., 2014), on preliminary immunoblots of stage 16 wt embryonic extracts, we detect a strong band of approximately 240 kDa corresponding to full length Mcr, as well as bands of lower molecular weight, which might represent degradation products or processed forms. The protein levels appear strongly reduced and almost absent in extracts of $mcr^{-/-}$ and $mcr^{-}/Df(2L)Trf\text{-}C6R31$ embryos, respectively and increased in embryos with pan-glial (*repo-Gal4*) and ubiquitous (*tub-Gal4*) *mcr* overexpression, demonstrating that the antibody is specific for Mcr (data not shown). To further check its specificity, we stained embryos ectopically expressing *mcr* in epidermal stripes using the *paired-Gal4* driver (Fig. 31B.3). In wt, embryos, the Mcr antibody stains the membranes of ectodermally-derived epithelia and PNS glia and recapitulates most of the expression revealed by RNA *in situ* (Fig. 31B.1-B.2). Collectively, our RNA and protein expression results show that *mcr* is expressed in embryonic epithelia and glia that form insulating SJs.

2.3.7 Mcr localizes at the SJ and its localization depends on other complex components

To examine if Mcr localizes at the SJ, we stained wt embryos with the Mcr and Cora antibodies and focused on the columnar tracheal and hindgut epithelia. We observed that Mcr colocalizes with Cora and exhibits the dynamic expression pattern of SJ

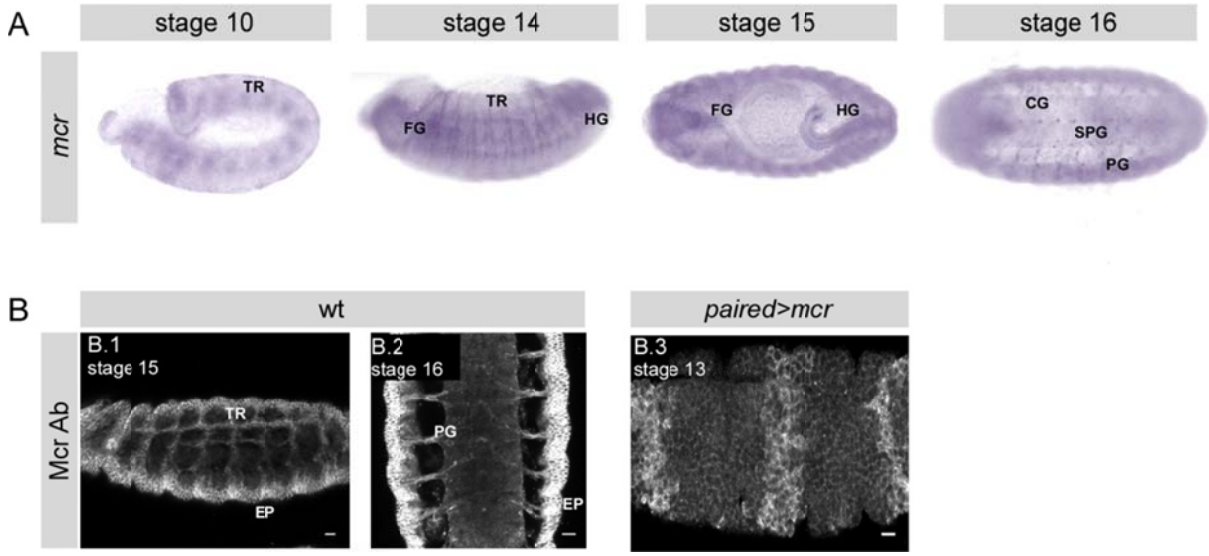

Figure 31. Mcr is expressed in SJ-forming embryonic epithelia and glia. (A) RNA *in situ* hybridization for *mcr* in w^{1118} embryos. *mcr* transcripts are detected from stage 10 onwards. Anterior is left. (B) The generated antibody successfully recognizes Mcr. (B.1-B.2) wt embryos stained with the Mcr antibody. Maximum projections of 5 (B.1) and 12 (B.2) µm z-stacks. Scale bars are 40 µm. (B.2) Lateral view of embryo overexpressing Mcr in epidermal stripes stained with the Mcr antibody. Maximum projection of 11 µm z-stack. Scale bar is 10 µm. epidermis (EP), foregut (FG), hindgut (HG), subperineurial glia (SPG), channel glia (CG), peripheral glia (PG), trachea (TR).

proteins: at stage 12, it accumulates along the lateral membrane, and at stage 15 is restricted apicolaterally (Fig. 32A). Overall, the Mcr antibody does not label SJs as strong as the Cora antibody, however, we certainly did not exhaust our efforts with these stainings. Similarly, N'-terminally tagged GFP-Mcr, when expressed with the *69B-Gal4* driver, colocalizes with Cora at SJs of stage 15 hindgut epithelial cells (Fig. 32B). Because SJ proteins typically display interdependence for localization, we sought to determine if Mcr localization also depends on other complex components. To this end, we analyzed the localization of GFP-Mcr (expressed with *69B-Gal4*) in the hindgut of $kune^{C309}$ and $cold^{f05607}$ SJ mutants. In both mutants, GFP-Mcr loses its restricted localization and spreads basolaterally (Fig. 32B). Therefore, Mcr localizes at the SJ and its accumulation there depends on other SJ proteins, suggesting that it likely is a core component of the SJ.

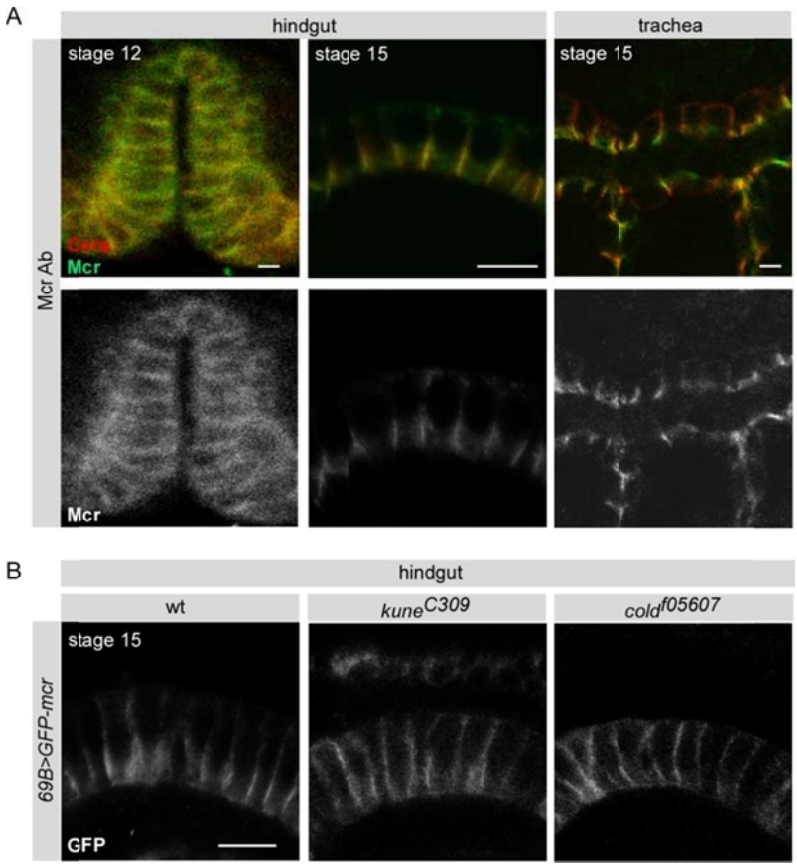

Figure 32 . Mcr localizes at SJs and its localization depends on other complex components. Single confocal sections of hindgut and trachea of fixed embryos. (A) In wt, endogenous Mcr co-localizes with Cora at SJs in stage 12 and stage 15 embryos. (B) N'-tagged GFP-Mcr localizes at the apicolateral membrane in wt hindgut epithelium, but spreads basolaterally in embryos mutant for SJ-associated proteins. Scale bars are 5 μm. n=5-6.

2.4 Discussion

2.4.1 Pasiflora proteins and Mcr are novel SJ components

Through our *in vivo* glial screens, we have identified three proteins, Pasiflora1, Pasiflora2 and Mcr and showed that they are novel components of the *Drosophila* SJ. Pasiflora1 and Pasiflora2 were previously uncharacterized proteins that belong to the same family (With et al., 2003) and Mcr, based on experiments conducted in S2 cells, was reported to be a secreted protein involved in phagocytosis of pathogens (Stroschein-Stevenson et al., 2006). Several lines of evidence support that all three proteins are SJ components. First, the mutants exhibit the characteristic

phenotypes associated with disrupted SJs: breakdown of blood-brain and tracheal barriers, over-elongated dorsal trunks, and mislocalization of SJs in a variety of tissues. In the BBB, SJs appear discontinuous and severely disorganized and in columnar epithelia, SJ proteins fail to localize at the apicolateral membrane and spread basolaterally. At least in columnar epithelia, the SJ mislocalization is not a result of disturbed cell polarity as the apical accumulation of Crb is preserved. Second, the genes are co-expressed in embryonic epithelia and glia that rely on SJs for their function and the proteins co-localize with Cora at the apicolateral membrane of columnar epithelia, where SJs form. Similar to known SJ proteins, their restricted localization depends on other complex members, as they spread at the basolateral membrane in SJ mutants. Finally, for the Pasiflora proteins we use FRAP and demonstrate that they are core components. At stage 15 epidermal cells, when SJ complexes have fully assembled, the core component Nrg-GFP displays limited lateral mobility after photobleaching due to its incorporation in the large multi-protein complex. In contrast, in *pasiflora* mutants, Nrg-GFP diffuses fast in the bleached region, indicating that complex formation is compromised. Overexpressed Pasiflora proteins also move slowly within the membrane of wt cells, while they display fast diffusion in mutants with disrupted SJs, showing that they are themselves associated with the SJ complex.

A puzzling observation is that SJ fluorescence never recovers to 100% in our FRAP experiments or those of others (Laval et al., 2008; Oshima and Fehon, 2011) as would be expected from full recovery of diffusing GFP-proteins. This reveals the presence of an immobile or extremely slow fraction of GFP-proteins within our observation time whose nature remains largely obscure. One of the factors contributing to the two distinct populations of diffusing proteins may lie in the genetics. *pasiflora1* is studied in zygotic mutant embryos although the gene is also maternally expressed and *pasiflora2* by RNAi; these incomplete loss of function conditions contribute to the broader distribution of fluorescence recovery times. However, more surprisingly, partial recovery is also observed for mCD8-GFP, suggesting the existence of additional sources of traps for the proteins. One possibility is that at early stages, before insulating SJ complexes have formed, SJs already operate as a fence limiting free mobility within the plane of the membrane, hindering diffusion of a fraction of the GFP-proteins. The fact that in SJ mutant

backgrounds the mobile fractions of Pasiflora-GFP proteins are larger compared to that of mCD8-GFP in wt epidermal cells further supports such a fence function.

2.4.2 Potential roles of Pasiflora proteins

Pasiflora1 and Pasiflora2 are predicted to be small proteins with four transmembrane domains, two extracellular loops of which the first is bigger, and both termini located intracellularly. Although the proteins lack putative conserved motifs that can classify them as orthologues of any known proteins and thus define a distinct family, in a wider context, they show structural similarity to a large superfamily of small tetra-spanning membrane glycoproteins. The superfamily includes proteins that play roles in specialized cell contacts, such as TJ-associated claudins, PMP22/EMP/MP20 proteins, voltage-gated calcium channel γ subunits (CACNGs), TMEM47 family members, clarins, tetraspanins and even the larger gap junction proteins connexins and innexins (Adato et al., 2002; Simske, 2013) . Based on structural and topological similarity and the shared role as occluding junction components, Pasiflora proteins mostly resemble claudins. Claudins have been shown to oligomerize homo- and heterophilically on the same cell and homo- and hetero-typically on adjacent cells with heterophilic oligomerization appearing to be more frequent than heterotypic binding (Koval, 2013). In addition, in electron micrographs, both TJs and SJs appear as a set of linear arrays, and vertebrate and invertebrate claudins may contribute to the formation of these structures. An important question will be to determine whether Pasiflora proteins can interact with each other in a similar fashion and together with claudins build the stacks of regularly spaced SJ septa that span the intercellular space. It is also tempting to speculate that similarly to vertebrate claudins, the first extracellular loop of Pasiflora proteins participates in regulating tightness of SJs. However, such functions have not been demonstrated for *Drosophila* claudins either, and *Drosophila* SJs do not contain fusions of adjacent cell membranes like TJs, but rather maintain a separation across the paracellular space at the junction. Alternatively, Pasiflora1 and Pasiflora2 might associate with each other to organize and build on the membrane an interacting network of SJ proteins. Tetraspanins play such roles in organizing other proteins into multimolecular membrane microdomains, called the tetraspanin web (Fradkin et al., 2002; Charrin et al., 2009). Finally, Pasiflora proteins might be palmitoylated; one such site is predicted for Pasiflora1 in position 7 (http://csspalm.biocuckoo.org). In claudins and tetraspanins, palmitoylation

has been shown to promote their partitioning into membrane microdomains and assembly into higher order structures (Findley and Koval, 2009). In any case, the highly transmembrane nature of Pasiflora1 and Pasiflora2 suggests a role for the proteins as central structural subunits of the SJ.

Pasiflora1 and Pasiflora2 belong to a previously uncharacterized family of four-pass membrane proteins conserved in *Drosophila* and *Anopheles*. The fly encodes nine family members, albeit distantly related (With et al., 2003). We demonstrated that Pasiflora proteins are expressed in embryonic epithelia and glia and act non-redundantly in SJ formation. So far, little is known about the expression of other family members and there are no data as to their function or subcellular localization. Interestingly, during epithelial morphogenesis large families of junctional proteins, such as the tetraspan claudins and innexins and the single-pass cadherins are often used in a tissue-specific manner to generate epithelia with diversified properties. It would therefore be interesting to examine if more family members are required for SJ formation in the same or different epithelia. Interestingly, *fire exit*, the founding member, is expressed in exit and peripheral glia but has not been assigned a function (With et al., 2003) and *CG15098* is expressed in the embryonic midgut (BDGP), which forms a different subtype of SJs, smooth SJs. Alternatively, the other family members might not be associated with SJs but play distinct roles at cell-cell contacts.

2.4.3 Mcr - Is there a link between epithelial barrier function and immunity?

We have reported a novel role for the TEP member Mcr as an integral plasma membrane protein and SJ component. This finding is further substantiated by the recent MS-based identification of Mcr along with many membrane-associated SJ proteins as components of the Claudin complex (Jaspers et al., 2012). Currently, the exact role of Mcr within the complex is unknown, however, based on its large extracellular region and its very small intracellular tail, we hypothesize that Mcr plays roles in organizing the extracellular components of the junction. Moreover, Mcr molecules on opposing cells might homophilically interact similar to invertebrate soluble α2M, which acts as a homodimer (Quigley and Armstrong, 1994). To approach elucidating the function of Mcr within SJs, deletion constructs could be generated to analyze the role of individual domains in barrier function. For example, the C'-terminal domain of α2M is required for receptor-mediated endocytosis of the

α2M/protease complex and is conserved in Mcr. Since SJ morphogenesis also involves complex endocytosis from the basolateral membrane, it would be interesting to examine if the Mcr C'-terminal α2M domain is involved in this process.

Many TEPs are secreted proteins that play roles in innate immunity and similarly, full-length Mcr was shown to be secreted by S2 cells and mediate the clearance of pathogenic *C.albicans* (Stroschein-Stevenson et al., 2006). In our experiments we were not able to detect C'-terminally tagged Mcr in S2 cell media. However, Stroschein-Stevenson et al. used an Mcr-specific antibody that targets an N'-terminal epitope, therefore it is possible that part of the Mcr protein pool is cleaved just upstream of the transmembrane domain and appears as a band of almost the full size in culture media. We also did not detect secreted Mcr in the embryonic hemocoel or tracheal lumen *in vivo*, either with N'-tagged Mcr or Mcr-specific antibody, suggesting that the majority of the protein is stably associated with the plasma membrane. However, low levels of secreted Mcr might be present that are poorly immobilized by fixation, whereas the membrane-bound locally concentrated pool is readily detected by immunofluorescence. The notion that Mcr is proteolytically processed is further supported by the presence of multiple Mcr-specific bands on our preliminary immunoblots and those of others (Bätz et al., 2014; Hall et al., 2014). Vertebrate α2M is also cleaved by proteases, which are then inhibited through covalent thioester bond formation with α2M. Mcr has a mutated thioester motif and presumably does not act as a protease inhibitor, however its hypervariable region is expected to render the protein sensitive to cleavage. The Mcr cleavage products might include both transmembrane and secreted species, which could carry out distinct functions *in vivo*. Perhaps membrane-localized isoforms are part of the SJ complex and mediate barrier function in epithelial cells and SPG, while secreted isoforms by *mcr*-expressing hemocytes (Bou Aoun et al., 2011; Hall et al., 2014) are involved in the anti-microbial response.

Another intriguing scenario is that SJ-forming cells express both transmembrane and secreted Mcr isoforms, which play dual roles in barrier function and immunity or that the transmembrane Mcr species is itself also involved in the defense mechanism. Barrier epithelia frequently come into contact with microorganisms and thus need to fulfill the important task of preventing their penetration. To perform this function, barrier epithelia express antimicrobial peptides that likely create a hostile environment for the attachment of microbes (Wagner et

al., 2008; Davis and Engström, 2012). SJs might also be actively involved in the antimicrobial mechanism and in preventing pathogens from crossing epithelia, with Mcr strategically placed to provide a first line of defense. Perhaps Mcr expressed on the apicolateral membrane of epithelial cells, such as the epidermis, trachea and hindgut, provides an immune function in compartments that are in direct contact with the outside world. Similarly, smooth SJs in the midgut of adult flies are components of the gut immune barrier and are required to maintain the subtle balance between immune response to pathogenic bacteria and immune tolerance to the endogenous flora (Bonnay et al., 2013). SJs in the BBB-forming SPG might similarly be involved in the clearance of pathogens approaching the nervous system. In addition, from the time the BBB is formed, circulating macrophages cannot enter the CNS and glia are the principal phagocytes within the nervous system. Given that different glial subtypes are able to perform phagocytosis in *Drosophila*, it is plausible to suggest that SPG also perform this function. Indeed, among the candidates identified in our SPG-specific *moody-Gal4* screen, we also find other genes likely involved in phagocytosis, such as *beta-*, *zeta-COP*, and *nucampholin*. Furthermore, it is tempting to speculate that SPG SJs are actively involved in phagocytosis; interestingly, the major type of engulfing glia in the injured brain, ensheathing glia also form SJs (Kremer et al., in preparation). Intriguingly, the clearance of large pathogens from the hemocoel in insect larvae also involves the formation of SJ-like structres. When circulating hemocytes encounter an invader that is too large to engulf, such as a parasitic wasp egg, they spread to form a multi-layered epithelium surrounding the pathogen and enable melanization of the capsule. This encapsulating epithelium has ultrastructural characteristics of SJs and expresses Nrg and Cora (Russo et al., 1996; Williams et al., 2005; Williams, 2009). These observations, together with the identification of Mcr as both a SJ protein and component of the antimicrobial response highlight an interesting connection between SJs, barrier function and immunity.

2.4.4 Open questions on SJs

Over the last two decades much progress has been made in understanding the molecular composition of SJs, and over 20 components have been identified mainly through genetic screens. However, most likely, SJs are molecularly still partially defined. Neutral screens for SJ phenotypes, such as the easily identifiable

overelongated tracheal tubes, and biased approaches (sequence similarities, miR-184 targets, mass spectrometry of SJ complex, co-expression data) will help identify such candidates. Although the repertoire of SJ proteins will likely continue to be growing, the field's focus is moving towards additional aspects of SJs, such as their involvement in functions other than barrier establishment and the pathways and mechanisms governing their morphogenesis and maintenance.

In addition, a comprehensive biochemical and structural characterization of the SJ complex is missing and nothing is known about its stoichiometry due to lack of quantitative MS data. An emerging idea is that not all SJ proteins are as interdependent as previously thought and that distinct subcomplexes exist within the large, highly ordered, multi-protein complex. The observations by us and others (Nelson et al., 2010; Oshima and Fehon, 2011; Hall et al., 2014) that in SJ mutants the localization of other complex members is differentially affected and that the fluorescence of GFP-tagged SJ proteins does not fully recover after photobleaching further support this notion. Therefore, it will be of particular interest to characterize the network of interactions bridging together SJ proteins and clarify if distinct subcomplexes exist. So far, only few direct interaction partners have been reported, mostly derived from studies of the mammalian paranode. Finally, surprisingly little is known about the specific roles of individual SJ proteins within the complex.

The multi-protein composition of the SJ complex suggests an elaborate mechanism for its biogenesis. The formation of intact junctions is a multi-step process and likely requires tight and coordinated regulation of SJ proteins at different levels, i.e. transcriptional and post-transcriptional regulation of expression, post-translational modification, control of trafficking and assembly into (sub)complexes and restricted membrane localization. The notion that SJ protein expression levels are tightly co-regulated is supported by the observation that more than half of the known SJ-encoding mRNAs are predicted targets of miR-184 (Hong et al., 2009; Iovino et al., 2009; www.microrna.org). Importantly, SPG-specific overexpression of miR-184 results in dramatic disruption of SJs, suggesting a central role of the microRNA in (fine-)tuning SJ protein levels (Iovino and Gaul, unpublished data). Such miRNA regulons, in which one miRNA targets many functionally related mRNAs, have also been described in other contexts, e.g. miR-19b that regulates NF-κB signaling, miR-124 that mediates endothelial recruitment and metastasis, and *Drosophila* miR-8 that regulates multiple growth factor hormones produced by the fat

body (Gantier et al., 2012; Png et al., 2012; Lee et al., 2014). Furthermore, there is evidence that SJ mRNAs, such as *Drosophila nrx-IV* and the vertebrate homologue of *nrg* are subject to cell-type specific alternative splicing that generate glial and neuronal isoforms. In *Drosophila, nrg*, as well as other SJ mRNAs also have multiple isoforms, while *nrx-IV* and *cora* splicing is co-regulated by the RNA-binding protein Held out wings (HOW) (Hortsch et al., 1990; Genova and Fehon, 2003; Basak et al., 2007; Rodrigues et al., 2012).

Recently, FRAP experiments have succeeded in uncoupling the processes of complex assembly and maturation into stable junctions and have started elucidating the dynamics of SJ morphogenesis (Oshima and Fehon, 2011). Despite the progress, we still lack a detailed understanding of SJ development, how the proteins cluster to form complexes and which pathways control their maturation. Finally, the maintenance of SJs remains obscure. SJs need to be stably maintained both in developing epithelia, where the number, morphology and arrangement of cells change due to morphogenetic processes, and in mature epithelia, where SJ proteins might need to be replenished. In mature dividing epithelia, where cells are actively rearranging contacts, the immobility of SJ proteins persists, indicating that the core components might assemble into intracellular complexes, which are slowly trafficked to the SJ (Oshima and Fehon, 2011). Future research will help decipher the pathways and mechanisms regulating the different steps of SJ development from transcription to stable membrane complexes.

3. Materials and methods

3.1 Genome-wide screening for adult viability

Through small scale preliminary screens, the exact number of parents and the duration of egg lay were determined to ensure that the F1 generation will grow under non-overcrowded, non-competitive conditions. In the primary screen, 5 *repo-Gal4/TM3* virgin females were crossed with 4 *UAS-RNAi* males; the parents were discarded after 4 days of egg lay. *repo-Gal4* is homozygous lethal and therefore the stock retains the TM3 balancer. *moody-Gal4* is homozygous viable, therefore at a first step *moody-Gal4* females were crossed at a large scale with *D/TM3* males. 4 *moody-Gal4/TM3* virgin females were crossed with 4 *UAS-RNAi* males and discarded after 2 days of egg lay. In both screens, approximately 150 progeny eclosed per cross and were scored at adult days 8-10. During the whole screening, flies were reared at optimal and strictly controlled conditions of temperature and humidity (25°C and 60%, respectively). For analysis of the screen results, GO terms by Flybase were used (www.flybase.org).

3.2 Constructs

pasiflora constructs

Rescue constructs were generated by PCR amplification of the coding sequence from the full length cDNA clones RE54605 (*pasiflora1*), and LD42595 (*pasiflora2*) (*Drosophila* Genomics Resource Center, DGRC, Indiana, USA) (the latter not used in this study) with primers containing 5′ *NotI* and 3′ *XbaI* restriction sites, and cloning into the pJFRC2 and pJFRC4 vectors that contain *10x-* and *3x-UAS*, respectively (Addgene). Tagged proteins were generated by in-frame fusion of a *Drosophila*-optimized GFP (pJFRC14, Addgene) or 3x-FLAG to the C'-terminus, using the Golden Gate *BsaI*-based method (Engler et al., 2008; Engler et al., 2009) and cloned into the pMT vector that contains an inducible metallothionein promoter for S2 cell expression (U. Gaul, unpublished). To separate the protein and tag, 8-15 amino acids-long alanine-rich linkers were used. Pasiflora1-FLAG/GFP and Pasiflora2-FLAG/GFP were amplified from pMT with primers containing 5′ *NotI* and 3′ *XbaI* restriction sites and cloned into pJFRC2 and pJFRC4 vectors for *in vivo* expression. Pasiflora2-GFP fusions overall showed stronger expression compared to Pasiflora1-

GFP; the *3x-UAS-pasiflora1-GFP* constructs led to almost undetectable expression with some drivers.

mcr constructs

The *mcr* rescue construct was generated by PCR amplification of the coding sequence from the full length cDNA clone LD23292 (DGRC) with primers containing 5′ and 3′ *NotI* restriction sites and cloning into *NotI*-cut dephosphorylated pJFRC2 and pJFRC4. All tagged versions of Mcr were initially cloned into the pMT vector (*BsaI*) for S2 cell expression and subsequently into pJFRC2 for *in vivo* expression (*NotI*). Mcr was tagged at the C'-terminus with FLAG (15 amino acids linker), at the C'-terminus with GFP and two different sizes of linkers (24 and 34 amino acids), and at two different positions at the N' terminus (after amino acid 25 and 35) without linker. Only N'-terminally tagged constructs showed *in vivo* expression of the tag. For faster cloning of the long *mcr* CDS, for some of the constructs *mcr* was amplified as two fragments that were ligated with the *BsaI* method, which does not leave extra nucleotides. The primers were designed so that they introduce silent mutations in the internal *BsaI* recognition site of *mcr*.

RNAi constructs

The *shRNAi* constructs for *pasiflora2* and *mcr* were generated using the design by Ni et al., 2011 by inserting an inverted repeat into *NheI/EcoRI*-cut pWalium20 vector that contains *10x-UAS* (Transgenic RNAi Project, TRiP, Harvard Medical School). Transcription of the inverted repeat generates 21 nt long siRNAs. The shRNAs were designed using the DSIR algorithm (http://biodev.cea.fr/DSIR/DSIR.html) and their sequences were: For *pasiflora2*: sense strand: TACAATGTGATTATGGTGCTC, antisense strand: GAGCACCATAATCACATTGTA; for *mcr*: sense strand: TTTGACAAGAACATCACGCTA, antisense strand: TAGCGTGATGTTCTTGTCAAA.

All constructs were sequenced.

3.3 Fly strains

The following fly strains were obtained from published sources: *repo-Gal4* (V. Auld), *moody-Gal4* (Schwabe et al., 2005), *tubulin-Gal4* (E. Arama), GFP traps Nrg^{G00305}, Lac^{G00044}, and $ATP\alpha^{G00109}$ (W. Chia), *UAS-mCD8-GFP* (L. Luo), *Df(3R)BSC566*,

Df(3R)ED5785, *Df(2L)Trf-C6R31, P{EPgy2}mcr*^{EY07421}, *nrx-IV*^{4304}, *nrg*^{l4}, *kune*^{C309}, *mega*^{G0012}, *cold*^{f05607}, *crok*^{KG06053a}, *69B-Gal4*, *paired-Gal4* and *breathless-Gal4* (Bloomington *Drosophila* Stock Center, BDSC, Indiana, USA). The glial screens were performed using the KK (phi3C1) library obtained from the Vienna *Drosophila* Resource Center (VDRC, Austria). The lines *UAS-dicer2*, *pasiflora1*^{KK102223}, *pasiflora2*^{KK105806}, *pasiflora2*^{GD43952}, *mcr*^{KK100197}, *lkb1*^{KK108356} and *CG7379*^{KK103928}, were further used in our studies (VDRC). *w*^{1118} was used as wt except if mentioned otherwise.

For generation of transgenic lines we used the phiC31 integrase method and inserted constructs in attP2 and attP40 docking sites (Groth et al., 2004; Markstein et al., 2008; Pfeiffer et al., 2010). The *pasiflora1*$^{\Delta}$ genomic mutant line was generated by imprecise excision of the P-element of the *P{EP}G4182* strain (BDSC). *pasiflora1*$^{\Delta}$ was sequenced and the deletion spans the region 17794826-17796435 and removes the entire *pasiflora1* locus and 59 bp of the *CG7379* 3'UTR. The line *mcr*^{Pex1} was sequenced and has a precise excision of the P-element of the *P{EPgy2} mcr*^{EY07421} strain (BDSC). For genotyping, mutant and transgenic lines were balanced with *Kr::GFP* (Casso et al., 2000) or *Dfd-YFP* (G.Beitel) obtained from BDSC. All strains were raised at 25°C.

3.4 Immunohistochemistry

For all experiments, embryos were raised at 25°C and staged based on gut morphology (according to Atlas of *Drosophila* development by Hartenstein V.) except if mentioned otherwise.

Immunohistochemistry of embryos was performed following standard procedures: embryos were dechorionated for 5 min in 50% commercial bleach, fixed in 4% formaldehyde in PBS/heptane for 20 min, and devitellinized by shaking in methanol/heptane. Washes were performed in PBTw (PBS+0.1% Tween 20); unspecific staining was blocked with BBTw (PBT+0.1% BSA+ 5% normal serum). Primary and secondary antibodies were diluted in BBTw and incubated overnight at 4°C and 2h at RT, respectively. Stained embryos were mounted in 80% glycerol in PBS+ 2% DABCO antifading agent.

Primary antibodies used were: mouse anti-Repo (1:5, Developmental Studies Hybridoma Bank, DSHB), rabbit anti-GFP (1:100, Molecular Probes, Life Technologies, mouse IgM 2A12 (1:5, DSHB), mouse anti-Cora (1:5, DSHB), mouse anti-FasIII (1:5, DSHB), mouse anti-Crb (1:5, DSHB), rabbit anti-Mcr (1:50, our generated antibody). Alexa- (Molecular Probes) and Cy- (Jackson ImmunoResearch) conjugated secondary antibodies were used at dilutions of 1:400 and 1:200, respectively.

3.5 Live imaging of embryos and larvae

For live imaging of BBB SJs, 20 h AEL embryos were dechorionated, rinsed, mounted on coverslip coated with heptane glue and covered with halocarbon oil (Huile 10S VOLTALEF). To subdue their movement, embryos were injected with 100mM KCN (2-3% of egg volume), and imaged 45 min post-injection. Third instar larval cephalic complexes were dissected, mounted in PBS and imaged directly.

3.6 Confocal image acquisition and analysis

All confocal images were acquired using a Zeiss LSM 710 system and the ZEN acquisition software (Carl Zeiss). Image analysis was performed using ImageJ (National Institutes of Health) except if mentioned otherwise.

3.7 Dye penetration assay and quantification

For the dye penetration assay, embryos were aligned on agar, transferred on glue-coated coverslip and covered with halocarbon oil. At 20 h AEL (visibility of tracheal tubes and/or subtle movement were used as criteria for staging), a fluorescent dye (Texas red coupled dextran, 10 kDa, 2.5 mM, Molecular probes) dissolved in standard injection buffer was injected from posterior into the body cavity (needle penetration into not more than 15% of egg length to avoid hitting the nerve cord) (Schwabe et al., 2005). Penetration into or exclusion from the CNS or dorsal trunks was followed 15 min after injection using the confocal microscope. Every genotype was tested in parallel to negative and positive controls.

Dye penetration in the CNS was quantified using a home-written *Definiens* script that automatically measures pixel intensity after excluding overexposed areas, such as the body cavity and channels that run through the CNS. To quantify dye penetration, mean pixel intensity was taken as readout value and the percentage of

embryos showing visible dye penetration was calculated. To assess significance, one-way Anova was performed over all groups with Student-Newman-Keuls post hoc test.

3.8 RNA *in situ* hybridization

Whole-mount *in situ* RNA hybridization on embryos was performed as previously described (Lehmann and Tautz, 1994) with the following modifications: post-fix step between embryo rehydration and proteinase K treatment was removed, incubation with anti-digoxigenin antibodies was overnight at 4°C. Anti-sense probes were generated by in vitro transcription from the full length clones RE54605 (*pasiflora1*), LD42595 (*pasiflora2*) and LD23292 (*mcr*).

3.9 Embryonic viability assay

To measure lethality, stage 15 embryos were dechorionated, rinsed, mounted on glue coated-coverslip, covered with halocarbon oil, and placed on agar plate facing a pile of yeast. Embryos were followed during late embryogenesis and every 24 h for the following three days and the stage they died was scored.

3.10 FRAP experiments and analysis

FRAP experiment

Embryos were dechorionated, rinsed, mounted on coverslips with glue, and covered with halocarbon oil. Imaging and photobleaching were performed with a c-Apochromat 40x/1.20 W Korr M27 objective. Two images were acquired before photobleaching and then GFP was bleached using maximal output power of 488 nm laser. The bleached membrane was located in the lateral epidermis and had a length of approximately 3 µm. A time series of images was started immediately after photobleaching, with one image every 30 sec for 10 min, except for *paired-Gal4;UAS-mCD8-GFP*, *kune*^{C309}*; paired-Gal4, UAS-Pasiflora1-GFP*, and *kune*^{C309}*; paired-Gal4, UAS-Pasiflora2-GFP* for which images were captured every 4 sec for 3 min.

Image Registration and analysis

Embryo movements are unavoidable and pose severe challenges for the analysis of time-lapse recordings. We used a home-written *Definiens* script to correct for lateral

drift and non-linear distortions of the raw confocal images due to changes of cellular shape. In brief, for a confocal stack of n images with index 1..n, a *built-in* image registration algorithm was first applied to three reference images with rounded indexes n/6, n/2 and 5n/6, respectively (the middle image was used as reference image for registration). The remaining images were then registered with respect to the reference image closest in index number. Given the strong embryo movements and drift that we observed, this strategy ensured a more robust alignment compared to a registration procedure based on only one reference image for the whole stack.

A second *Definiens* script was then used to automatically extract the fluorescence intensity trajectories of the photobleached membrane regions. To detect the photobleached region we applied to registered images a 2D-Gaussian filter with a kernel size of 5x5x3 pixels, followed by an edge 3D filter. This filter is sensitive to signal variations between successive time-lapse images, and is thus ideal to detect the photobleached region that exhibits a strong decrease in fluorescence intensity just after the photobleaching step. The average fluorescence intensity in the identified region can then be extracted for each time point, and normalized with respect to its maximal and minimal values at the time points before and immediately after photobleaching, respectively.

FRAP data analysis

In a first approximation, the diffusion in the thin photobleached membrane can be modeled by one-dimensional free diffusion. The experimental data were fitted to the empirical formula given in Eq. 1, which agrees within 5% with the solution of the diffusion equation in one dimension for recovery into an interval of zero intensity (Ellenberg et al., 1997; Ellenberg and Lippincott-Schwartz, 1999)

$$I(t) = I(fina\square)\left(1 - \sqrt{\frac{\tau_D}{\tau_D + \pi \cdot t}}\right) \qquad \textbf{Eq. 1}$$

with I(t) = intensity as a function of time; t_0= time right after photobleaching; I(final) = final intensity reached after complete recovery; τ_D = characteristic time of diffusion.

The fitting procedure was performed using *Origin 8.5*. We kept t_0 constant, and extracted I(final) and τ_D from the fitted curves. Mobile fractions were calculated as ratios of fluorescence intensity in the bleached area just before photobleaching to fluorescence intensity in the bleached after recovery of the fluorescence signal.

Another common approach used to analyze FRAP recovery curves is the calculation of half-time ($t_{1/2)}$ as the time required for the bleached fluorescence to recover to half of its maximum recovery value (Yguerabide et al., 1982; Oshima and Fehon, 2011). We extracted $t_{1/2}$ from exponential fits of the recovery curves and found for Nrg-GFP $t_{1/2}$= 0.7±0.1 min, 1.1±0.1 min and 7.6±5.4 min in *pasiflora1*$^{\Delta}$, *tubulin-Gal4;UAS-pasiflora2-RNAi* and wt embryos, respectively. For overexpressed Pasiflora1- and Pasiflora2-GFP, we calculated $t_{1/2}$= 0.9±0.1 min and 1.9±0.2 min, respectively, while for the control membrane-bound mCD8-GFP $t_{1/2}$= 11±1 sec. For overexpressed Pasiflora1- and Pasiflora2-GFP in the *kune*^{C309} mutant background, we calculated $t_{1/2}$= 0.31 min and 0.26 min, respectively. All these values are in the same order of magnitude with both the characteristic times of diffusions τ_D calculated using a one-dimensional free diffusion model and the results obtained by Oshima and Fehon. Minor quantitative differences between our results and those of Oshima and Fehon (e.g. mobile fractions of mCD8-GFP) might result from the usage of different drivers (*paired-Gal4* vs *engrailed-Gal4*) and pipelines of data analysis.

3.11 Production of antibodies

Pasiflora antibodies

For each protein two 15-16 amino acids-long peptides were synthetically generated and their mixture was injected in rabbit and guinea pig (for Pasiflora1) and hen (for Pasiflora2) (Eurogentec, Seraing, Belgium). The epitopes were selected based on antigenicity and were: for Pasiflora1: SPLFETDIRSSMPVA, IIWSDNVRTGSYAVA, and for Pasiflora2: NLHSKMSRSTRSVRI, STANSLAGSRPTTPHS. The sera, as well as affinity-purified antibodies were tested by immunostainings in wt embryos in various concentrations (including 1:2). The full length proteins were also cloned (see protocol for production of Mcr antibody), but their expression in *E.coli* following standard procedures was toxic to the bacteria.

Mcr antibody

To produce the Mcr-specific antibody, we PCR amplified nucleotides 1096-1446 from the LD23292 cDNA clone with primers containing 5′ *EcoRI* and 3′ *NotI* restriction sites and cloned it into pHAT-2 vector that contains a 6x-His tag for N'-terminal tagging (EMBL protein expression and purification facility). The sequence amplified encodes a non-conserved 116 amino acids long sequence corresponding to the

hypervariable region between the two N'-terminal α2M domains of Mcr (amino acids 366-482). The plasmid was transfected into *E. coli* BL21 Star (DE3) cells, protein expression was induced with IPTG at 37°C and cells were harvested 4 h after induction (time chosen after checking IPTG time series). The His-tagged Mcr peptide was extracted from inclusion bodies (pellets), solubilized in binding buffer (100 mM NaH_2PO_4, 10 mM Tris-Cl pH 8.0, 6 M GuHCl), and purified through Ni^{2+} affinity chromatography (cOmplete HIS-Tag purification resin, Roche). Protein was dialyzed against buffer with 100 mM NaH_2PO_4, 10 mM Tris-Cl, 3.5 M Urea, 10% glycerol, 0.05% NP-40 and injected in two rabbits (Eurogentec, Seraing, Belgium) and their sera were used.

3.12 Cell culture and immunohistochemistry

S2 cells were cultured at 25°C in serum-free medium (Express Five, Gibco) supplemented with L-glutamine, penicillin and streptomycin. 50.000 cells in 100 µl were plated in 96-well poly-L-lysine coated plates for imaging (Greiner Bio-one) and transfected with pMT vectors using FuGene HD reagent (Roche) 24h post-plating. Cells were induced with 0.2-0.5 mM $CuSO_4$ 24h post-transfection, and imaged live or fixed 24h post-induction. For immunohistochemistry, cells were fixed with 2% paraformaldehyde for 25 min, post-fixed with 4% paraformaldehyde for 25 min, permeabilized with PBT (PBS+0.1% Triton X-100) and stained following standard procedures. Washes were performed with PBS and blocking with PBS+2% BSA+4% normal serum. Primary monoclonal anti-FLAG antibody (Sigma) was incubated overnight at 4°C (1:500) and secondary Alexa488 (Molecular Probes) 1h at RT (1:500). To stain the cytoplasm and nucleus, cells were incubated at RT with 15 µM Cell tracker (Molecular Probes) for 20 min and Hoechst 33342 for 5 min, respectively.

3.13 Western blotting

Polyacrylamide SDS-PAGE gel electrophoresis, immunoblotting and chemiluminescent detection were performed as previously described (Zhang and Ward, 2011). 7.5% polyacrylamide gels were used for the separation. For Western blots of embryonic extracts, 40 embryos were homogenized in RIPA buffer (150 Mm NaCl, 1% Triton X-100, 0.5% sodium deoxycholate, 0.1% SDS, 50 Mm Tric-HCl, pH=8.0) with protease inhibitor and 30 µg were loaded per sample. For Western

blots from S2 cells, 500.00 cells were plated in 24-well plates, transfected 24 h post-plating with pMT vector and induced with 0.5 mM $CuSO_4$ 24 h post-transfection. Cells and media were collected separately and cells were lysed using cOmplete Lysis-M, EDTA-free (Roche). Immunoblots were hybridized with mouse anti-FLAG (1:500, Sigma), rabbit anti-Mcr (1:1500, our generated antibody) and mouse anti-actin (1:5000, Abcam).

References

Abbott, N.J. (1991). Permeability and transport of glial blood-brain barriers. Annals of the New York Academy of Sciences *633*, 378-394.

Abbott, N.J. (2013). Blood-brain barrier structure and function and the challenges for CNS drug delivery. Journal of inherited metabolic disease *36*, 437-449.

Abbott, N.J., Lane, N.J., and Bundgaard, M. (1986). The blood-brain interface in invertebrates. Annals of the New York Academy of Sciences *481*, 20-42.

Abbott, N.J., Ronnback, L., and Hansson, E. (2006). Astrocyte-endothelial interactions at the blood-brain barrier. Nature reviews Neuroscience *7*, 41-53.

Adato, A., Vreugde, S., Joensuu, T., Avidan, N., Hamalainen, R., Belenkiy, O., Olender, T., Bonne-Tamir, B., Ben-Asher, E., Espinos, C.*, et al.* (2002). USH3A transcripts encode clarin-1, a four-transmembrane-domain protein with a possible role in sensory synapses. European journal of human genetics : EJHG *10*, 339-350.

Altenhein, B., Becker, A., Busold, C., Beckmann, B., Hoheisel, J.D., and Technau, G.M. (2006). Expression profiling of glial genes during Drosophila embryogenesis. Developmental biology *296*, 545-560.

Asano, A., Asano, K., Sasaki, H., Furuse, M., and Tsukita, S. (2003). Claudins in Caenorhabditis elegans: their distribution and barrier function in the epithelium. Current biology : CB *13*, 1042-1046.

Auld, V.J., Fetter, R.D., Broadie, K., and Goodman, C.S. (1995). Gliotactin, a novel transmembrane protein on peripheral glia, is required to form the blood-nerve barrier in Drosophila. Cell *81*, 757-767.

Awasaki, T., and Ito, K. (2004). Engulfing action of glial cells is required for programmed axon pruning during Drosophila metamorphosis. Current biology : CB *14*, 668-677.

Awasaki, T., Lai, S.L., Ito, K., and Lee, T. (2008). Organization and postembryonic development of glial cells in the adult central brain of Drosophila. The Journal of neuroscience : the official journal of the Society for Neuroscience *28*, 13742-13753.

Awasaki, T., Tatsumi, R., Takahashi, K., Arai, K., Nakanishi, Y., Ueda, R., and Ito, K. (2006). Essential role of the apoptotic cell engulfment genes draper and ced-6 in programmed axon pruning during Drosophila metamorphosis. Neuron *50*, 855-867.

Bachmann, A., Draga, M., Grawe, F., and Knust, E. (2008). On the role of the MAGUK proteins encoded by Drosophila varicose during embryonic and postembryonic development. BMC developmental biology *8*, 55.

Bainton, R.J., Tsai, L.T., Schwabe, T., DeSalvo, M., Gaul, U., and Heberlein, U. (2005). moody encodes two GPCRs that regulate cocaine behaviors and blood-brain barrier permeability in Drosophila. Cell *123*, 145-156.

Balda, M.S., and Matter, K. (2008). Tight junctions at a glance. Journal of cell science *121*, 3677-3682.

Banerjee, S., Bainton, R.J., Mayer, N., Beckstead, R., and Bhat, M.A. (2008). Septate junctions are required for ommatidial integrity and blood-eye barrier function in Drosophila. Developmental biology *317*, 585-599.

Banerjee, S., Pillai, A.M., Paik, R., Li, J., and Bhat, M.A. (2006). Axonal ensheathment and septate junction formation in the peripheral nervous system of Drosophila. The Journal of neuroscience : the official journal of the Society for Neuroscience *26*, 3319-3329.

Basak, S., Raju, K., Babiarz, J., Kane-Goldsmith, N., Koticha, D., and Grumet, M. (2007). Differential expression and functions of neuronal and glial neurofascin isoforms and splice variants during PNS development. Developmental biology *311*, 408-422.

Bassett, A.R., Tibbit, C., Ponting, C.P., and Liu, J.L. (2013). Highly efficient targeted mutagenesis of Drosophila with the CRISPR/Cas9 system. Cell reports *4*, 220-228.

Batz, T., Forster, D., and Luschnig, S. (2014). The transmembrane protein Macroglobulin complement-related is essential for septate junction formation and epithelial barrier function in Drosophila. Development *141*, 899-908.

Baumgartner, S., Littleton, J.T., Broadie, K., Bhat, M.A., Harbecke, R., Lengyel, J.A., Chiquet-Ehrismann, R., Prokop, A., and Bellen, H.J. (1996). A Drosophila neurexin is required for septate junction and blood-nerve barrier formation and function. Cell *87*, 1059-1068.

Beckervordersandforth, R.M., Rickert, C., Altenhein, B., and Technau, G.M. (2008). Subtypes of glial cells in the Drosophila embryonic ventral nerve cord as related to lineage and gene expression. Mechanisms of development *125*, 542-557.

Behr, M., Riedel, D., and Schuh, R. (2003). The claudin-like megatrachea is essential in septate junctions for the epithelial barrier function in Drosophila. Developmental cell *5*, 611-620.

Bhat, M.A., Rios, J.C., Lu, Y., Garcia-Fresco, G.P., Ching, W., St Martin, M., Li, J., Einheber, S., Chesler, M., Rosenbluth, J.*, et al.* (2001). Axon-glia interactions and the domain organization of myelinated axons requires neurexin IV/Caspr/Paranodin. Neuron *30*, 369-383.

Bier, E. (2005). Drosophila, the golden bug, emerges as a tool for human genetics. Nature reviews Genetics *6*, 9-23.

Bishop, D.L., Misgeld, T., Walsh, M.K., Gan, W.B., and Lichtman, J.W. (2004). Axon branch removal at developing synapses by axosome shedding. Neuron *44*, 651-661.

Blandin, S., and Levashina, E.A. (2004). Thioester-containing proteins and insect immunity. Molecular immunology *40*, 903-908.

Bonnay, F., Cohen-Berros, E., Hoffmann, M., Kim, S.Y., Boulianne, G.L., Hoffmann, J.A., Matt, N., and Reichhart, J.M. (2013). big bang gene modulates gut immune tolerance in Drosophila. Proceedings of the National Academy of Sciences of the United States of America *110*, 2957-2962.

Booth, G.E., Kinrade, E.F., and Hidalgo, A. (2000). Glia maintain follower neuron survival during Drosophila CNS development. Development *127*, 237-244.

Borth, W. (1992). Alpha 2-macroglobulin, a multifunctional binding protein with targeting characteristics. FASEB journal : official publication of the Federation of American Societies for Experimental Biology *6*, 3345-3353.

Bossing, T., Udolph, G., Doe, C.Q., and Technau, G.M. (1996). The embryonic central nervous system lineages of Drosophila melanogaster. I. Neuroblast lineages derived from the ventral half of the neuroectoderm. Developmental biology *179*, 41-64.

Bou Aoun, R., Hetru, C., Troxler, L., Doucet, D., Ferrandon, D., and Matt, N. (2011). Analysis of thioester-containing proteins during the innate immune response of Drosophila melanogaster. Journal of innate immunity *3*, 52-64.

Boyle, M.E., Berglund, E.O., Murai, K.K., Weber, L., Peles, E., and Ranscht, B. (2001). Contactin orchestrates assembly of the septate-like junctions at the paranode in myelinated peripheral nerve. Neuron *30*, 385-397.

Brankatschk, M., Dunst, S., Nemetschke, L., and Eaton, S. (2014). Delivery of circulating lipoproteins to specific neurons in the Drosophila brain regulates systemic insulin signaling. eLife *3*.

Brown, N.H. (2000). Cell-cell adhesion via the ECM: integrin genetics in fly and worm. Matrix biology : journal of the International Society for Matrix Biology *19*, 191-201.

Buchanan, R.L., and Benzer, S. (1993). Defective glia in the Drosophila brain degeneration mutant drop-dead. Neuron *10*, 839-850.

Bundgaard, M., and Abbott, N.J. (2008). All vertebrates started out with a glial blood-brain barrier 4-500 million years ago. Glia *56*, 699-708.

Casso, D., Ramirez-Weber, F., and Kornberg, T.B. (2000). GFP-tagged balancer chromosomes for Drosophila melanogaster. Mechanisms of development *91*, 451-454.

Charrin, S., le Naour, F., Silvie, O., Milhiet, P.E., Boucheix, C., and Rubinstein, E. (2009). Lateral organization of membrane proteins: tetraspanins spin their web. The Biochemical journal *420*, 133-154.

Chell, J.M., and Brand, A.H. (2010). Nutrition-responsive glia control exit of neural stem cells from quiescence. Cell *143*, 1161-1173.

Daneman, R., and Prat, A. (2015). The blood-brain barrier. Cold Spring Harbor perspectives in biology *7*, a020412.

Davis, M.M., and Engstrom, Y. (2012). Immune response in the barrier epithelia: lessons from the fruit fly Drosophila melanogaster. Journal of innate immunity *4*, 273-283.

DeSalvo, M.K., Hindle, S.J., Rusan, Z.M., Orng, S., Eddison, M., Halliwill, K., and Bainton, R.J. (2014). The Drosophila surface glia transcriptome: evolutionary conserved blood-brain barrier processes. Frontiers in neuroscience *8*, 346.

Dietzl, G., Chen, D., Schnorrer, F., Su, K.C., Barinova, Y., Fellner, M., Gasser, B., Kinsey, K., Oppel, S., Scheiblauer, S.*, et al.* (2007). A genome-wide transgenic RNAi library for conditional gene inactivation in Drosophila. Nature *448*, 151-156.

Dodds, A.W., and Law, S.K. (1998). The phylogeny and evolution of the thioester bond-containing proteins C3, C4 and alpha 2-macroglobulin. Immunological reviews *166*, 15-26.

Egger, B., Leemans, R., Loop, T., Kammermeier, L., Fan, Y., Radimerski, T., Strahm, M.C., Certa, U., and Reichert, H. (2002). Gliogenesis in Drosophila: genome-wide analysis of downstream genes of glial cells missing in the embryonic nervous system. Development *129*, 3295-3309.

Einheber, S., Zanazzi, G., Ching, W., Scherer, S., Milner, T.A., Peles, E., and Salzer, J.L. (1997). The axonal membrane protein Caspr, a homologue of neurexin IV, is a component of the septate-like paranodal junctions that assemble during myelination. The Journal of cell biology *139*, 1495-1506.

Ellenberg, J., and Lippincott-Schwartz, J. (1999). Dynamics and mobility of nuclear envelope proteins in interphase and mitotic cells revealed by green fluorescent protein chimeras. Methods *19*, 362-372.

Ellenberg, J., Siggia, E.D., Moreira, J.E., Smith, C.L., Presley, J.F., Worman, H.J., and Lippincott-Schwartz, J. (1997). Nuclear membrane dynamics and reassembly in living cells: targeting of an inner nuclear membrane protein in interphase and mitosis. The Journal of cell biology *138*, 1193-1206.

Engler, C., Gruetzner, R., Kandzia, R., and Marillonnet, S. (2009). Golden gate shuffling: a one-pot DNA shuffling method based on type IIs restriction enzymes. PloS one *4*, e5553.

Engler, C., Kandzia, R., and Marillonnet, S. (2008). A one pot, one step, precision cloning method with high throughput capability. PloS one *3*, e3647.

Faivre-Sarrailh, C., Banerjee, S., Li, J., Hortsch, M., Laval, M., and Bhat, M.A. (2004). Drosophila contactin, a homolog of vertebrate contactin, is required for septate junction organization and paracellular barrier function. Development *131*, 4931-4942.

Farina, C., Aloisi, F., and Meinl, E. (2007). Astrocytes are active players in cerebral innate immunity. Trends in immunology *28*, 138-145.

Farquhar, M.G., and Palade, G.E. (1963). Junctional complexes in various epithelia. The Journal of cell biology *17*, 375-412.

Fehon, R.G., Dawson, I.A., and Artavanis-Tsakonas, S. (1994). A Drosophila homologue of membrane-skeleton protein 4.1 is associated with septate junctions and is encoded by the coracle gene. Development *120*, 545-557.

Findley, M.K., and Koval, M. (2009). Regulation and roles for claudin-family tight junction proteins. IUBMB life *61*, 431-437.

Flower, N.E., and Filshie, B.K. (1975). Junctional structures in the midgut cells of lepidopteran caterpillars. Journal of cell science *17*, 221-239.

Fradkin, L.G., Kamphorst, J.T., DiAntonio, A., Goodman, C.S., and Noordermeer, J.N. (2002). Genomewide analysis of the Drosophila tetraspanins reveals a subset with similar function in the formation of the embryonic synapse. Proceedings of the National Academy of Sciences of the United States of America *99*, 13663-13668.

Franke, W.W. (2009). Discovering the molecular components of intercellular junctions--a historical view. Cold Spring Harbor perspectives in biology *1*, a003061.

Freeman, M.R., Delrow, J., Kim, J., Johnson, E., and Doe, C.Q. (2003). Unwrapping glial biology: Gcm target genes regulating glial development, diversification, and function. Neuron *38*, 567-580.

Freeman, M.R., and Doherty, J. (2006). Glial cell biology in Drosophila and vertebrates. Trends in neurosciences *29*, 82-90.

Fuentes-Medel, Y., Logan, M.A., Ashley, J., Ataman, B., Budnik, V., and Freeman, M.R. (2009). Glia and muscle sculpt neuromuscular arbors by engulfing destabilized synaptic boutons and shed presynaptic debris. PLoS biology *7*, e1000184.

Furuse, M., Fujita, K., Hiiragi, T., Fujimoto, K., and Tsukita, S. (1998a). Claudin-1 and -2: novel integral membrane proteins localizing at tight junctions with no sequence similarity to occludin. The Journal of cell biology *141*, 1539-1550.

Furuse, M., Sasaki, H., Fujimoto, K., and Tsukita, S. (1998b). A single gene product, claudin-1 or -2, reconstitutes tight junction strands and recruits occludin in fibroblasts. The Journal of cell biology *143*, 391-401.

Furuse, M., and Tsukita, S. (2006). Claudins in occluding junctions of humans and flies. Trends in cell biology *16*, 181-188.

Gantier, M.P., Stunden, H.J., McCoy, C.E., Behlke, M.A., Wang, D., Kaparakis-Liaskos, M., Sarvestani, S.T., Yang, Y.H., Xu, D., Corr, S.C.*, et al.* (2012). A miR-19 regulon that controls NF-kappaB signaling. Nucleic acids research *40*, 8048-8058.

Genova, J.L., and Fehon, R.G. (2003). Neuroglian, Gliotactin, and the Na+/K+ ATPase are essential for septate junction function in Drosophila. The Journal of cell biology *161*, 979-989.

Graveley, B.R., Brooks, A.N., Carlson, J.W., Duff, M.O., Landolin, J.M., Yang, L., Artieri, C.G., van Baren, M.J., Boley, N., Booth, B.W.*, et al.* (2011). The developmental transcriptome of Drosophila melanogaster. Nature *471*, 473-479.

Grosjean, Y., Grillet, M., Augustin, H., Ferveur, J.F., and Featherstone, D.E. (2008). A glial amino-acid transporter controls synapse strength and courtship in Drosophila. Nature neuroscience *11*, 54-61.

Groth, A.C., Fish, M., Nusse, R., and Calos, M.P. (2004). Construction of transgenic Drosophila by using the site-specific integrase from phage phiC31. Genetics *166*, 1775-1782.

Gunzel, D., and Yu, A.S. (2013). Claudins and the modulation of tight junction permeability. Physiological reviews *93*, 525-569.

Hall, S., Bone, C., Oshima, K., Zhang, L., McGraw, M., Lucas, B., Fehon, R.G., and Ward, R.E.t. (2014). Macroglobulin complement-related encodes a protein required for septate junction organization and paracellular barrier function in Drosophila. Development *141*, 889-898.

Halter, D.A., Urban, J., Rickert, C., Ner, S.S., Ito, K., Travers, A.A., and Technau, G.M. (1995). The homeobox gene repo is required for the differentiation and maintenance of glia function in the embryonic nervous system of Drosophila melanogaster. Development *121*, 317-332.

Hidalgo, A., and Booth, G.E. (2000). Glia dictate pioneer axon trajectories in the Drosophila embryonic CNS. Development *127*, 393-402.

Hidalgo, A., Kinrade, E.F., and Georgiou, M. (2001). The Drosophila neuregulin vein maintains glial survival during axon guidance in the CNS. Developmental cell *1*, 679-690.

Hidalgo, A., Urban, J., and Brand, A.H. (1995). Targeted ablation of glia disrupts axon tract formation in the Drosophila CNS. Development *121*, 3703-3712.

Hong, X., Hammell, M., Ambros, V., and Cohen, S.M. (2009). Immunopurification of Ago1 miRNPs selects for a distinct class of microRNA targets. Proceedings of the National Academy of Sciences of the United States of America *106*, 15085-15090.

Hortsch, M., Bieber, A.J., Patel, N.H., and Goodman, C.S. (1990). Differential splicing generates a nervous system-specific form of Drosophila neuroglian. Neuron *4*, 697-709.

Hosoya, T., Takizawa, K., Nitta, K., and Hotta, Y. (1995). glial cells missing: a binary switch between neuronal and glial determination in Drosophila. Cell *82*, 1025-1036.

Ile, K.E., Tripathy, R., Goldfinger, V., and Renault, A.D. (2012). Wunen, a Drosophila lipid phosphate phosphatase, is required for septate junction-mediated barrier function. Development *139*, 2535-2546.

Iovino, N., Pane, A., and Gaul, U. (2009). miR-184 has multiple roles in Drosophila female germline development. Developmental cell *17*, 123-133.

Ito, K., Urban, J., and Technau, GM. (1995). Distribution, classification and development of Drosophila glial cells in the late embryonic and early larval ventral nerve cord. Roux's Arch Dev Biol 204: 284-307.

Izumi, Y., and Furuse, M. (2014). Molecular organization and function of invertebrate occluding junctions. Seminars in cell & developmental biology *36*, 186-193.

Jacobs, S., and Doering, L.C. (2010). Astrocytes prevent abnormal neuronal development in the fragile x mouse. The Journal of neuroscience : the official journal of the Society for Neuroscience *30*, 4508-4514.

Jaspers, M.H., Nolde, K., Behr, M., Joo, S.H., Plessmann, U., Nikolov, M., Urlaub, H., and Schuh, R. (2012). The claudin Megatrachea protein complex. The Journal of biological chemistry *287*, 36756-36765.

Jones, B.W., Fetter, R.D., Tear, G., and Goodman, C.S. (1995). glial cells missing: a genetic switch that controls glial versus neuronal fate. Cell *82*, 1013-1023.

Knust, E., and Bossinger, O. (2002). Composition and formation of intercellular junctions in epithelial cells. Science *298*, 1955-1959.

Kondo, S., and Ueda, R. (2013). Highly improved gene targeting by germline-specific Cas9 expression in Drosophila. Genetics *195*, 715-721.

Koval, M. (2013). Differential pathways of claudin oligomerization and integration into tight junctions. Tissue barriers *1*, e24518.

Kurant, E., Axelrod, S., Leaman, D., and Gaul, U. (2008). Six-microns-under acts upstream of Draper in the glial phagocytosis of apoptotic neurons. Cell *133*, 498-509.

Lal-Nag, M., and Morin, PJ. (2009). The Claudins. Genome Biol 10(8):235.

Lamb, R.S., Ward, R.E., Schweizer, L., and Fehon, R.G. (1998). Drosophila coracle, a member of the protein 4.1 superfamily, has essential structural functions in the septate junctions and developmental functions in embryonic and adult epithelial cells. Molecular biology of the cell *9*, 3505-3519.

Laprise, P., Lau, K.M., Harris, K.P., Silva-Gagliardi, N.F., Paul, S.M., Beronja, S., Beitel, G.J., McGlade, C.J., and Tepass, U. (2009). Yurt, Coracle, Neurexin IV and the Na(+),K(+)-ATPase form a novel group of epithelial polarity proteins. Nature *459*, 1141-1145.

Laprise, P., and Tepass, U. (2011). Novel insights into epithelial polarity proteins in Drosophila. Trends in cell biology *21*, 401-408.

Laval, M., Bel, C., and Faivre-Sarrailh, C. (2008). The lateral mobility of cell adhesion molecules is highly restricted at septate junctions in Drosophila. BMC cell biology *9*, 38.

Ledger, P.W. (1975). Septate junctions in the calcareous sponge Sycon ciliatum. Tissue & cell *7*, 13-18.

Lee, G.J., Jun, J.W., and Hyun, S. (2014). MicroRNA miR-8 regulates multiple growth factor hormones produced from Drosophila fat cells. Insect molecular biology.

Lehmann, R., and Tautz, D. (1994). In situ hybridization to RNA. Methods in cell biology *44*, 575-598.

Lemke, G. (2001). Glial control of neuronal development. Annual review of neuroscience *24*, 87-105.

Leys, S.P., and Riesgo, A. (2012). Epithelia, an evolutionary novelty of metazoans. Journal of experimental zoology Part B, Molecular and developmental evolution *318*, 438-447.

Lin, M., Sutherland, D.R., Horsfall, W., Totty, N., Yeo, E., Nayar, R., Wu, X.F., and Schuh, A.C. (2002). Cell surface antigen CD109 is a novel member of the alpha(2) macroglobulin/C3, C4, C5 family of thioester-containing proteins. Blood *99*, 1683-1691.

Llimargas, M., Strigini, M., Katidou, M., Karagogeos, D., and Casanova, J. (2004). Lachesin is a component of a septate junction-based mechanism that controls tube size and epithelial integrity in the Drosophila tracheal system. Development *131*, 181-190.

Luschnig, S., Batz, T., Armbruster, K., and Krasnow, M.A. (2006). serpentine and vermiform encode matrix proteins with chitin binding and deacetylation domains that limit tracheal tube length in Drosophila. Current biology : CB *16*, 186-194.

MacDonald, J.M., Beach, M.G., Porpiglia, E., Sheehan, A.E., Watts, R.J., and Freeman, M.R. (2006). The Drosophila cell corpse engulfment receptor Draper mediates glial clearance of severed axons. Neuron *50*, 869-881.

Markstein, M., Pitsouli, C., Villalta, C., Celniker, S.E., and Perrimon, N. (2008). Exploiting position effects and the gypsy retrovirus insulator to engineer precisely expressed transgenes. Nature genetics *40*, 476-483.

Mayer, F., Mayer, N., Chinn, L., Pinsonneault, R.L., Kroetz, D., and Bainton, R.J. (2009). Evolutionary conservation of vertebrate blood-brain barrier chemoprotective mechanisms in Drosophila. The Journal of neuroscience : the official journal of the Society for Neuroscience *29*, 3538-3550.

Miklos, G.L., and Rubin, G.M. (1996). The role of the genome project in determining gene function: insights from model organisms. Cell *86*, 521-529.

Miller, G. (2005). Neuroscience. The dark side of glia. Science *308*, 778-781.

Miyamoto, T., Morita, K., Takemoto, D., Takeuchi, K., Kitano, Y., Miyakawa, T., Nakayama, K., Okamura, Y., Sasaki, H., Miyachi, Y.*, et al.* (2005). Tight junctions in Schwann cells of peripheral myelinated axons: a lesson from claudin-19-deficient mice. The Journal of cell biology *169*, 527-538.

Morin, X., Daneman, R., Zavortink, M., and Chia, W. (2001). A protein trap strategy to detect GFP-tagged proteins expressed from their endogenous loci in Drosophila. Proceedings of the National Academy of Sciences of the United States of America *98*, 15050-15055.

Moyer, K.E., and Jacobs, J.R. (2008). Varicose: a MAGUK required for the maturation and function of Drosophila septate junctions. BMC developmental biology *8*, 99.

Mudiganti, U., Hernandez, R., and Brown, D.T. (2010). Insect response to alphavirus infection--establishment of alphavirus persistence in insect cells involves inhibition of viral polyprotein cleavage. Virus research *150*, 73-84.

Napoli, I., and Neumann, H. (2009). Microglial clearance function in health and disease. Neuroscience *158*, 1030-1038.

Nelson, K.S., Furuse, M., and Beitel, G.J. (2010). The Drosophila Claudin Kune-kune is required for septate junction organization and tracheal tube size control. Genetics *185*, 831-839.

Ni, J.Q., Zhou, R., Czech, B., Liu, L.P., Holderbaum, L., Yang-Zhou, D., Shim, H.S., Tao, R., Handler, D., Karpowicz, P.*, et al.* (2011). A genome-scale shRNA resource for transgenic RNAi in Drosophila. Nature methods *8*, 405-407.

Nilton, A., Oshima, K., Zare, F., Byri, S., Nannmark, U., Nyberg, K.G., Fehon, R.G., and Uv, A.E. (2010). Crooked, coiled and crimpled are three Ly6-like proteins required for proper localization of septate junction components. Development *137*, 2427-2437.

Noirot-Timothee, C., Smith, D.S., Cayer, M.L., and Noirot, C. (1978). Septate junctions in insects: comparison between intercellular and intramembranous structures. Tissue & cell *10*, 125-136.

Nusslein-Volhard, C., and Wieschaus, E. (1980). Mutations affecting segment number and polarity in Drosophila. Nature *287*, 795-801.

Okamoto, N., Nakamori, R., Murai, T., Yamauchi, Y., Masuda, A., and Nishimura, T. (2013). A secreted decoy of InR antagonizes insulin/IGF signaling to restrict body growth in Drosophila. Genes & development *27*, 87-97.

Olofsson, B., and Page, D.T. (2005). Condensation of the central nervous system in embryonic Drosophila is inhibited by blocking hemocyte migration or neural activity. Developmental biology *279*, 233-243.

Oshima, K., and Fehon, R.G. (2011). Analysis of protein dynamics within the septate junction reveals a highly stable core protein complex that does not include the basolateral polarity protein Discs large. Journal of cell science *124*, 2861-2871.

Paul, S.M., Ternet, M., Salvaterra, P.M., and Beitel, G.J. (2003). The Na+/K+ ATPase is required for septate junction function and epithelial tube-size control in the Drosophila tracheal system. Development *130*, 4963-4974.

Pfeiffer, B.D., Ngo, T.T., Hibbard, K.L., Murphy, C., Jenett, A., Truman, J.W., and Rubin, G.M. (2010). Refinement of tools for targeted gene expression in Drosophila. Genetics *186*, 735-755.

Pfrieger, F.W., and Barres, B.A. (1995). What the fly's glia tell the fly's brain. Cell *83*, 671-674.

Pillai, A.M., Thaxton, C., Pribisko, A.L., Cheng, J.G., Dupree, J.L., and Bhat, M.A. (2009). Spatiotemporal ablation of myelinating glia-specific neurofascin (Nfasc NF155) in mice reveals gradual loss of paranodal axoglial junctions and concomitant disorganization of axonal domains. Journal of neuroscience research *87*, 1773-1793.

Png, K.J., Halberg, N., Yoshida, M., and Tavazoie, S.F. (2012). A microRNA regulon that mediates endothelial recruitment and metastasis by cancer cells. Nature *481*, 190-194.

Poliak, S., and Peles, E. (2003). The local differentiation of myelinated axons at nodes of Ranvier. Nature reviews Neuroscience *4*, 968-980.

Quigley, J.P., and Armstrong, P.B. (1994). Invertebrate alpha 2-macroglobulin: structure-function and the ancient thiol ester bond. Annals of the New York Academy of Sciences *712*, 131-145.

Rival, T., Soustelle, L., Strambi, C., Besson, M.T., Iche, M., and Birman, S. (2004). Decreasing glutamate buffering capacity triggers oxidative stress and neuropil degeneration in the Drosophila brain. Current biology : CB *14*, 599-605.

Rodrigues, F., Thuma, L., and Klambt, C. (2012). The regulation of glial-specific splicing of Neurexin IV requires HOW and Cdk12 activity. Development *139*, 1765-1776.

Russo, J., Dupas, S., Frey, F., Carton, Y., and Brehelin, M. (1996). Insect immunity: early events in the encapsulation process of parasitoid (Leptopilina boulardi) eggs in resistant and susceptible strains of Drosophila. Parasitology *112 (Pt 1)*, 135-142.

Schmidt, H., Rickert, C., Bossing, T., Vef, O., Urban, J., and Technau, G.M. (1997). The embryonic central nervous system lineages of Drosophila melanogaster. II. Neuroblast lineages derived from the dorsal part of the neuroectoderm. Developmental biology *189*, 186-204.

Schulte, J., Charish, K., Que, J., Ravn, S., MacKinnon, C., and Auld, V.J. (2006). Gliotactin and Discs large form a protein complex at the tricellular junction of polarized epithelial cells in Drosophila. Journal of cell science *119*, 4391-4401.

Schulte, J., Tepass, U., and Auld, V.J. (2003). Gliotactin, a novel marker of tricellular junctions, is necessary for septate junction development in Drosophila. The Journal of cell biology *161*, 991-1000.

Schwabe, T., Bainton, R.J., Fetter, R.D., Heberlein, U., and Gaul, U. (2005). GPCR signaling is required for blood-brain barrier formation in drosophila. Cell *123*, 133-144.

Shilo, B.Z. (2014). The regulation and functions of MAPK pathways in Drosophila. Methods *68*, 151-159.

Simon, M.A. (1994). Signal transduction during the development of the Drosophila R7 photoreceptor. Developmental biology *166*, 431-442.

Simske, J.S. (2013). Claudins reign: The claudin/EMP/PMP22/gamma channel protein family in C. elegans. Tissue barriers *1*, e25502.

Solomon, K.R., Sharma, P., Chan, M., Morrison, P.T., and Finberg, R.W. (2004). CD109 represents a novel branch of the alpha2-macroglobulin/complement gene family. Gene *327*, 171-183.

Sonnenfeld, M.J., and Jacobs, J.R. (1995). Macrophages and glia participate in the removal of apoptotic neurons from the Drosophila embryonic nervous system. The Journal of comparative neurology *359*, 644-652.

Sousa-Nunes, R., Yee, L.L., and Gould, A.P. (2011). Fat cells reactivate quiescent neuroblasts via TOR and glial insulin relays in Drosophila. Nature *471*, 508-512.

Speder, P., and Brand, A.H. (2014). Gap junction proteins in the blood-brain barrier control nutrient-dependent reactivation of Drosophila neural stem cells. Developmental cell *30*, 309-321.

St Johnston, D. (2002). The art and design of genetic screens: Drosophila melanogaster. Nature reviews Genetics *3*, 176-188.

St Johnston, D. (2013). Using mutants, knockdowns, and transgenesis to investigate gene function in Drosophila. Wiley interdisciplinary reviews Developmental biology *2*, 587-613.

St Johnston, D., and Ahringer, J. (2010). Cell polarity in eggs and epithelia: parallels and diversity. Cell *141*, 757-774.

Stork, T., Engelen, D., Krudewig, A., Silies, M., Bainton, R.J., and Klambt, C. (2008). Organization and function of the blood-brain barrier in Drosophila. The Journal of neuroscience : the official journal of the Society for Neuroscience *28*, 587-597.

Stroschein-Stevenson, S.L., Foley, E., O'Farrell, P.H., and Johnson, A.D. (2006). Identification of Drosophila gene products required for phagocytosis of Candida albicans. PLoS biology *4*, e4.

Suh, J., and Jackson, F.R. (2007). Drosophila ebony activity is required in glia for the circadian regulation of locomotor activity. Neuron *55*, 435-447.

Tasdemir-Yilmaz, O.E., and Freeman, M.R. (2014). Astrocytes engage unique molecular programs to engulf pruned neuronal debris from distinct subsets of neurons. Genes & development *28*, 20-33.

Tepass, U. (1997). Epithelial differentiation in Drosophila. BioEssays : news and reviews in molecular, cellular and developmental biology *19*, 673-682.

Tepass, U., and Hartenstein, V. (1994). The development of cellular junctions in the Drosophila embryo. Developmental biology *161*, 563-596.

Tiklova, K., Senti, K.A., Wang, S., Graslund, A., and Samakovlis, C. (2010). Epithelial septate junction assembly relies on melanotransferrin iron binding and endocytosis in Drosophila. Nature cell biology *12*, 1071-1077.

Unhavaithaya, Y., and Orr-Weaver, T.L. (2012). Polyploidization of glia in neural development links tissue growth to blood-brain barrier integrity. Genes & development *26*, 31-36.

Wagner, C., Isermann, K., Fehrenbach, H., and Roeder, T. (2008). Molecular architecture of the fruit fly's airway epithelial immune system. BMC genomics *9*, 446.

Wang, S., Jayaram, S.A., Hemphala, J., Senti, K.A., Tsarouhas, V., Jin, H., and Samakovlis, C. (2006). Septate-junction-dependent luminal deposition of chitin deacetylases restricts tube elongation in the Drosophila trachea. Current biology : CB *16*, 180-185.

Ward, R.E.t., Lamb, R.S., and Fehon, R.G. (1998). A conserved functional domain of Drosophila coracle is required for localization at the septate junction and has membrane-organizing activity. The Journal of cell biology *140*, 1463-1473.

Ward, R.E.t., Schweizer, L., Lamb, R.S., and Fehon, R.G. (2001). The protein 4.1, ezrin, radixin, moesin (FERM) domain of Drosophila Coracle, a cytoplasmic component of the septate junction, provides functions essential for embryonic development and imaginal cell proliferation. Genetics *159*, 219-228.

Watts, R.J., Schuldiner, O., Perrino, J., Larsen, C., and Luo, L. (2004). Glia engulf degenerating axons during developmental axon pruning. Current biology : CB *14*, 678-684.

Whitlock, K.E. (1993). Development of Drosophila wing sensory neurons in mutants with missing or modified cell surface molecules. Development *117*, 1251-1260.

Williams, M.J. (2009). The Drosophila cell adhesion molecule Neuroglian regulates Lissencephaly-1 localisation in circulating immunosurveillance cells. BMC immunology *10*, 17.

Williams, M.J., Ando, I., and Hultmark, D. (2005). Drosophila melanogaster Rac2 is necessary for a proper cellular immune response. Genes to cells : devoted to molecular & cellular mechanisms *10*, 813-823.

With, S., Rice, T., Salinas, C., and Auld, V. (2003). Fire exit is a potential four transmembrane protein expressed in developing Drosophila glia. Genesis *35*, 143-152.

Woods, D.F., and Bryant, P.J. (1991). The discs-large tumor suppressor gene of Drosophila encodes a guanylate kinase homolog localized at septate junctions. Cell *66*, 451-464.

Woods, D.F., Wu, J.W., and Bryant, P.J. (1997). Localization of proteins to the apico-lateral junctions of Drosophila epithelia. Developmental genetics *20*, 111-118.

Wu, V.M., and Beitel, G.J. (2004). A junctional problem of apical proportions: epithelial tube-size control by septate junctions in the Drosophila tracheal system. Current opinion in cell biology *16*, 493-499.

Wu, V.M., Schulte, J., Hirschi, A., Tepass, U., and Beitel, G.J. (2004). Sinuous is a Drosophila claudin required for septate junction organization and epithelial tube size control. The Journal of cell biology *164*, 313-323.

Wu, V.M., Yu, M.H., Paik, R., Banerjee, S., Liang, Z., Paul, S.M., Bhat, M.A., and Beitel, G.J. (2007). Drosophila Varicose, a member of a new subgroup of basolateral MAGUKs, is required for septate junctions and tracheal morphogenesis. Development *134*, 999-1009.

Xiao, X., Liu, Y., Zhang, X., Wang, J., Li, Z., Pang, X., Wang, P., and Cheng, G. (2014). Complement-related proteins control the flavivirus infection of Aedes aegypti by inducing antimicrobial peptides. PLoS pathogens *10*, e1004027.

Xie, X., and Auld, V.J. (2011). Integrins are necessary for the development and maintenance of the glial layers in the Drosophila peripheral nerve. Development *138*, 3813-3822.

Yguerabide, J., Schmidt, J.A., and Yguerabide, E.E. (1982). Lateral mobility in membranes as detected by fluorescence recovery after photobleaching. Biophysical journal *40*, 69-75.

Yi, P., Johnson, A.N., Han, Z., Wu, J., and Olson, E.N. (2008). Heterotrimeric G proteins regulate a noncanonical function of septate junction proteins to maintain cardiac integrity in Drosophila. Developmental cell *15*, 704-713.

Zhang, L., and Ward, R.E.t. (2011). Distinct tissue distributions and subcellular localizations of differently phosphorylated forms of the myosin regulatory light chain in Drosophila. Gene expression patterns : GEP *11*, 93-104.

Zlokovic, B.V. (2008). The blood-brain barrier in health and chronic neurodegenerative disorders. Neuron *57*, 178-201.